Table of Contents

List of Tables

List of Figures

APPLICATION OF THE SWAN WAVE MODEL TO A HIGH-ENERGY CONTINENTAL SHELF

by

MARGARET L. PALMSTEN

An Abstract

of a thesis submitted in partial fulfillment
of the requirements for the degree of
Master of Science
College of Marine Science
University of South Florida

May 2001

Major Professor: Peter Howd, Ph.D.

This thesis initiated an investigation of wave shoaling over the southwest Washington inner continental shelf. To better understand wave characteristics along the southwest Washington coast, the SWAN (Simulating WAves Nearshore) model will be implemented for this narrow high-energy shelf and sensitivity to changes in model formulation will be investigated. Pressure and velocity data collected at five stations near Grays Harbor, Washington between October and December 1999 will be used to calibrate and validate the model. The study was conducted in fall because of the variable wave climate in the Pacific Northwest. The data were deglitched and processed to produce estimates of significant wave height, peak direction, and peak period. Wave heights ranged between approximately 1 m and 8 m during the experiment. Wave direction was generally from the northwest during low wave conditions and the southwest during storm events. Peak period ranged from approximately 10 s to 20 s during the study. Processed data and results of the sensitivity study are used to calibrate and validate the SWAN model. Modeled wave characteristics were most like field measurements when the Madsen formulation for bottom friction was used with K_N = 0.05 m, and the Janssen formulation for wind input/whitecapping was used with C_{ds1} = 4 .5. The SWAN model reproduced wave shoaling over model domain well. The greatest difficulty in using the SWAN model on the southwest Washington inner continental shelf is inadequate input at the model boundary. An an application of validated model results, along-isobath energy flux was interpreted at the Grays Harbor ebb tidal delta. Using along-isobath energy flux as a proxy for a component of sediment transport, the stability of the ebb tidal delta was examined. Along-isobath energy flux appears to contribute to the northward component of ebb tidal delta movement.

Abstract Approved: _____

Major Professor: Peter Howd, Ph.D.
Assistant Professor, College of Marine Science

Date Approved: _____

Chapter One

Introduction

Background

The purpose of this study is apply a wave model to the high energy environment on the southwest Washington inner continental shelf and use model results to interpret stability of the Grays Harbor ebb tidal delta as an example of model application. To complete this goal, wave conditions along the southwest Washington coast must be accurately modeled. The difficulties in accurately representing the wave climate of southwest Washington will also be addressed. Accurate modeling is achieved by completing a series of three objectives. The SWAN (Simulating WAves Nearshore) model, developed at Deft University of Technology, must be implemented and a study of changes in formulations driving the SWAN model completed to determine sensitivity of the model. The SWAN model is calibrated by adjusting model formulations and comparing the results with conditions measured during a field experiment. The data collected during the field experiment consist of wave pressure and horizontal velocity measurements processed using linear wave theory to estimate wave statistics (significant wave height, peak direction, and peak period). Model formulations are calibrated for a simple condition, with medium wave height and wind and waves from the same direction. Results of the calibrated model are verified for a variety of wave conditions observed during the field experiment. The calibrated model will then be used to examine influence of waves on the stability of the Grays Harbor ebb tidal delta.

The motivation for this work is the Southwest Washington Coastal Erosion Study. The two goals of this larger study are to understand regional sediment system dynamics and predict coastal behavior at management scales (Gelfenbaum and Kaminsky, 2000). These goals necessitate a coastal wave-modeling component to the study. Such a component improves

understanding of nearshore sediment transport and regional shoreline change. Coastal change near the mouth of Grays Harbor is strongly influenced by the movement of the ebb tidal delta (Buijsman, 2000). Therefore, understanding of the wave climate that transports sand composing the ebb tidal delta at Grays Harbor will have implications for nearby coastal change.

The SWAN model provides the link between offshore wind and wave conditions and the nearshore conditions that drive longshore transport. The result of SWAN model simulations are detailed descriptions of the wave field, which may be used as input for a sediment transport model. Sediment transport models characterize sediment dynamics and are very sensitive to wave input which provides energy to suspend sediment. This requires modeled wave height results that compare well with field data. Modeled wave refraction must also reproduce field data well because wave direction is important in sediment transport modeling. A thorough understanding of the strengths and weaknesses of the SWAN model allows for better constraints on model error.

On a large scale, coastal change is important as humans interact with the dynamic coastal environment. Greater than 50 percent of the United States population lives within 50 miles of the coast. Billions of dollars are spent annually in coastal communities (Thornton et al., 1998). Like many coastal areas, the southwest Washington coast derives economic value from tourism, agriculture, housing and roadways along the coast, as well as use of channels and harbors for navigation. Coastal change has a great influence on this value.

Historical Change at Grays Harbor Ebb Tidal Delta

The study area extends from south of the Columbia River to Point Grenville in the north (Figure 1). Below is a summary of the investigation of historical ebb tidal delta and shoreline change at Grays Harbor by Kaminsky and Gelfenbaum (in press). Prior to jetty construction the Grays Harbor ebb tidal delta was located in a stable position at the mouth of the inlet at Grays Harbor. Jetty construction at Grays Harbor began in 1898 on the southern side of the inlet entrance in an effort to confine ebb tidal currents and scour the delta and channel for improved navigation. The jetty has been continually rehabilitated to the present. The jetty on the north

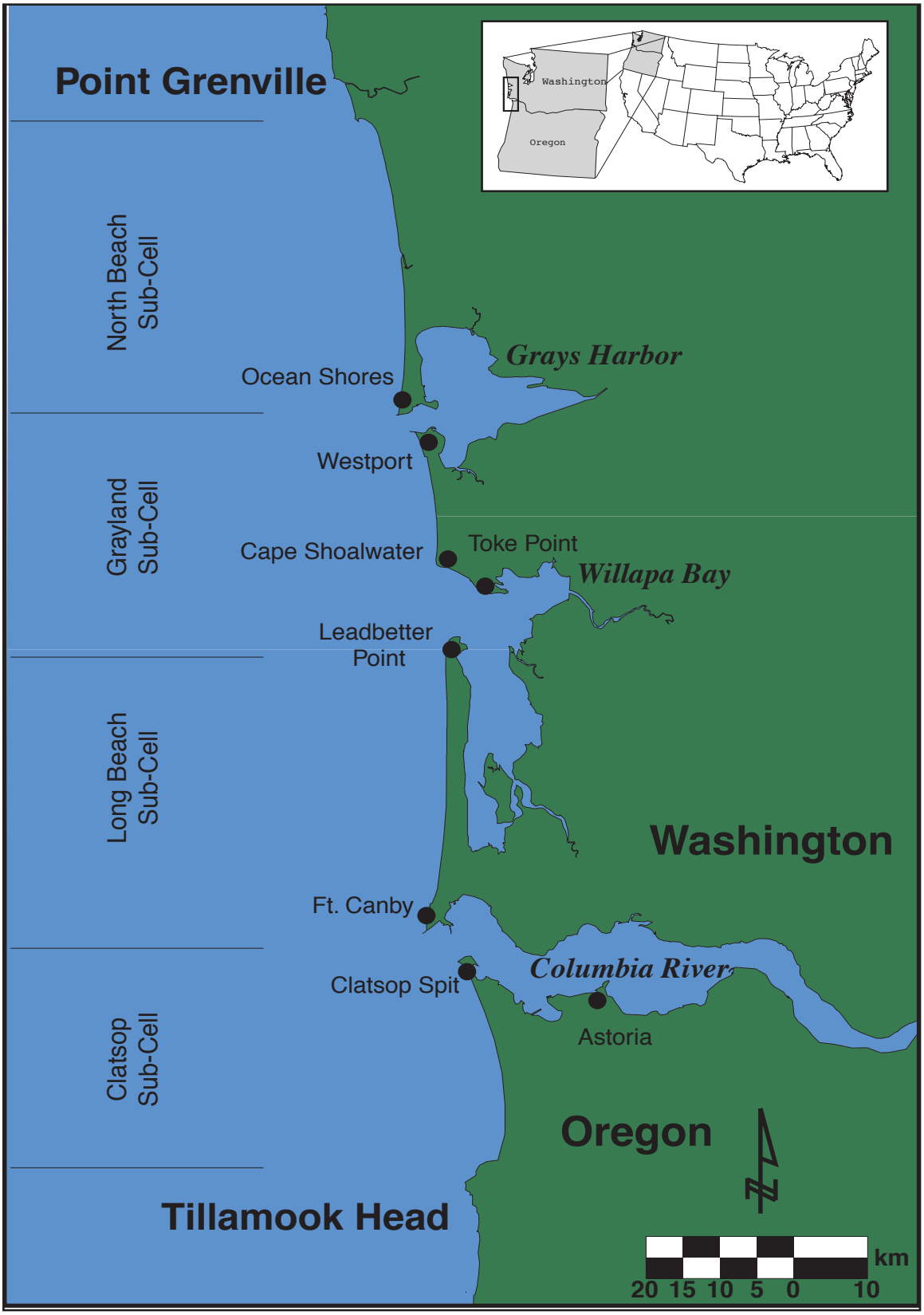

Figure 1. The study area extends the length of the Columbia River Littoral Cell, from point Grenville, WA to Tillamook Head, OR.

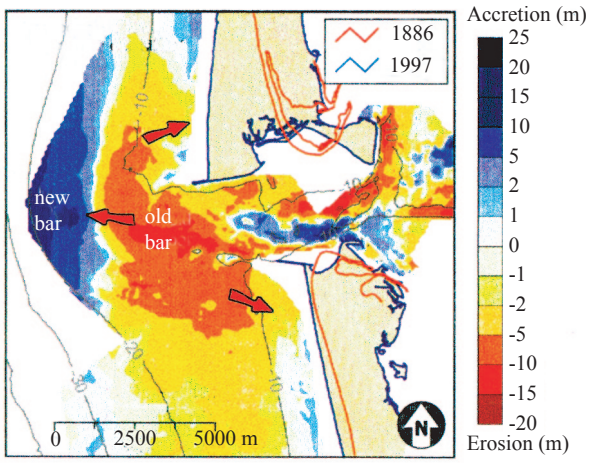

Figure 2. Bathymetric change at the entrance to Grays Harbor, 1900 - 1999 (modified from Buijsman (in press)).

side of the inlet began construction in 1908 to increase scour of the delta and channel by further confining ebb tidal currents. The north jetty has also been maintained to the present time. The result of jetty construction was erosion of the original delta at a rate of 0.9 Mm^3/yr and deposition of sand at a more offshore location at a rate of 1.4 Mm^3/yr (Kaminsky et al., in press). Shorelines near the inlet mouth accreted as wave action moved sediment from the flanks of the ebb tidal delta landward (Kaminsky et al., in press) (Figure 2).

Study Area Surficial Geology

Figure 3 shows the variety of facies described by Twitchell et al. (2000) in the study area. Continental shelf sediments may be divided in to two zones. South of Willapa Bay is a thick cover of Holocene sediments (Cross et al., 1998). Sediment cover on this part of the shelf is up to 45 m thick (Twitchell et al., 1998). Surface sediments are very fine sands (Twitchell et al., 2000). The origin of this layer is sediment from the Columbia River transported north (Herb, 1999). Bed forms on the lower beach face and inner shelf are oscillatory ripples with wavelengths of approximately 20 cm during the study (Twitchell, 2000). Bioturbated relict ripples covering the middle shelf region are composed of silty sands with >25% mud (Twitchell, 2000).

Sediment from the Columbia River has not been transported on the shelf north of Willapa Bay in significant quantity (Herb, 1999). Beaches in the northern part of the Columbia River

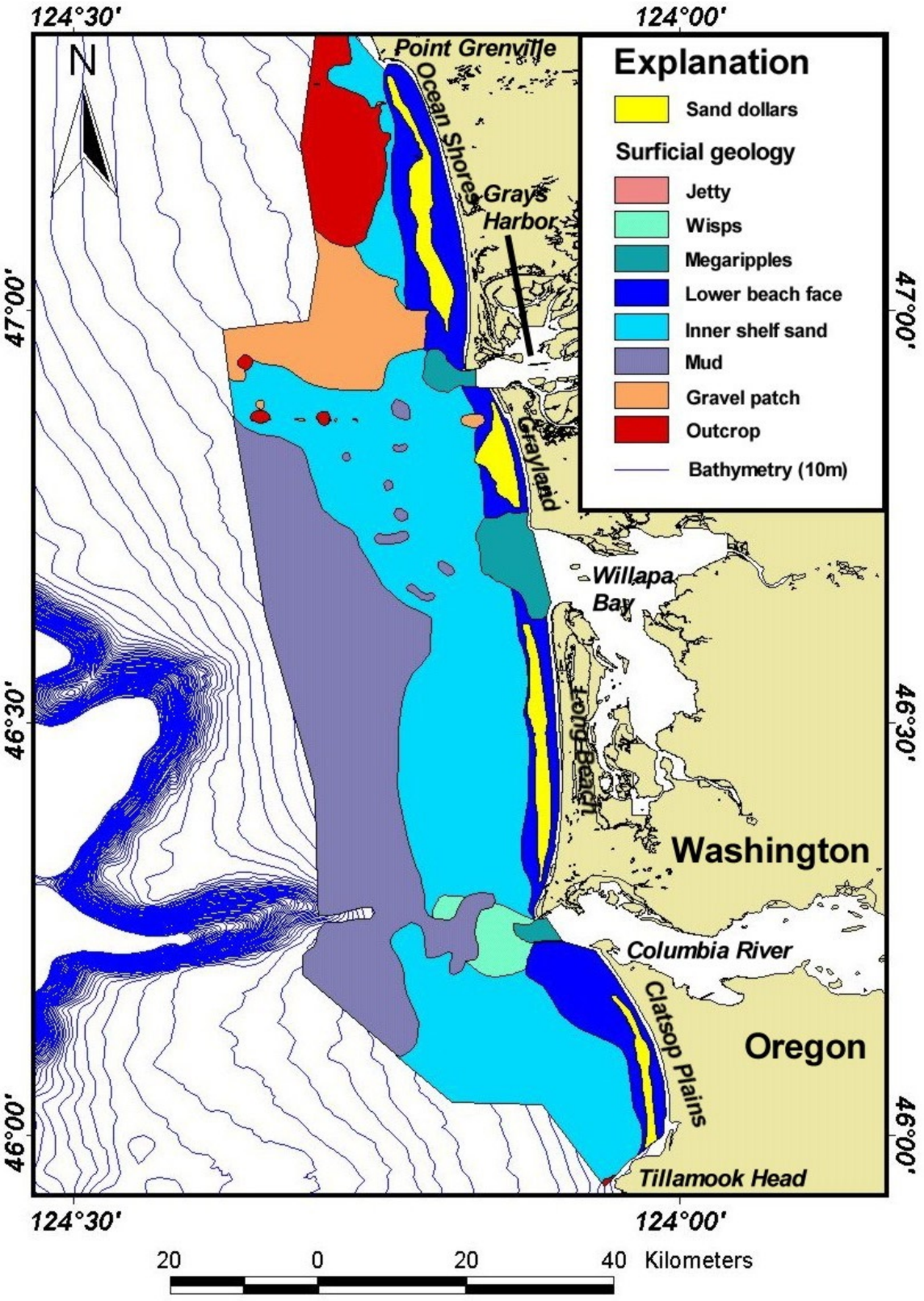

Figure 3. Surficial geology of the Columbia River Littoral Cell (modified from Twitchell et al., 2000).

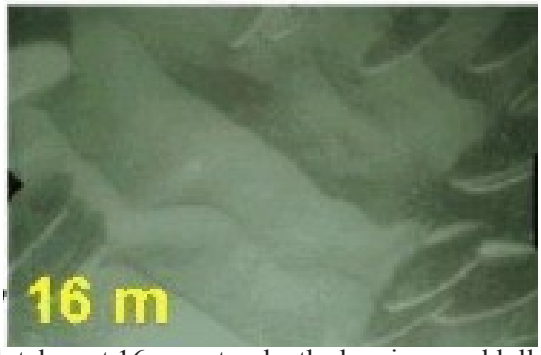

Figure 4. Photograph taken at 16 m water depth showing sanddollars aligned perpendicular to ripple crests (modified from Twitchell et al, 2000).

littoral cell began accreting at a later date than beaches near the mouth of the Columbia River (Woxell, 1998). The shelf area north of the Willapa Bay has a thin, discontinuous cover of medium to coarse sand with very little fine sand relative to the south (Twitchell, 2000). Gravel patches outcrop where the Holocene deposit thins to 1-2 m or is completely absent. Gravel patches are oriented E-W to NE-SW with sharp transitions to overlying sediment on the north side and gradational transitions on the south side (Twitchell, 2000). Megaripples with 2-4 m spacing are present in the patches (Twitchell, 2000). The gravel consists of 2 mm to 2 cm pebbles (Twitchell, 2000). The gravel patches are glacial in origin from the Chehalis River flowing out of Grays Harbor and onto the shelf at lower sea level (Venkatarathnam, 1973). Tertiary rock composed of altered basalt also outcrops where the relict shelf is exposed (Venkatarathnam, 1973). These rocks underlie the surficial sediment throughout the study area (Twitchell, 2000).

Sand dollars are present along the lower beach face throughout the study area (Figure 4). They are located in 7-18 m water depth and are oriented perpendicular to the crests of oscillatory ripples, which are roughly parallel to the shoreline (Twitchell, 2000). Tidally generated megaripples with wavelengths of 2-4 m and crests oriented parallel to the shoreline are located off the mouth of all three inlets in the study area (Twitchell, 2000). Patches of gravel located off the mouth of the Columbia River are interpreted to be fluvial sands or relict ebb tidal delta sediments (Twitchell, 2000).

Study Area Wave Climate

Wave climate along the Pacific Northwest coastline is spatially uniform (Tillotson and Komar, 1997). This study takes advantage of the spatial uniformity and assumes the same wave characteristics along the 435 km western boundary of the model domain. Wave heights and periods at National Data Buoy Center (NDBC) deep-water buoys and wave heights and periods at Coastal Data Information Program (CDIP) buoys transformed to their deep-water equivalents compare well. This check proves that the buoys are making reliable measurements, validating the assumption that we are initializing with accurate offshore boundary conditions. Wave heights computed by Wave Information Study (WIS) hindcasts are 30% to 60% higher than measured by NDBC buoys. Hence, WIS is not a good choice for offshore boundary conditions.

Allen and Komar (1999) summarized temporal variations of the wave climate in the Pacific Northwest. Spring and summer waves are the result of locally generated winds that blow over short fetches producing wave heights of less than 2.0 m and peak periods of less than 10 sec. Wave energy increases in the fall and peaks in December due to intensification of the Aleutian low and the southeasterly propagation of storms toward the West Coast. Winter storms have an average significant wave height of 3.3 m to 3.5 m. Since 1978, annual average significant wave height has increased at a rate of 0.027 m/year, for a total increase of 0.54 m. Annual average peak period has increased at a rate of 0.059 sec/year, resulting in a total increase of 1.1 seconds for the 19-year record. Causes of the long-term increase in wave height are unclear. The long-term increase in wave characteristics does not allow us to extrapolate a probable wave climate for longer time periods. Allen and Komar believe short-term trends in wave characteristics may be related to the East Pacific Teleconnection Pattern (EP), a measure of strength of westerly winds and the position of the jet stream, as well as El Nino/La Nina events. Wave directional records are only available for a short period of time and are poor during storm events so long-term direction is poorly constrained (Tillotson and Komar, 1997). The lack of directional information makes long term estimates of wave direction for the Pacific Northwest impossible.

Model Description

In an effort to understand wave transformation on the continental shelf and coastal orientation in southwest Washington, the SWAN wave model was implemented to describe wave conditions in nearshore waters. The SWAN model is a phase averaged spectral wave model developed at Delft University of Technology (Ris, 1997). This model accounts for nearly all of the physical processes that modify the wave field of coastal and inland waters. The SWAN model uses an Eulerian approach and assumes wave properties vary slowly over a wavelength. Rather than model the shape of the wave trains, phase averaged models compute the change in wave spectra over complex coastal bathymetry while maintaining computational efficiency. The most important advancement of the SWAN model is that the spectrum of waves is described as the net effect of a number of waves of different frequencies. Models of this type are called "third generation". In contrast, the older "second generation" models considered only the spectrum as a single, undivided entity. It is advantageous to resolve each frequency in a wave model because the evolution of a single wave (having one frequency) is a more fundamental and better-understood concept than is the evolution of the entire spectrum. Furthermore, the wave spectrum, which describes wave energy as a function of frequency, has a shape that varies considerably in space and time. The small number of parameters used in second-generation models cannot exactly describe this shape. The collections of waves described by third generation models are free to describe a far wider range of spectral shapes. This model is freely available on the Internet and has a variety of users, making it an attractive choice for this modeling effort.

Although the SWAN model was developed with state of the art formulations for physical processes, little work has occurred to understand sensitivity of model results to various parameters or to validate the model in a variety of coastal settings. The SWAN model was validated for environments including a wave tank, a fetch and depth limited shallow lake, and several complex low energy estuarine environments in the Netherlands and Germany (Ris, 1997). However, no model validation occurred in high wave energy, narrow shelf environment analogous to southwestern Washington. Absence of model verification in the field emphasizes the importance

of validating model results.

An alternate class of wave models designed for the coastal zone is termed “phase-resolving”. These models attempt to fully describe the temporally and spatially varying sea surface. Phase resolving models are capable of accounting for effects of diffraction and reflection. These models, however, do not include the effects of wave generation by wind or whitecapping. REF/DIF S, written by James Kirby of the University of Delaware, is a prominent phase resolving model. Phase resolving models are also more computationally demanding than phase averaged models.

The SWAN model describes the evolution of wave spectra, input at the offshore model boundary, propagating over geographic space with variations in water depth and depth averaged horizontal currents. The action balance equation drives the SWAN model.

$$\frac{\partial}{\partial t} N + \frac{\partial}{\partial x} c_x N + \frac{\partial}{\partial y} c_y N + \frac{\partial}{\partial \sigma} c_\sigma N + \frac{\partial}{\partial \theta} c_\theta N = \frac{S}{\sigma} \quad (1)$$

$N(\sigma,\theta)$ represents the action density spectrum, equal to the energy density spectrum divided by wave frequency, where σ is frequency and θ is direction. N is used because action density is conserved in the presence of currents, while energy density is not conserved. The first term in Equation 1 represents local rate of change in N with time. This term reduces to zero as only one time step is considered in the stationary version of the SWAN model. The second and third terms represent propagation in x and y space with c_x and c_y the propagation velocities in the x and y directions. The fourth term represents shifting of the relative frequency due to variations in water depth and currents. The fifth term represents depth-induced refraction. Energy source term, S, on the right side of the equation accounts for generation, dissipation, and nonlinear interactions between waves.

$$S = S_{in} + S_{ds} + S_{nl} \quad (2)$$

Energy input in SWAN results from wind (S_{in}). Three mechanisms for dissipation in SWAN (S_{ds}) are whitecapping, bottom friction, and depth-induced breaking. Energy is redistributed over the wave spectrum by nonlinear interactions (S_{nl}). Spectral evolution in shallow water is the result of triad interactions, while four-wave interactions, termed quadruplets, are important at intermediate and deep depths (Ris, 1997).

The source term for dissipation includes a contribution from bottom friction, $S_{ds,bf}$. Intuitively, bottom friction is the dominant form of dissipation in shallow water prior to the onset of depth limited breaking. This formulation may be adjusted to better represent wave and sediment characteristics in the model domain. The general form for the bottom friction dissipation equation is (Weber, 1991),

$$S_{ds,bf} = -C \frac{k}{\sinh kh} E(\sigma,\theta) \tag{3}$$

Where k is wave number, h is water depth, and E(s,q) is the energy density spectrum. The most influential factor in modeling wave dissipation due to bottom friction is the dissipation coefficient (C). Several formulations for C have are available for use in the SWAN model. The JOint North Sea WAve Project (JONSWAP) dissipation coefficient was developed to model decay of swell in the North Sea.

$$C_j = \frac{2\,c}{g} \tag{4}$$

c was empirically determined to have a mean value of 0.038 m^2s^{-3}. This value of c assigns a constant bed velocity of 0.259 ms^{-1}, which is reasonable over a wide range of conditions (Young and Gorman, 1995). Bouws and Komen found this value of c too low for a depth limited wind sea (1983). They determined a more appropriate value for wind seas of 0.067 m^2s^{-3}. This value is the default coefficient for bottom friction in SWAN because this formulation produced results most similar to field data (Ris, 1997). According to Weber (1991) C_j = 0.067 m^2s^{-3} is too high for fully developed, shallow water seas. Spectra produced using C_j has the highest energy levels and lowest peak frequencies of any bottom friction coefficients available in the SWAN model (Luo and Mondaliu, 1994).

Collins (1972) developed a value for C from a simplified version of the quadratic drag friction law using the wave induced bottom velocity.

$$C_{dc} = 2C_f \left\langle U^2 \right\rangle^{1/2} \tag{5}$$

Where,

$$\left\langle U^2 \right\rangle^{1/2} = \sqrt{\iint \frac{2gk}{\sinh 2kh} E(f,\theta)\,df\,d\theta} \tag{6}$$

C_f is the drag coefficient experimentally determined during Hurricane Betsy (1965) near Panama City, FL. The value for C_f of 0.015, is a function of bottom roughness scale. < > denotes an ensemble average. Computations using C_f yield spectra with intermediate energy levels and the low peak frequencies (Luo and Mondaliu, 1994). In contrast to C_j, C_{dc} assumes bed velocity is variable (Young and Gorman, 1995). Li and Mao (1991) found that for an idealized infinite region of finite water depth, both C_j and C_{dc} produce growth curves similar to Corps of Engineers Research Center (CERC) and Koninklijk Nederlands Meteorologisch Instituut (KNMI) growth curves.

Madsen et al. (1988) also developed a drag coefficient from the quadratic drag law. The friction factor, f_w is a function of roughness height (K_N) estimated by Jonsson (1960).

$$C_{dm} = f_w \frac{g}{\sqrt{2}} U_{rms} \tag{7}$$

m_f has a constant value of –0.08.

$$\frac{1}{4\sqrt{f_w}} + \log_{10} \frac{1}{4\sqrt{f_w}} = m_f + \log_{10} \frac{a}{K_N} \tag{8}$$

a_b represents bottom orbital velocity where,

$$a_b^{\,2} = 2\int_0^{2\pi} \int_0^{\infty} \frac{1}{\sinh^2(kd)} E(\sigma,\theta)\, d\sigma\, d\theta \tag{9}$$

K_N depends on flow field and sedimentary properties. A well-defined quantitative relationship for determining bottom roughness from grain size and bedform morphology does not exist. Values for bottom roughness are empirically determined. Tolman (1991) suggests K_N = 2 cm to 5 cm for a depth limited wind sea. For an environment with small sand ripples Weber (1991) used K_N = 4 cm where bottom roughness is two to four times ripple height. Ris (1997) recommends K_N = 0.1 cm for a smooth fine clay lakebed. C_{dm} produces the lowest energy levels and highest peak frequencies of all formulations for bottom friction in the SWAN model (Luo and Mondaliu, 1994).

In deeper water whitecapping surpasses bottom friction in energy dissipation. Whitecapping is the second component to the dissipation source term in the SWAN model. The

general form for dissipation of wave energy due to whitecapping is derived from the pulse-based model of Hasselman (1974) reformulated in terms of wave number is:

$$S_{ds} = -\Gamma \tilde{\sigma} \frac{k}{\tilde{k}} E(\sigma, \theta) \tag{10}$$

Where Γ is the steepness dependent coefficient,

$$\Gamma = C_{ds}\left[(1-\delta) + \delta \frac{k}{\tilde{k}}\right]\left[\frac{\tilde{s}}{\tilde{s}_{PM}}\right]^m \tag{11}$$

$\tilde{s}$ represents mean frequency, $\tilde{s}$ is the overall wave steepness, $\tilde{s}$ is the overall wave steepness parameter for the Pierson-Moskowitz spectrum. C_{ds} and m are constants.

The SWAN model contains two formulations for whitecapping. In the Komen formulation, $C_{ds} = 2.36 \times 10^{-5}$, $\delta = 0$, and $m = 4$ are obtained by closing the energy balance of waves in idealized wave growth conditions (Ris, 1997). This method of estimating dissipation due to whitecapping assumes the length scale between whitecaps and waves is large and weak in the mean, resulting in a linear dissipation source term. This formulation tends to underestimate peak frequency and wave height for steep waves while over estimating energy over short fetches. Despite these shortcomings, the Komen formulation produced valid results for swell near Hawaii and in the Southern Ocean (Zambresky, 1989; Bender, 1996). The default formulation for whitecapping in the SWAN model is the Komen formulation.

Janssen (1989, 1991) developed the alternative formulation for whitecapping. Janssen retuned the coefficients for whitecapping from the Komen formulation to $C_{ds} = 4.10 \times 10^{-5}$, $\delta = 0.5$, and $m = 4$. These values were determined by closing the energy balance and assuming the length scale between whitecaps and high frequency waves is not large for the Janssen formulation for wind input. In this form dissipation may depend on wavenumber rather than a linear relationship described by Komen et al. (Janssen, 1991). Consequently, there is stronger dissipation of high frequency waves and weaker dissipation at low frequencies. This resulted in a more realistic spectrum than that produced with the Komen formulation for wind input and whitecapping. This formulation for whitecapping tends to overestimate energy and underestimate peak frequency over short fetches. It underestimates energy and introduces spurious oscillations over long fetches (Ris, 1997).

The calculation for depth-induced wave breaking in the SWAN model ($S_{ds,br}$) is a spectral version of the bore-based model developed by Battjes and Janssen (1978). The model is capable of predicting wave height decay and setup for plane or bar-trough beach in the laboratory. Dissipation in the model is estimated as

$$S_{ds,br}(\sigma,\theta) = -\frac{\alpha_{BJ} Q_b \bar{\sigma} H_m^{\ 2}}{8\pi} \frac{E(\sigma,\theta)}{E_{tot}} \tag{12}$$

Where α_{BJ} is a free parameter with a value near 1. Q_b is the fraction of waves breaking.

$$H_m = \gamma d \tag{13}$$

γ can be constant or depend on slope. The formulation for dissipation due to breaking waves was not altered from the default as this was beyond the scope of the present study.

The source term for wind input (S_{in}) in the SWAN model is tied to the formulation for whitecapping. Komen et al (1984) determined exponential wave growth (B) using a constant drag coefficient when calculating U*. This formulation is an adaptation of Snyder's (1981) formulation developed from direct measurements of atmospheric pressure fluctuations on waves.

$$B = \max\left[0, 0.25 \frac{\rho_a}{\rho_w} 28 \frac{U_*}{c} \cos(\theta - \theta_w) - 1\right] \sigma \tag{14}$$

Where ρ_a and ρ_w are the densities of air and water, respectively. θ is wave direction and θ_w is wind direction. c is phase speed and U* is,

$$U_* = C_D^{\ 1/2} U_{10} \tag{15}$$

The second expression for exponential wave growth from Janssen is an extension of Komen's formulation, but depends on waves affecting the wind velocity profile. For a young wind sea, wave induced stress on the wind profile is large, thereby reducing the transfer of momentum from wind to waves. For an old wind sea, there is little transfer of momentum between the wind and waves, therefore less aerodynamic drag. The Janssen formulation parameterizes this effect by assuming a logarithmic wind profile with a roughness that depends on wave induced stress. Wave growth in this formulation is calculated with a variable value for U*.

$$B = \beta \frac{\rho_a}{\rho_w} \left(\frac{U_*}{c}\right)^2 \max\left[0, \cos(\theta - \theta_w)\right]^2 \sigma \tag{16}$$

β is the Miles parameter, which depends on a dimensionless value for surface roughness, becomes constant for high frequencies, resulting in constant wave growth. This differs from the Komen formulation where wave growth at high frequencies is linear. This generally results in the underestimation of wind input for high frequency waves and therefore wave induced stress.

Nonlinear interactions, which are responsible development of wave spectra through the transfer of energy between spectral components, are represented in the source term S_{nl} in the SWAN model. Nonlinear interactions in deep water are the result of quadruplet interactions. The transfer of energy by quadruplets occurs when resonance conditions described below are satisfied,

$$k_1 + k_2 = k_3 + k_4 \tag{17}$$

$$\omega_1 + \omega_2 = \omega_3 + \omega_4 \tag{18}$$

Where ω is related to k by the dispersion relation from linear wave theory.

Hasselman (1963) described quadruplet interactions in terms of action density using the Boltzmann integral

$$\frac{\partial N_1}{\partial t} = \iiint G\left(\vec{k}_1,\vec{k}_2,\vec{k}_3,\vec{k}_4\right) \times \delta\left(\vec{k}_1 + \vec{k}_2 - \vec{k}_3 - \vec{k}_4\right) \times \delta\left(\omega_1 + \omega_2 - \omega_3 - \omega_4\right) \times \left[n_1 n_3 \left(n_4 - n_2\right) + n_2 n_4 \left(n_3 - n_1\right)\right] d\vec{k}_1 d\vec{k}_2 d\vec{k}_3 \tag{19}$$

$N_i = N(k_i)$ is the action density at wavenumber k_i, G is a coupling coefficient, δ functions ensure that contributions to the integral occur only at quadruplets that satisfy the resonant conditions (Equations 17 and 18). The direct solution of the Boltzmann integral is computationally intensive. Therefore the SWAN model uses a modified form of the Discrete Interaction Approximation (DIA) developed by Hasselman et al (1985). The DIA in the SWAN model considers a small number of quadruplets of the configuration.

$$\sigma_1 = \sigma_2 = \sigma \tag{20}$$

$$\sigma_3 = \sigma(1+\lambda) = \sigma^+ \tag{21}$$

$$\sigma_4 = \sigma(1+\lambda) = \sigma^- \tag{22}$$

Lambda is set to 0.25 based on observation. $k_1 = k_2$ and k_3 and k_4 are of different magnitude and angle than the first two wavenumbers. In the SWAN model k_3 lies at an angle of -11.5^o

k_1 in the first quadruplet and 11.5° in the second quadruplet. k_4 is at an angle of 33.6° from k_2 in the first quadruplet and –33.6° in the second quadruplet. The source term is result of addition of the first and second quadruplets.

$$S_{nl4}(\sigma,\theta) = S^{*}_{nl4}(\sigma,\theta) + S^{**}_{nl4}(\sigma,\theta) \tag{23}$$

Where δS_{nl4} is the rate of change of the energy density,

$$\delta S_{nl4}(\alpha_i\sigma,\theta) = C_{nl4}(2\pi)^2 g^{-4}\left(\frac{\sigma}{2\pi}\right)^{11} E^2(\alpha_i\sigma,\theta)\left[\frac{E(\alpha_i\sigma^+,\theta)}{(1+\lambda)^4} + \frac{E(\alpha_i\sigma^-,\theta)}{(1-\lambda)^4} - 2\frac{E(\alpha_i\sigma,\theta)E(\alpha_i\sigma^+,\theta)E(\alpha_i\sigma^-,\theta)}{(1-\lambda^2)^4}\right] \tag{24}$$

C is a constant equal to 3 x 10^7. $E(\alpha,\sigma,\theta)$ is the energy density at the interacting wavenumbers. The nonlinear energy transfer is calculated by considering all interactions between the four wavenumbers that satisfy the resonant conditions by looping over all wavenumbers in the spectrum with the central wavenumber $k = k_1 = k_2$. This reduces the problem to a two dimensional integral, rather than the six dimensional Boltzmann integral. Although this reduces the number of interactions calculated by three orders of magnitude, it reproduces the physical properties and of the Boltzmann integral (Young and Van Vledder, 1993). Spectra produced by the DIA have broader directional spreading than spectra calculated by the full solution (Young and Van Vledder, 1993).

Quadruplet interactions in finite water depth are scaled by R, where R is,

$$R(k_p d) = 1 + \frac{5.5}{k_p d}\left[1 - \frac{5k_p d}{6}\right]\exp(-1.25k_p d) \tag{25}$$

$k_p = 0.75$(mean k). $k_p d = 0.5$ is the lower limit for which the scaling factor is applied.

Triad-wave interactions are the second form of nonlinear interactions in the SWAN model. Triad interactions transfer energy from the peak frequency to higher and lower frequencies in steep waves in very shallow water (Ris, 1997). The Lumped Triad Approximation (LTA) is used to calculate nonlinear transfer due to triads in the SWAN model. Only transfer of energy to super harmonics are calculated in the SWAN model as,

$$S_{nl3}(\sigma,\theta) = S^{+}_{nl3}(\sigma,\theta) + S^{-}_{nl3}(\sigma,\theta) \tag{26}$$

where

$$S_{nl3}^{+}(\sigma,\theta) = \max\left[0, \alpha_{EB} 2\pi c_{g,\sigma} J^2 \left|\sin(\beta)\right| \left(\frac{\sigma}{k_\sigma} E^2(\sigma/2,\theta) - 2\frac{\sigma/2}{k_{\sigma/2}} E(\sigma/2,\theta) E(\sigma,\theta)\right)\right] \quad (27)$$

and

$$S_{nl3}^{-}(\sigma,\theta) = -2S_{nl3}^{+}(2\sigma,\theta) \quad (28)$$

α_{EB} controls the magnitude of the triad interactions and is set to 0.5. β is the parameterized biphase depending on the Ursell number, Ur,

$$\beta = \frac{-(\log Ur + 1)\pi}{4} \quad (29)$$

where Ur is given by

$$Ur = \frac{g}{2\sqrt{2}} \frac{H_s}{d^2 \bar{\sigma}^2}$$

$\bar{\sigma}$ is mean frequency. J is an interaction coefficient given by

$$J = \frac{g\alpha_{nl3}}{\beta_{nl3}} \quad (31)$$

with

$$\alpha_{nl3} = \left(2k_{\sigma/2}\right)^2 \left[\frac{1}{2} + \frac{c_{\sigma/2}^2}{gd}\right] \quad (32)$$

and

$$\beta_{nl3} = -2k_\sigma \left[gd + 1.3gd^3 k_\sigma^2 - 0.46\sigma^2 d^2\right] \quad (33)$$

Chapter Two

Methods

Sensitivity Analysis

The SWAN model has many parameters that may be adjusted by the modeler. The purpose of this sensitivity study is to determine which SWAN model parameters produce significant change in the wave characteristics over an area. This will also provide insight into which parameters must be varied to produce a physically accurate model and model results that agree well with observed wave characteristics. Two suites of model tests, totaling more than 100 model runs were performed to measure the sensitivity of SWAN to several of these parameters.

Three wave states were utilized for the sensitivity study representing typical small, medium, and large wave conditions for fall in southwest Washington. The range of conditions was chosen to represent possible wave conditions during the field experiment used to validate the model. The "small wave" case had a significant wave height of 2.3 m, a peak period of 8 s, and a wave direction of 305^{o}. This corresponds to stable conditions observed over several hours at NDBC 46005 in September of 1998. In the "medium wave" case, significant wave height was 4.8 m, peak period was 11s, and wave direction was 260^{o}. This was based on a stable time period in November of 1998. A "large wave" case (8.1 m, 16.7 sec, 280^{o}; December 1998) was used in a few tests. Wave direction in these cases was taken from peak wave direction measured at the Grays Harbor CDIP buoy. Several of the sensitivity runs were initialized using a one dimensional energy spectrum from the small and large wave cases. Wave direction in model runs with observed spectra at the boundary condition were determined at the Grays Harbor CDIP buoy and a value of directional spreading was calculated at each frequency using the Donnelan-Banner method described by Ewans (1998). The formulation for directional distribution $H(\sigma,\theta)$ is calculated using directional characteristics of second order Stokes wave groups and analysis of data.

$$H(\sigma,\theta) = 0.5\beta\ sech^2\beta(\theta-\theta_1(\sigma)) \quad (34)$$

Where β depends on relative frequency and θ_1 is mean wave direction.

If wind was used in a particular model run, wind speed in ms^{-1} was set equal to the wave height in m. Winds of this speed were chosen because they were a negligible source of wave energy and yet had a significant impact of whitecapping. Wind direction in the sensitivity study was set as a following wind. For small wave case this is 305^o and for the medium case this is 260^o. Alternatively, it was set as a crossing wind 40^o to the south in the small wave case (245^o) and 40^o to the north in the medium wave case (320^o).

Four model elements were tested in the sensitivity study. The elements are boundary conditions, model formulations, formulation coefficients, and currents. One parameter of one element was varied per model run; all other parameters were set to the default value. The first set of sensitivity runs investigated model elements including: bottom friction formulation, exponential wave growth formulation, method of computing quadruplet interactions, use of a linear wave growth term, use of observed or parameterized boundary spectra, and wind input. Conceptually, the elements were treated as "on" and "off" switches. The purpose of these runs was to determine differences in model results when the elements included or excluded from the calculations. Model elements tested in the second suite of model runs were the formulation coefficients, which are continuously variable settings or values. The continuously varying parameters were associated with four physical mechanisms: dissipation due to whitecapping, dissipation due to bottom friction, triad interactions, frequency resolution, and directional resolution. In each test, a coefficient was increased or decreased by doubling or halving the default value. These new values were doubled or halved repeatedly until a 3% difference in wave height occurred between model runs in a coastal subset of the model domain. A 3% difference in wave height was defined as the significant because this value is near the limit of accuracy for wave height statistics calculated from pressure measurements.

Two bathymetry data sets were used in these model runs. Both have a resolution of 750 m, cover roughly 100 km in longitude, and are based on the National Ocean Survey (NOS) 1927 data. The "short" set is show in Figure 5 and covers about 225 km in latitude. The "tall" set is identical except that it includes another 40 km to the north and 170 km to the south. The reason for two bathymetry data sets is the null-boundary effect. Boundary conditions are specified along

the offshore (western) boundary but not along the lateral (northern and southern) boundaries. This is equivalent to specifying that no waves are present along the lateral boundaries; this in turn corrupts the model results some distance inward of the lateral boundaries. Thus, the "short" bathymetry is used only when the null boundary effect does not include the study region.

Model results were analyzed in two ways. First, images were generated showing differences in wave height and peak direction between pairs of runs (Figure 5). This form of comparison resulted in a qualitative view of differences in wave characteristics, showing general spatial trends. Second, criteria were devised for characterizing the differences in wave height and direction over a subset of the domain (Figure 6). This calculation resulted in a quantitative comparison of wave characteristics. For significant wave height, the criterion was the mean percent difference in wave height between wave height calculated with default coefficient and wave height calculated with test coefficient.

For wave direction, the criterion was the mean angular difference between direction calculated with default coefficient and direction calculated with test coefficient. Four areas (Figure 6) were selected from within the model domain. A so-called "large area" was defined to encompass the entire domain deeper than 15 m and excluding areas near the lateral boundaries where results are corrupted by those boundaries. Three "coastal areas" bounded by the 15 and 40 m isobaths were defined, with one near the straight coast of Grayland and one over each of the ebb-tidal deltas of Grays Harbor and Willapa Bay. (Note in Figure 6 how poorly the coastline is represented. This does not reflect errors in the bathymetry, which is based on data deeper than 5 m).

In the SWAN model the user indicates the wind velocity at 10 m elevation in ms^{-1} as well as the wind direction at 10 m elevation at every model grid point with the wind-input command. The sensitivity of the SWAN model to wind-input was tested by increasing wind from 0 ms^{-1} to 5 ms^{-1}, 5 ms^{-1} to 7 ms^{-1}, and 7 ms^{-1} to 10 ms^{-1}. Wind direction was also varied between a following wind from 260^{o} and a crossing wind of 320^{o}. The medium wave case was used in this test.

The major dissipation source term in shallow water within the SWAN model is bottom friction. It may be formulated in three ways within the SWAN model. The Madsen formulation for bottom friction and the Collins formulation for bottom friction are based on the quadratic drag law, while the JONSWAP formulation for bottom friction comes from empirical measurements.

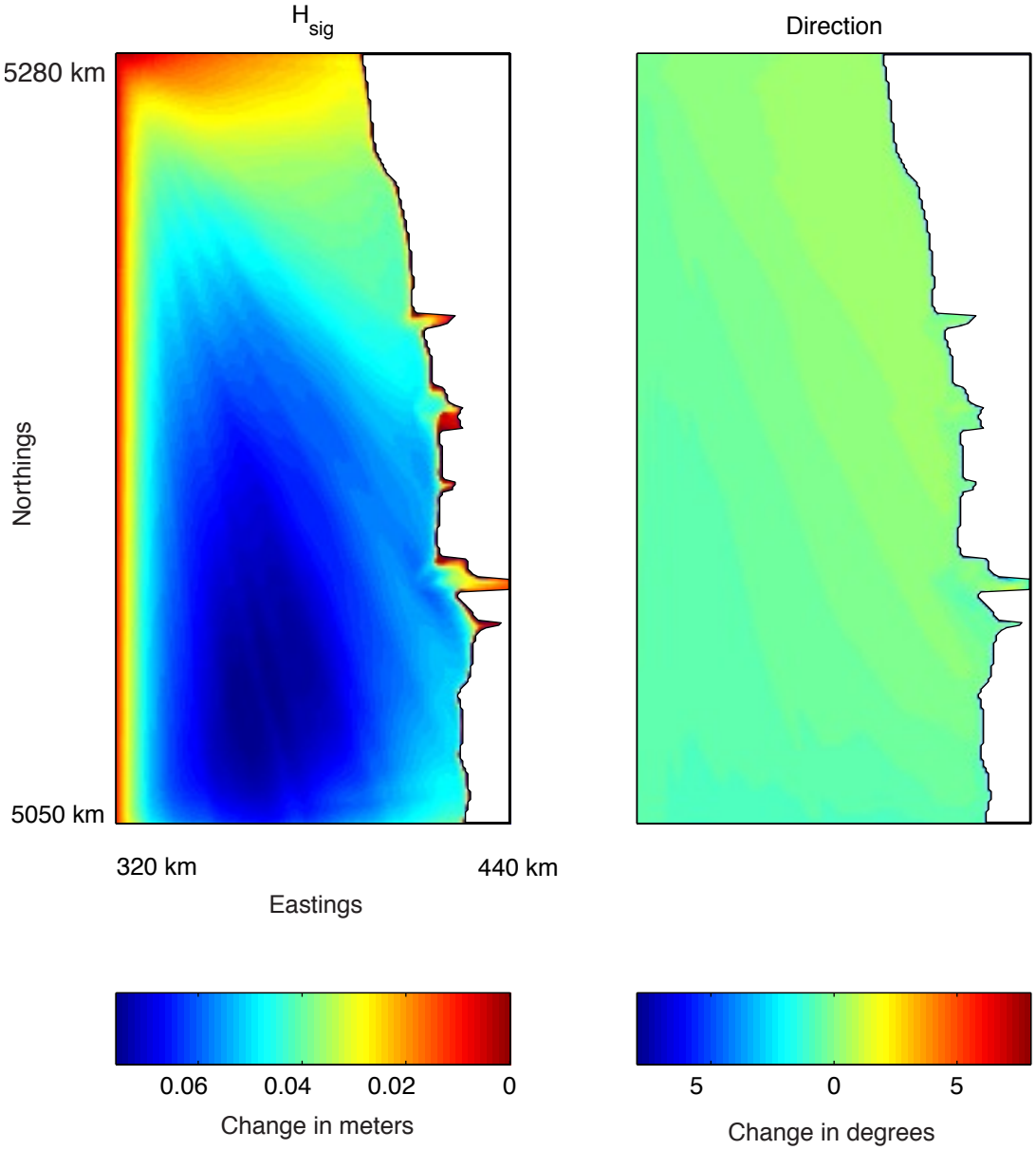

Figure 5. Example of format for plotting results of the sensitivity study. Plot on the left represents change in significant wave height (H_{sig}) in meters due to change in formulation for exponential growth. Right plot represents change in degrees due to change in formulation for exponential growth.

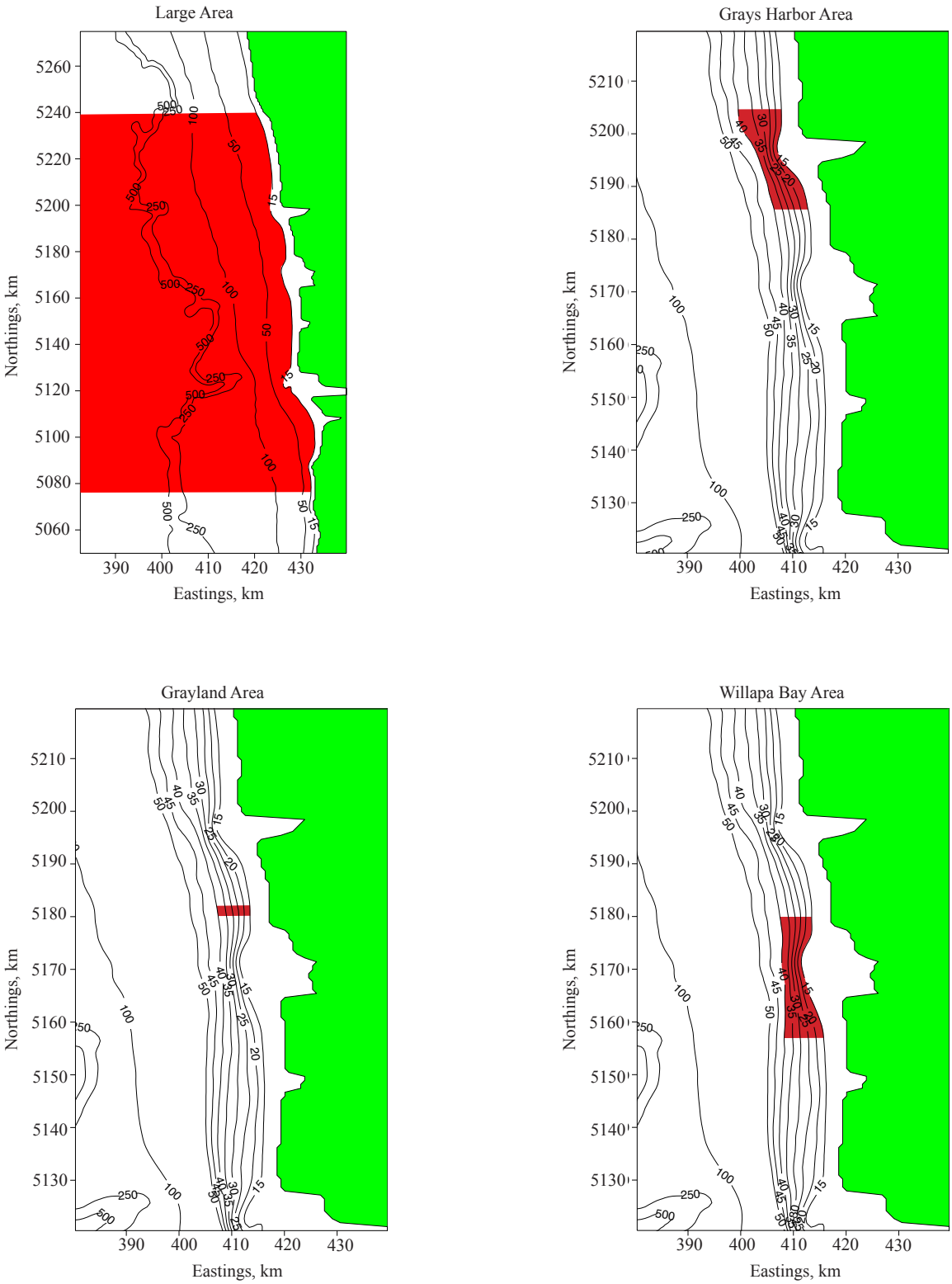

Figure 6. Subsets of model domain used in sensitivity calculation are depicted by red areas. Bathymetry contour levels are in meters.

These formulations are described in detail in the introduction. In this part of the sensitivity test the formulations for bottom friction are compared using the default values for the coefficient of dissipation given in the SWAN model. The default coefficient for the Madsen formulation is K_N = 0.05. The default value for the Collins bottom friction is 0.015. 0.038 is the default coefficient for bottom friction in the JONSWAP formulation. No wind was used during the comparison so energy was not lost to whitecapping. The small and medium parameterized wave cases as well as wave cases from September and December using one-dimensional spectrum with a varying directional spreading value were used.

In the second suite of model runs for sensitivity, bottom friction was revisited. This time the effect of varying the roughness value in the Madsen formulation was tested. Focus was placed on the Madsen formulation for bottom friction because it is considered the most physically accurate of the three choices for bottom friction available in the SWAN model (Luo and Monbalui, 1994). The small wave case was used with a following wind. The bottom roughness value (K_N) was varied by orders of magnitude from the default to 0.05 m to 0.5 and 0.005 and 0.0005.

One of the source terms in the SWAN model is dissipation due to whitecapping. Comparing model results with whitecapping turned on and turned off tested the relative importance of whitecapping to variation in wave height and direction. Both the Janssen formulation for exponential wave growth and the Komen formulation for exponential wave growth were used in this experiment. Small and medium wave cases were used in this comparison.

Formulations for whitecapping may be adjusted by varying several coefficients within the formulation. The coefficient for determining rate of dissipation due to whitecapping and delta in the Janssen formulation were varied until a significant change in wave height was produced. The coefficient for determining rate of dissipation due to whitecapping, C_{ds} and wave steepness parameter for the Pierson-Moskowitz spectrum, $\tilde{s}_{pm}$, were varied in the Komen formulation for whitecapping until a significant change in wave height was produced. Both small and medium wave conditions were modeled with following and crossing winds.

Model sensitivity to the formulation for exponential wave growth was tested. Sensitivity was determined by comparing model results using the Janssen formulation and model results

using the Komen formulation. Exponential wave growth is the result of wind input to pre-existing waves. The small and medium wave cases were tested using following and crossing winds. Whitecapping was also turned on and off. The linear growth term in SWAN facilitates the growth of waves from a calm sea state. This term was compared with results from applying the JONSWAP spectrum at the model boundary. Comparisons were made for small and medium wave conditions with following and crossing winds.

Non-linear interactions between waves are a source term in the SWAN model. This interaction occurs in deep and intermediate water depths as quadruplets. Within the SWAN model there are three methods of computing quadruplet interactions. The methods are listed in order of decreasing computational time. The first method uses a semi-implicit computation per sweep. The second method uses a fully explicit computation for nonlinear transfer per sweep. The third method uses a fully explicit computation for nonlinear transfer per iteration.

The second portion of the source term for nonlinear interactions is triad interactions in shallow water. Within the triad command in the SWAN model, the proportionality constant, α_{eb}, controls the magnitude of the interactions. The value of α_{eb} was increased and decreased an order of magnitude from the default value. The maximum frequency considered in triad computations is adjustable. This value was increased and decreased by an order of magnitude. Both parameters were tested using small and medium wave cases with crossing and following wind.

Sensitivity of the SWAN model to applied boundary conditions was tested. The parameterized JONSWAP spectrum (Ris, 1997) was used to initialize the model. Wave height, period, and direction and constant directional spreading are specified at the model boundary. This spectrum was compared with an observed frequency spectrum with direction specified and a constant value for directional spreading or and observed frequency spectrum with a specified direction and directional spreading varying with frequency according to Donnelan-Banner (Ewans, 1998). Observed spectra were from the small wave case and the large wave case. No wind was used.

The modeler may choose the directional resolution of the SWAN model. The size in degrees of directional bins is inversely proportional to computational time and smaller bin size results in greater model accuracy. Therefore, it was important to determine the most efficient bin size with regard to computational time and model accuracy. The default bin size was set at 6^{o}.

Maximum bin size modeled was 40°. Bin size was decreased in increments of five or ten degrees between 40° and 12°, two degrees between 12° and 6°, and increments of one degree between 6° and 3°. The percent difference between the results of a model run with the smallest bin size and a larger bin size was defined as sensitivity.

As with directional resolution, it is important to use the most efficient frequency resolution. Frequency resolution is proportional to computational time and model accuracy. Resolved frequency band with was defined by a minimum (0.04 Hz) and a maximum frequency (0.4 Hz) set by the modeler. Frequency resolution was determined by the number of frequencies (default was 15) modeled. Sensitivity to frequency resolution was determined by varying the number of frequencies modeled in increments of five or fewer between 8 and 35. The 35 frequency case was taken to be the most accurate, and sensitivity was defined as percent difference in wave height between this and other runs.

Field Experiment

A wave refraction experiment near the Grays Harbor ebb tidal delta was designed to complete the objective of calibrating and validating the SWAN model. The main goal of the field experiment was to collect data for many wave conditions. The experiment was conducted in the fall because wave climate for the Pacific Northwest is most variable. During this time dominant swell is from the northwest and storm events are from the southwest.

A number of experimental SWAN runs were completed in order to help identify optimal instrument locations for the field experiment. SWAN parameters were chosen using the results from the sensitivity study. Wave boundary conditions were selected from a climatology of Army Corp of Engineers (WIS) results. The small wave case (Hsig = 3.5 m) represents the case resulting in the largest value of (PDF * $Hsig^2$), where PDF is the probability density function. The quantity (PDF * $Hsig^2$) gives the rate of energy delivered by waves of that height and may be thought of as their "importance" from an energetic standpoint. The medium (5.1 m) and large (7.1 m) wave cases were chosen to characterize the effect of storms larger than 3.5 m. Wind input was taken from a climatology of the NDBC mooring 46005. Bathymetry input was the NOS 1926/Army Corps of Engineers (COE) 1998 merged bathymetry created by Gibbs (1999) at 500 m resolution (Figure 7). Modeled wave height and direction were extracted along the 15 m, 20 m, 25

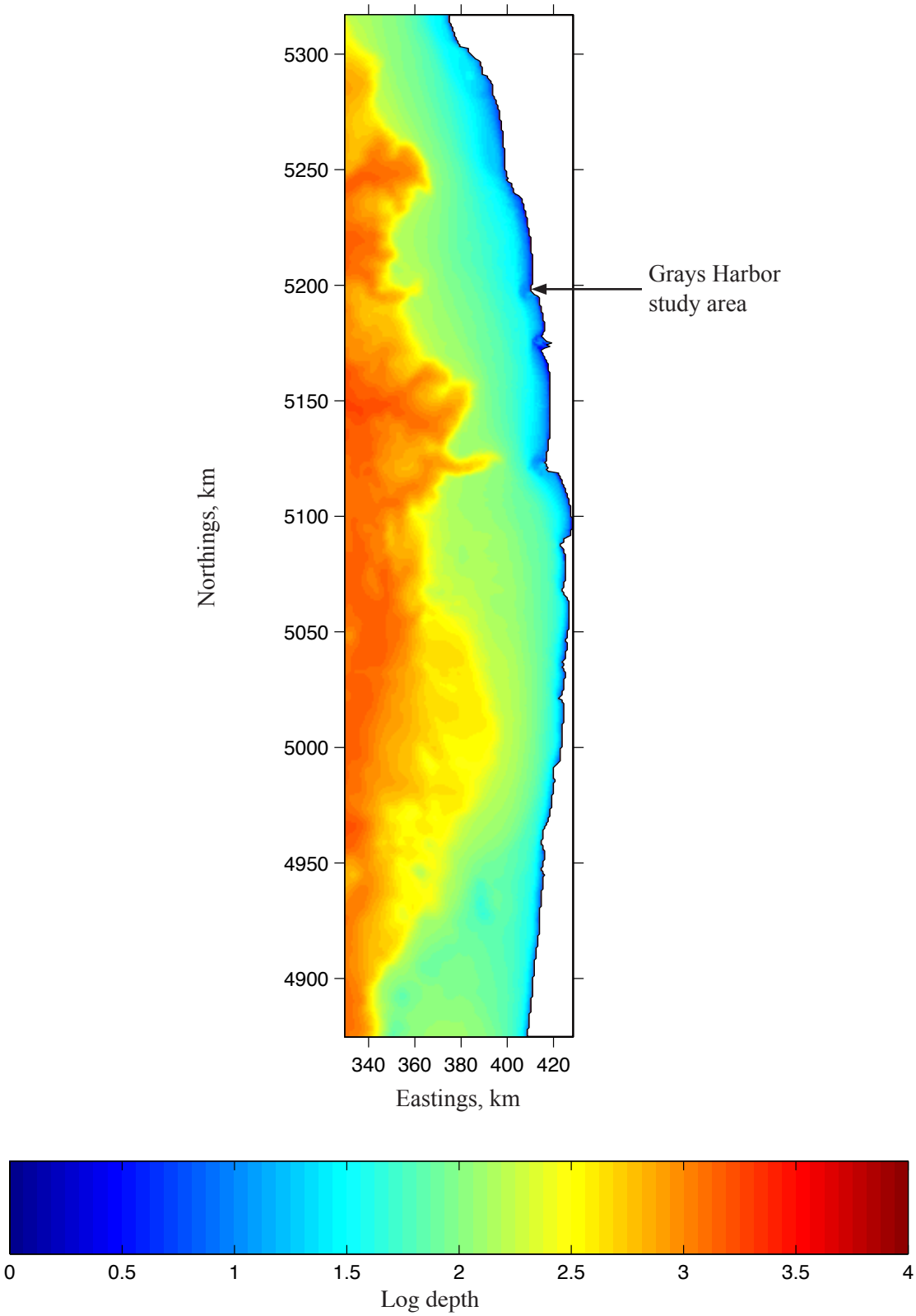

Figure 7. NOS 1926/COE 1998 merged bathymetry gridded at 750 m resolution used as input for the SWAN model.

m, 30 m, 35 m, and 40 m isobaths near Grays Harbor. Locations where SWAN showed maximum influence of the delta were identified on the north and south side of Grays Harbor ebb-tidal delta (ETD). The preliminary runs showed wave direction was much more dramatically impacted by the delta than was wave height. "Influence" was characterized by examining wave direction on an isobath and comparing the values on the delta with those on "straight" coast sections to the north and south. Tripod locations were chosen where influence was predicted to be the greatest.

An array of sensors was secured to each of five 2.4 m aluminum tripods deployed during the experiment (Figure 8 and Figure 9). Water depths and position of the tripods are given in Table 1 and Figure 10. Pressure data were collected at 5 (ND, NS, MD, SD, SS) stations using an external Paroscientific, Inc. Digiquartz pressure sensor. Pressure data were also collected using a Druck pressure sensor internally mounted on an upward looking Sontek acoustic doppler profiler (ADP) at two locations (ND and SD, Table 1). Wave orbital velocities were measured at 5 stations using a Sontek, Inc. three axis single point acoustic doppler velocimeter (ADV). ADV sampling volume was 0.5 cm^3 located 0.8 m above the base of the tripod. Data were recorded by Sontek Hydra dataloggers. Data were collected at a rate of 2 Hz over half-hour periods every two hours during the first deployment and every hour during the second deployment. A sampling rate of 2 Hz was chosen to allow the resolve surface gravity waves. This resulted in the collection of 111,837,184 pressure and velocity measurements. The first deployment took place October 1-2, 1999. The instruments were recovered, serviced and redeployed during November, 1999. The final recovery took place the end of December, 1999.

Data collected by instruments during the deployment were downloaded and stored on CD. Plots of raw horizontal and vertical velocities and pressure were created for each half-hour burst. Plots helped identify qualitative aspects of the data including character of errors in the data. General trends in the data were identified with plots of moving mean and variance. An autocorrelation was computed and plotted for each data burst. A histogram was created for each burst to visualize general trends in the data. Maximum, minimum, mean value per burst of velocity and pressure were calculated. The overall variance and number of points exceeding four standard deviations of the mean were determined for each burst.

Many statistics were calculated and plotted for each burst to check data quality. Plots of mean signal strength, standard deviation of the signal strength, mean correlation, and standard

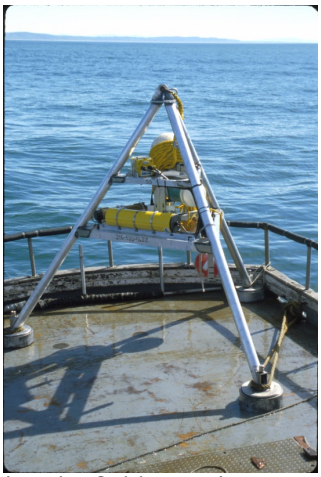

Figure 8. Tripod deployed during the field experiment. Tripod is equipped with an Sontek ADP, Sontek Hydra datalogger, Sontek battery pack, Sontek ADVO, buoy, pinger, OBS, and Paroscientific, Inc pressure sensor.

Figure 9. Detail of tripod showing location of the Paroscientific pressure senor and Sontek ADVO.

deviation of correlation gave quality estimates of ADV measurements. Velocity data of poor quality were identified with a low pass filter in the frequency domain. Within the low pass filter routine, written by Sherwood, 1989, the mean is removed from the data. A Fast Fourier Transform (FFT) is performed on the data. The cut off frequency was set to 0.3. The filter is created by multiplying the cutoff frequency by the number of frequencies computed in the FFT and the timestep of the timeseries. A three point taper is used between pass-band and stop band. The autocorrelation from the FFT is multiplied by the filter and and inverse FFT is computed from the result. Finally, the mean is added to the real result of the FFT. The residual of the velocity measurements is calculated by subtracting the raw velocity time series from the filtered velocity time series. If the absolute value of the residual is greater than four times the standard deviation of the residual of U or V, the point is replaced. A spline interpolation was used to replace poor quality data points.

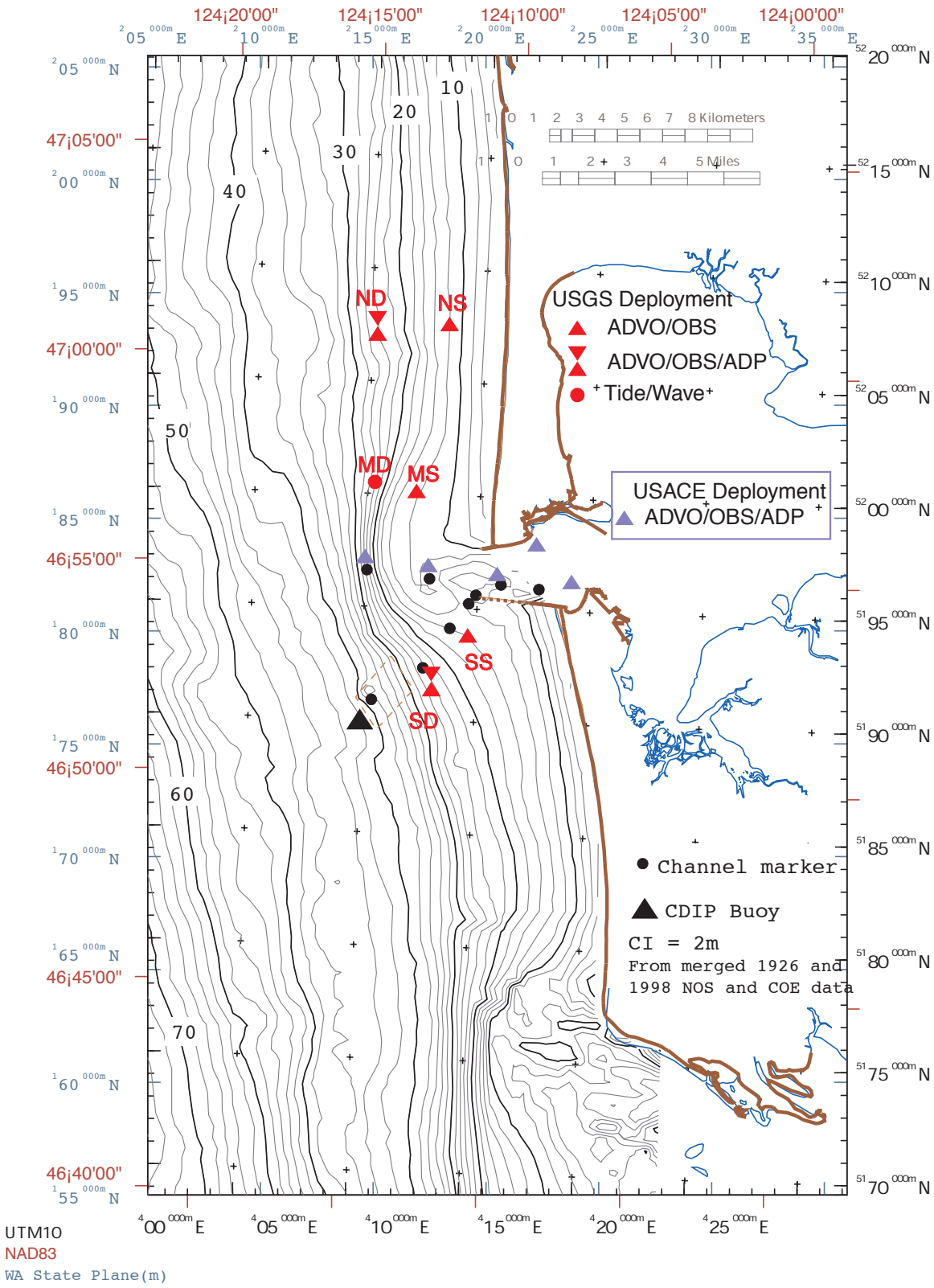

Figure 10. Instruments were deployed at locations SD, SS, MD, MS, where the SWAN model showed the greatest influence of the ETD. The SWAN model showed little influence of the ETD at ND and NS.

Station	First Deployment Dates	Second Deployment Dates	First Deployment Instrumentation	Second Deployment Instrumentation
ND	10/01/99 - 11/02/99	11/04/99 - 12/11/99	Paros Pressure Sensor Sontek ADV	Paros Pressure Sensor Sontek ADV
NS	No data collected	11/05/99 - 12/28/99		Druck Pressure Sensor Sontek ADV
MD	10/02/99 - 11/27/99	11/27/99 - 12/29/99	Paros Pressure Sensor Sontek ADV	Paros Pressure Sensor Sontek ADV
SD	10/02/99 - 11/27/99	11/27/99 - 12/29/99	Paros Pressure Sensor Sontek ADV	Paros Pressure Sensor Sontek ADV
SD	10/02/99 - 11/27/99	11/27/99 - 12/29/99	Paros Pressure Sensor Sontek ADV	Paros Pressure Sensor Sontek ADV

Table 1. Tripod station names, deployment dates, and instruments used to collect wave data.

In an effort to determine quality of the deglitched data a number of statistics were computed and plotted. The absolute and percent change between raw and deglitched burst averaged data were examined. The RMS absolute changes between raw and deglitched burst averaged data were calculated and plotted. Number of flagged points per burst was plotted to determine quality of the low pass filter. Change between raw and deglitched data was plotted against estimated significant wave height to determine relationship between velocity data points that were replaced and wave height.

Pressure spectra were depth corrected using the linear wave theory spectral transfer function described by Guza and Thornton (1980). Significant wave height was calculated for each burst using depth corrected pressure spectrum and integrating across the spectrum as described by Thornton and Guza (1982). Significant wave height from deglitched horizontal velocity was also calculated using the spectral transfer function for horizontal velocity (Guza and Thornton, 1980) and integrating across the horizontal velocity spectrum (Thornton and Guza, 1982). Frequencies of 0.05 Hz to 0.25 Hz were used to estimate significant wave height. These frequencies are also used to compute significant wave height at the Grays Harbor CDIP buoy. The ratio between wave height estimated from pressure and estimated from velocity data was plotted to determine whether estimates were accurate. Estimated wave heights were also compared with wave height data from the CDIP buoy as another check on accuracy. Wave direction was determined at each frequency by calculating inverse tangent of the cross spectra from pressure and U and the cross spectra from pressure and V. Peak direction for each burst was reported at the peak frequency. Wave direction was checked by producing sine and cosine waves and computing direction. Wave direction was

also compared with wave direction collected at the CDIP buoy as another check on method accuracy. Compass heading data were plotted to determine alterations in tripod orientation during the deployment.

Model Calibration and Validation

Currents were neglected in the calibration and validation study. The rationale for this simplification comes from the Froude number.

$$Fr = U/(gh)^{1/2} \tag{35}$$

The assumption is made that when current velocity (U) is small compared with group wave velocity in shallow water, $C_g = (gh)^{1/2}$, or when $Fr << 1$, U can be neglected. Fr was less than 0.1 for time periods used for model calibration and validation.

Plots of wave statistics for each burst at every tripod were used to determine time periods to reproduce with the model. Peak wave period at each tripod must be similar during the modeled time period, so similar wave characteristics are being compared. Wind velocity, peak period, and significant wave height at the offshore NDBC mooring 46005 (46.08 N, 131.00 W, water depth 2,779.8 m) during those time periods will be used to initialize the SWAN model. 46005 is located approximately 532 km from the study area. Using linear wave theory, wave travel times between 46005 and the study area were calculated to be on the order of hours and varying with wave period. Therefore, modeled time periods must be of the same duration as the wave travel time between 46005 and the study area. This eliminates error due to changing conditions. Wave direction for model initialization will come from the Coastal Data Information Program (CDIP) Datawell directional buoy located near the Grays Harbor navigational channel (46 51.47' N, 124 14.64' W, water depth 41.5 m). Direction at 46005 will be calculated from direction at the CDIP buoy using Snell's Law at increments of 10 m water depth.

$$\frac{\sin\theta}{C} = \frac{\sin\theta_o}{C_o} \tag{36}$$

Where θ is wave direction and C is wave celerity. Initially, the model will be run for a test case of medium energy conditions identified in the field data using the default formulations in SWAN. Model output at the tripod locations will be compared with wave statistics as a check on model validity. The statistical comparison of model output and field data is conducted using

four statistical parameters, rms-error, Scatter Index (SI), Model Performance Index (MPI), and Operational Performance Index (OPI), as described by Ris (1997). rms is calculated as

$$rms = \sqrt{\frac{1}{N}\sum_{i=1}^{N}(X_i - Y_i)^2} \tag{37}$$

Where N is the number of observations, X_i is the observed value at location i and Y_i is the computed value at location i. The SI is equal to rms normalized by mean of observed wave parameters.

$$SI = \frac{rms}{\overline{X}} \tag{38}$$

$\overline{X}$ represents mean of the observed wave parameter,

$$\overline{X} = \frac{1}{N}\sum_{i=1}^{N} X_i \tag{39}$$

The MPI is a test of how well the model performs relative to a perfect model run minus the ratio of rms-error of the model to rms-value of the modeled changes in wave parameters from the up-wave boundary. MPI is most useful when wave conditions vary greatly between offshore boundary conditions and nearshore output. MPI differs from SI in that it normalizes RMS by the change over the domain between observed and modeled conditions, while SI compares differences in observed and model conditions.

$$MPI = 1 - \frac{rms}{rms(X_{boundary}; X_i)} \tag{40}$$

OPI is rms-error normalized by the boundary conditions.

$$OPI = \frac{rms}{X_{boundary}} \tag{41}$$

OPI provides insight into the scale of error compared with model input.

Wave height, peak period, and peak direction were statistics used for model/data comparison. The rational for using these statistics for comparison is that it is known that the SWAN model reproduces these features well (Ris, 1997). To provide a robust comparison of a spectral model, some spectral comparisons were also made.

The SWAN model will be calibrated for the southwest Washington coast to produce realistic results. Appropriate coefficient values and formulations within the model will be chosen using the sensitivity study. Only three model formulations significantly alter modeled wave height and direction along the Washington coast. These formulations are form of boundary conditions, bottom friction, and dissipation due to whitecapping. Initially, the model will be

run using the parameterized JONSWAP spectra calculated using wave height and direction at the offshore model boundary. The JONSWAP spectrum was derived empirically from swell spectra in the North Sea (Ris, 1997). Model results using a JONSWAP spectrum and measured spectra with a directional spreading value will be compared.

The other processes affecting wave height and direction in the SWAN model along the southwest Washington coast are dissipation due to bottom friction and whitecapping. Intuitively, bottom friction is the most important dissipation mechanism in shallow water, while whitecapping is more important in deep water. These formulations may be adjusted to better represent wave characteristics in the study area. The method for determining the optimal value for the dissipation source term was to vary the term according to literature until the best comparison between modeled and field wave characteristics was achieved.

Chapter Three

Results

Sensitivity Study

The SWAN model displayed significant variation in model output with changes in several model formulations while many formulations were very insensitive to changes. Wind plays an important role in the wave evolution estimated by the SWAN model. Wind speeds of 0, 5, 7.5, and 10 ms^{-1} were tested for the medium wave case (Figure 11). Significant wave height was roughly 2% lower in coastal areas when a 5 ms^{-1} following wind was blowing than when no wind was present. This reduction in wave energy with increased wind speed is apparently due to increased whitecapping generation. Increasing wind speed above 5 ms^{-1} adds energy to waves in these runs. The 7.5 minus 5 ms^{-1} and 10 minus 7.5 ms^{-1} cases differed from the no wind case in wave height by about +0.5% and +4%, respectively. Both following (260^{o}) and crossing (320^{o}) winds were tested. Generally, the presence of a following wind produces greater changes in wave height than a crossing wind. Relatively small changes in wind speed produce less than significant changes in wave height. Wave direction was rather insensitive to increasing wind speed.

The modeler chooses directional resolution of the SWAN model. Bin sizes of 1^{o} and 2^{o} were not included in this test because the model became too computationally intensive. 3^{o} bin size was taken as the most accurate bin size. Maximum bin size modeled was 40^{o}. The percent difference between the results of the smallest bin size and larger bin sizes was defined as accuracy. Wave height increased with larger bin size (Figure 12). Coastal areas were more sensitive to differences in directional resolution than the large area. Wave refraction increased and waves became more shore-normal as bin size increased (Figure 13). Significant changes in wave direction occurred when bin size was 30^{o} or greater. In cases where bin size was less than 30^{o} wave direction in coastal areas and offshore was nearly equal. When bin size was greater than 30^{o}, wave direction in the large area was greater than wave direction in coastal areas.

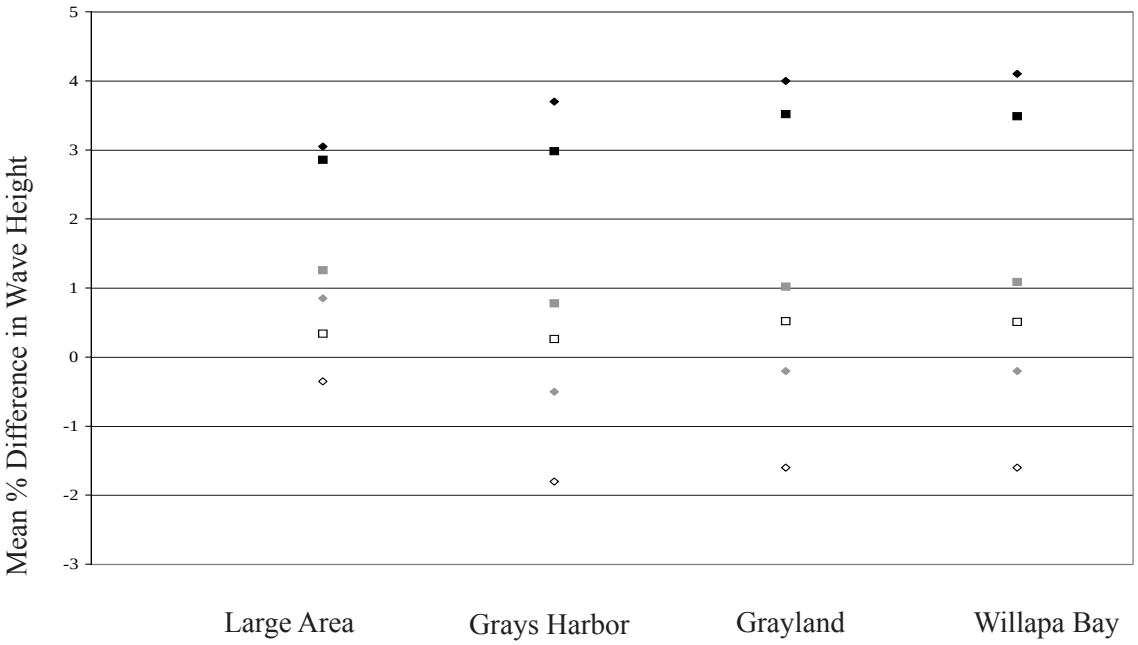

Figure 11. Graph showing wave height sensitivity to wind speed and direction. As expected, an increase in wind speed results in an increase in wave height. A following wind produces greater change in wave height than a crossing wind. Each symbol represents the difference between model results calculated with different wind speeds: 5 ms^{-1} compared to 0 ms^{-1} with a following wind (◇) or crossing wind (□), 7.5 ms^{-1} compared to 5 ms^{-1} with a following wind (◆) or crossing wind (■), 10 ms^{-1} compared to 5 ms^{-1} with a following wind (◆), or crossing wind (■).

Resolved frequency bandwidth was defined by a minimum (0.04 Hz) and a maximum frequency (0.4 Hz) set by the modeler. Frequency resolution is determined by the number of frequencies (default was 15) modeled. Sensitivity to frequency resolution was determined by varying the number of frequencies modeled between 8 and 35 in increments of five or fewer. The SWAN model was unable to compute runs with fewer that 8 frequencies. Runs with more than 35 frequencies were too computationally intensive. The 35 frequency case was taken to be the most accurate, and sensitivity was defined as percent difference in wave height between this and other runs. Model runs with 20 frequencies or more produced results within acceptable accuracy (Figure 14). There was little difference in accuracy due to frequency resolution between coastal areas and the large area. The effect of frequency resolution on wave direction is insignificant.

In the SWAN model, the whitecapping formulation is tied to the choice of the exponential wave growth term. It is one of several physical processes that dissipate waves in the SWAN model (Komen, 1984). We tested these two in tandem, turning whitecapping on and off for both the Janssen and Komen formulae for exponential wave growth. The effect of turning

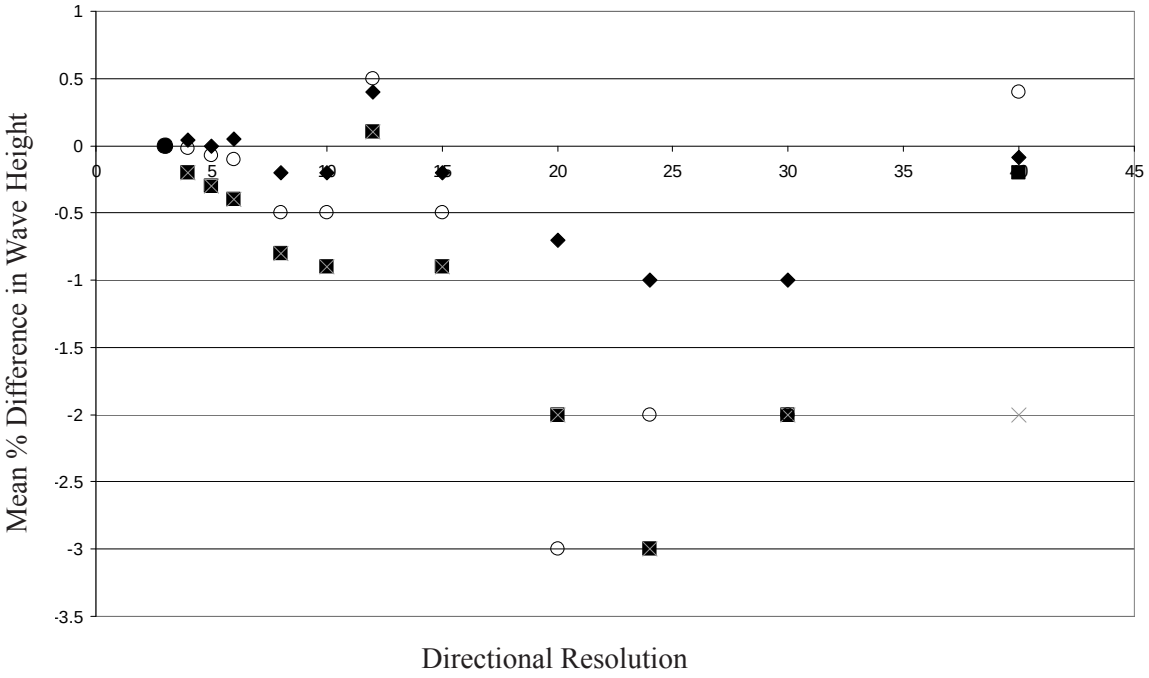

Figure 12. Plot of wave height sensitivity to directional resolution, initalizing the model with the medium wave case and a following wind. Each symbol represents difference between the default and tested directional resolution at an area in the model domain; Large Area (◆), Grays Harbor (■), Grayland (×), Willapa Bay (○). As noted in coastal modeling literature, directional bin sizes of less than 20° produce reliable results.

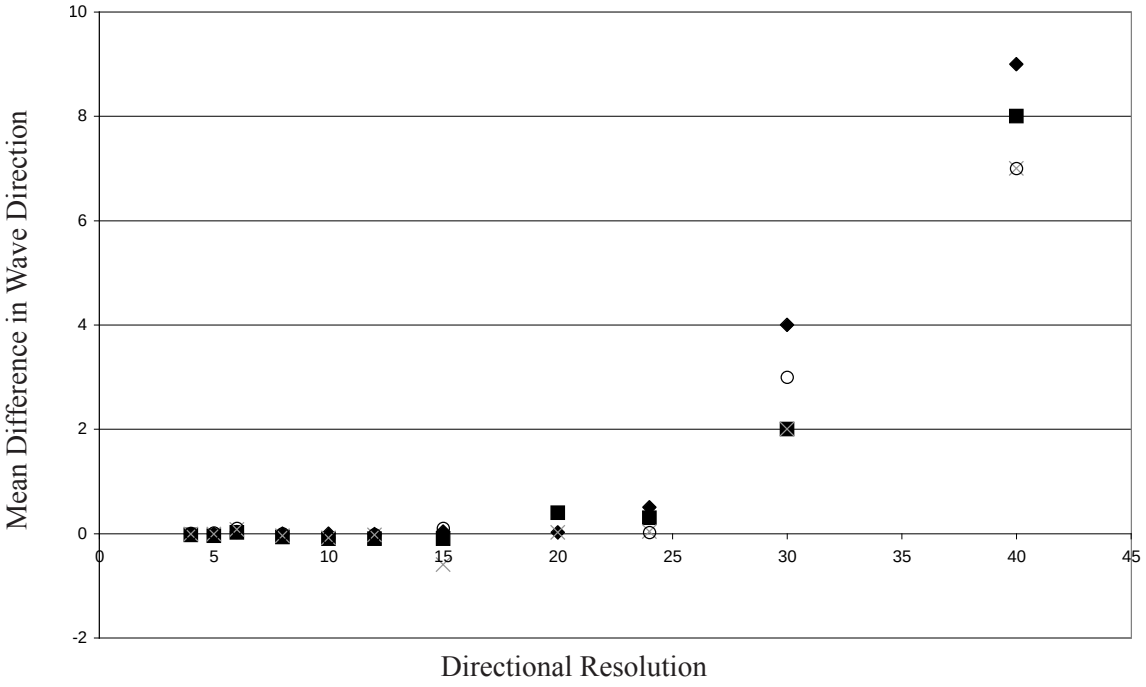

Figure 13. Plot of wave direction sensitivity to directional resolution, initalizing the model with the medium wave case and a following wind. Symbols are as in Figure 12.

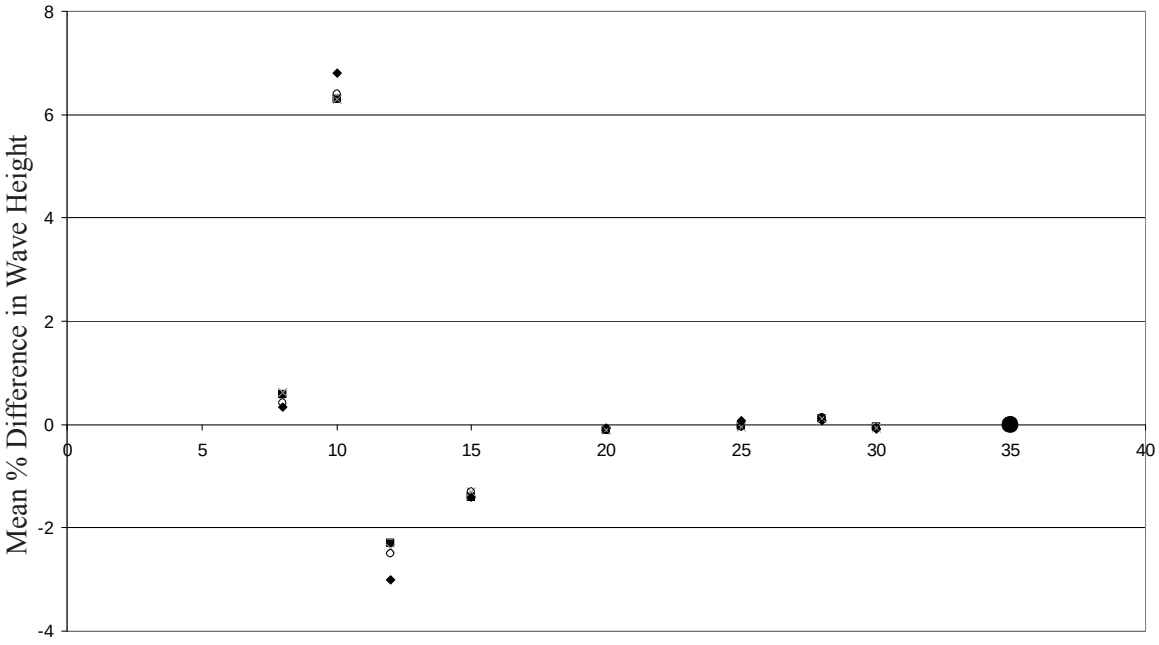

Figure 14. Plot of wave height sensitivity to frequency resolution for the medium wave case using a following wind. Modeling greater than 15 frequencies produces accurate results. Symbols are as in Figure 12.

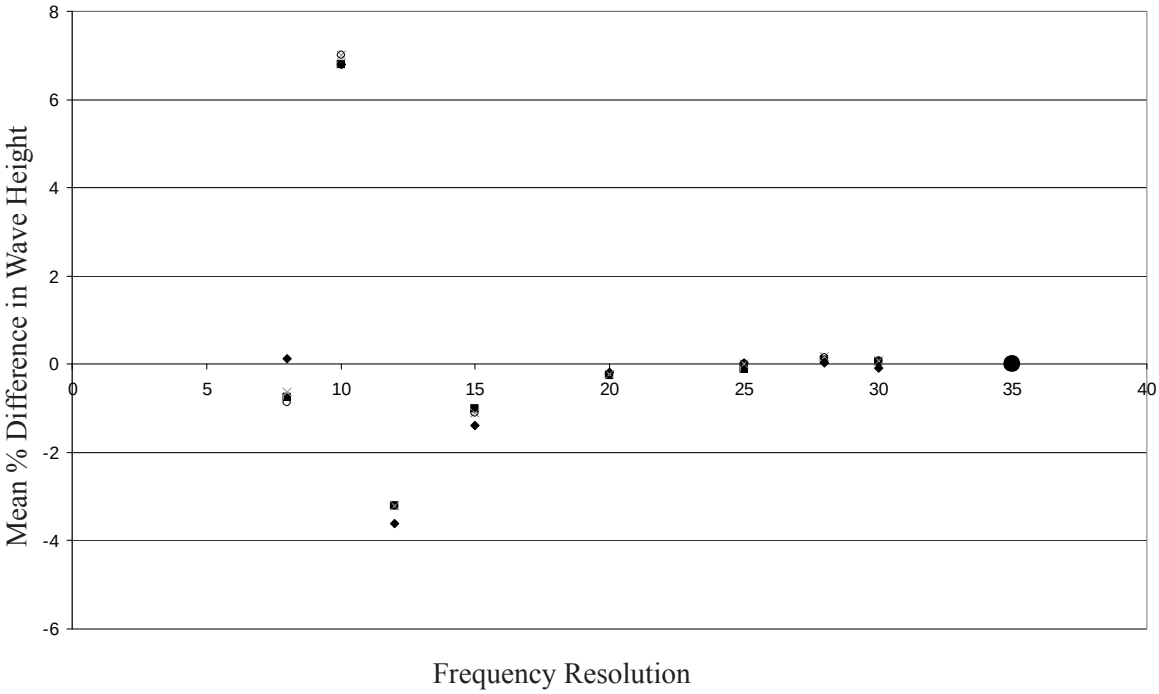

Figure 15. Plot of wave height sensitivity to frequency resolution for the medium wave case using a crossing wind. Modeling greater than 15 frequencies produces accurate results. Symbols are as in Figure 12.

whitecapping on and off is substantial irrespective of the choice of wave growth (Figure 16). In the large area, significant wave height was 2-4% larger when whitecapping was off, whereas in coastal areas, it was up to 7% greater. Greater whitecapping was the result of steeper waves due to bottom friction in coastal areas. Wave height differences were insignificant when varying the growth term with whitecapping turned off. However, with whitecapping on, wave height was 2% to 4% greater in the Komen case than in the Janssen case. Wave direction was insensitive both to the presence/absence of whitecapping and to the choice of growth term. The difference criteria were insensitive to whether winds were crossing or following.

The Janssen formulation for wave growth had two coefficients: the coefficient for determining rate of dissipation (C_{ds1}) and the coefficient for determining the dependency of whitecapping on wave number (δ). The default values for coefficients in this formulation were chosen to match observational data describing fetch-limited growth and dependence of surface stress on wave age (Komen et al, 1994). These coefficients should be tuned for each case that the formulation is used (Komen et al., 1994). A significant difference in SWAN wave height output occurred when C_{ds1} (default = 4.5) was adjusted to roughly one fourth or twice the default value in the small wave case or one half or twice the default value in the medium wave case. As expected from examination of the formula, C_{ds1} was positively correlated to dissipation and negatively correlated to wave height (Figure 17)

Doubling δ from the default value of 0.5 increased wave height 3%. Reducing δ produced varying differences in wave height. In the small wave case, reducing δ by six orders of magnitude did not produce significant changes in wave height. Reducing δ by one half produced significant changes in wave height in the medium wave case. Consistent with the formula, the relationship between δ and dissipation depends on the value of $k/\langle k \rangle$, where k is wave number and $\langle k \rangle$ is mean wave number. When $k/\langle k \rangle$ is greater than one, values of δ greater than one are negatively correlated to dissipation and positively correlated to wave height. The inverse is true of δ values smaller than one. There is no relationship between wave height at the boundary condition and sensitivity of the SWAN model to changes in δ. The large area is less sensitive to changes in δ than coastal areas.

The Komen formulation for wave growth contains a coefficient to determine rate of dissipation (C_{ds2}, default = 2.36×10^{-5}) and a coefficient to determine the value of wave steepness

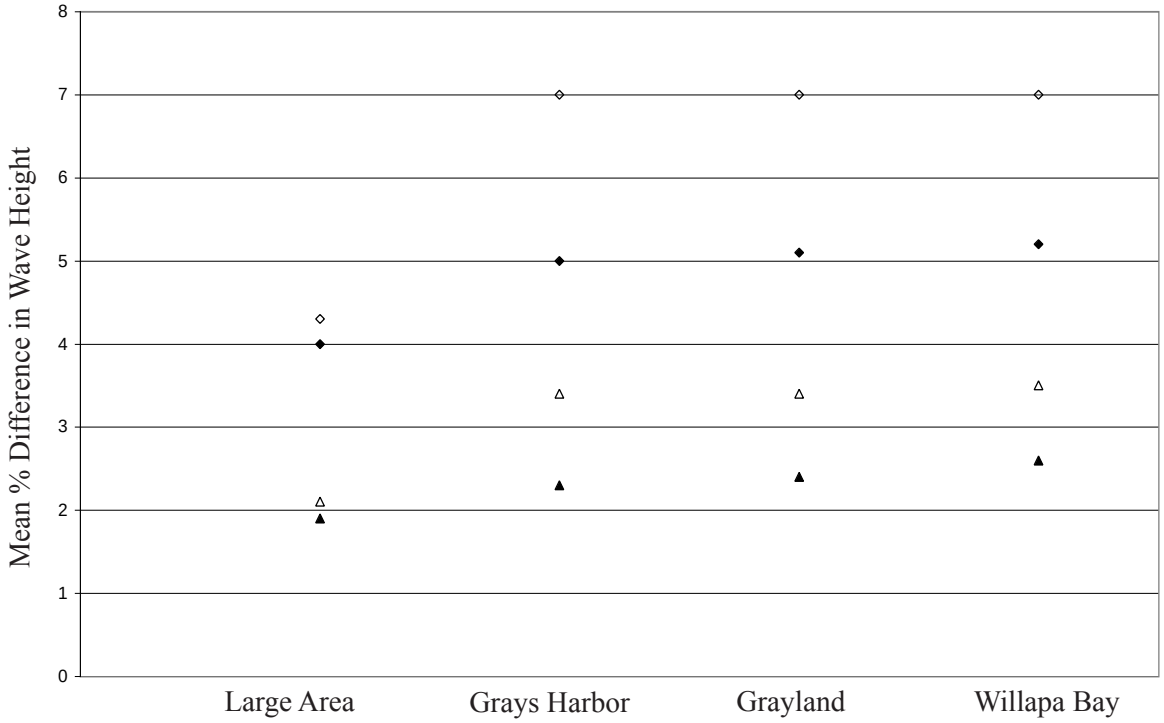

Figure 16. Plot showing wave height sensitivity to use of the whitecapping term for dissipation of wave energy in the SWAN model for several model formulations and boundary conditions including: the Janssen formulation for whitecapping with medium (◇) or small wave conditions (◆) and a following wind, or the Komen formulation for whitecapping with medium (△) or small wave conditions (▲) and a crossing wind. Use of the whitecapping term significantly reduces wave height.

for a Pierson-Moskowitz spectrum ($\tilde{s}_{pm}$, default = 3.02×10^{-3}). Wave height computed by SWAN was significantly different when the default value of C_{ds2} was reduced two orders of magnitude or quadrupled in the small wave case and reduced by one fourth or doubled in the large wave case. Like C_{ds1} in the Janssen formulation, C_{ds2} was directly correlated to dissipation and inversely correlated to wave height. Decreasing the default value of $\tilde{s}_{pm}$ by half resulted in a significant difference in wave height for both small and medium wave heights at the boundary. Increasing $\tilde{s}_{pm}$ by a factor of two in the medium wave case or by a factor of eight in the small wave case produced significant changes in wave height. As inferred from the formula, $\tilde{s}_{pm}$ was inversely correlated to dissipation and directly correlated to wave height. Wave height output from the medium wave state with following wind was 1% to 2% more sensitive to changes in the C_{ds2} and $\tilde{s}_{pm}$ than the small wave state.

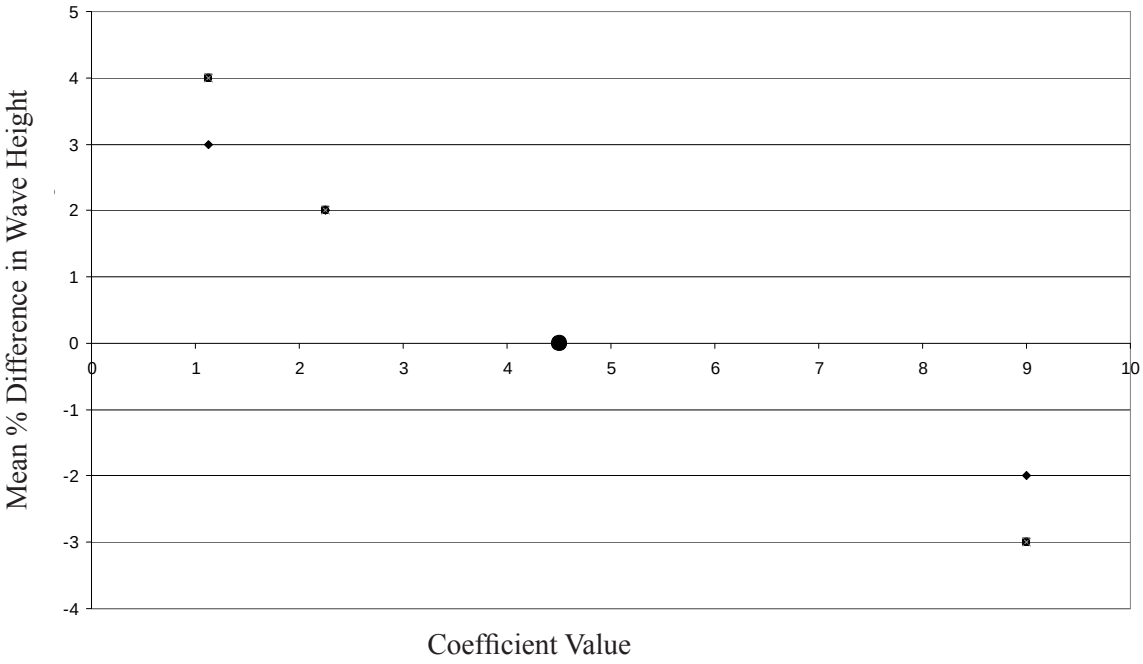

Figure 17. Using the small wave case with a following wind, the value of the coefficient for determining rate of dissipation within the Janssen formulation for exponential wave growth produced significant change in wave height. The black circle represents the default value of the coefficient. Other symbols are as in Figure 12.

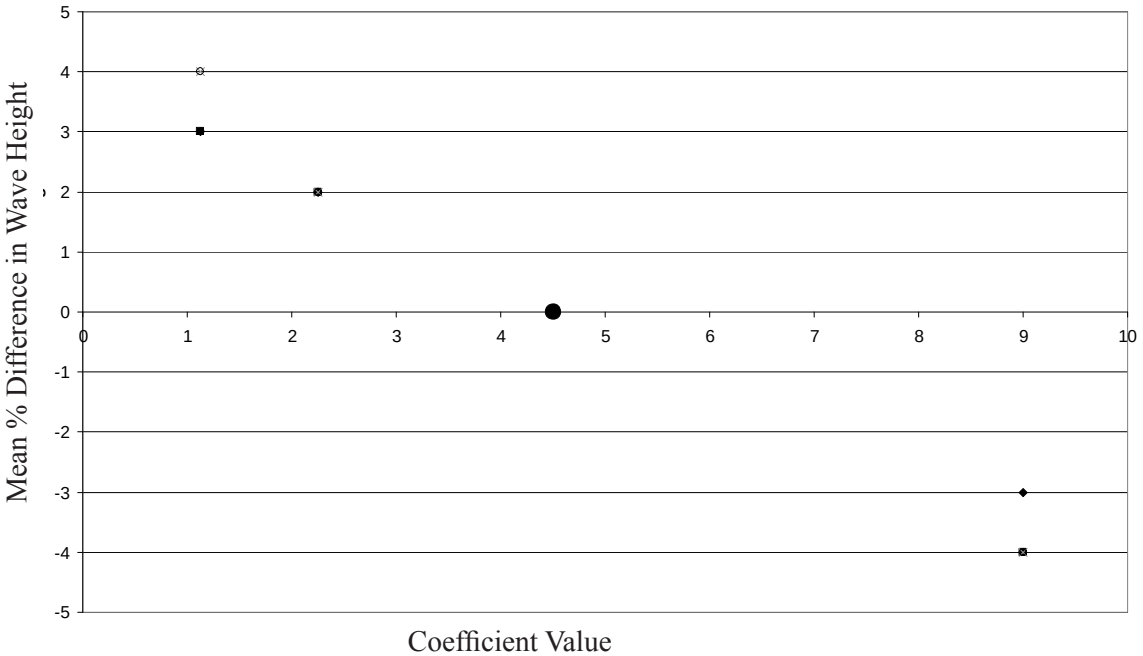

Figure 18. Using the small wave case with a crossing wind, the value of the coefficient for determining rate of dissipation within the Janssen formulation for exponential wave growth produced significant change in wave height. Symbols are as in Figure 12.

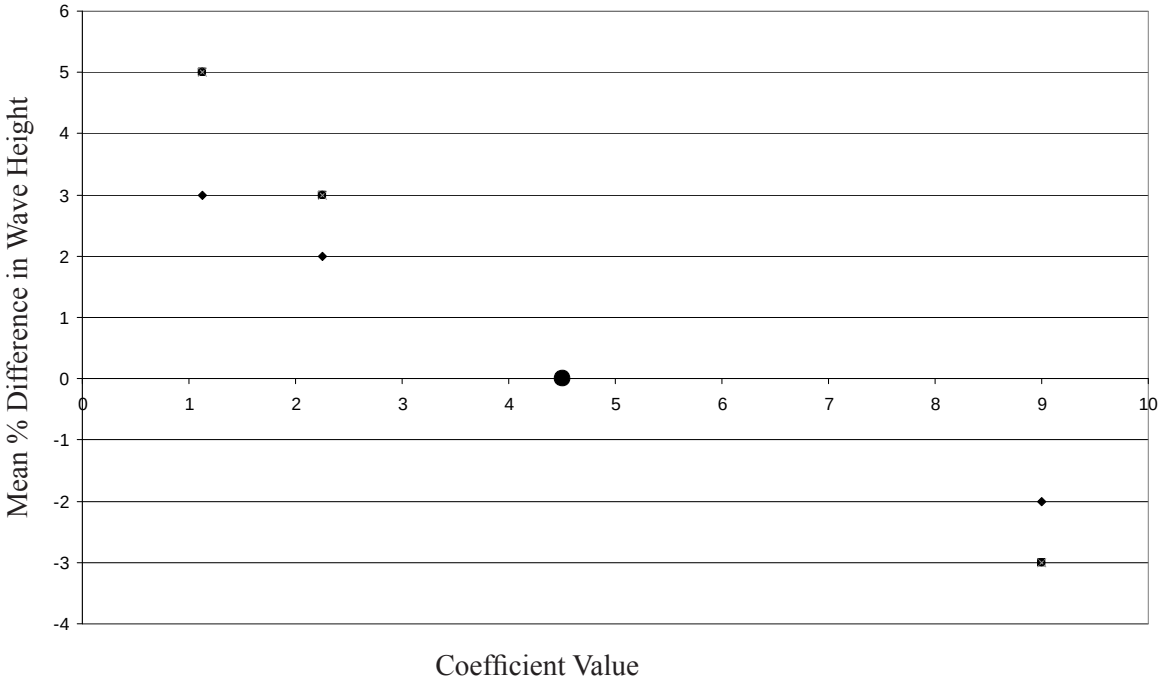

Figure 19. Using the medium wave case with a following wind, the value of the coefficient for determining rate of dissipation within the Janssen formulation for exponential wave growth produced significant change in wave height. Symbols are as in Figure 12.

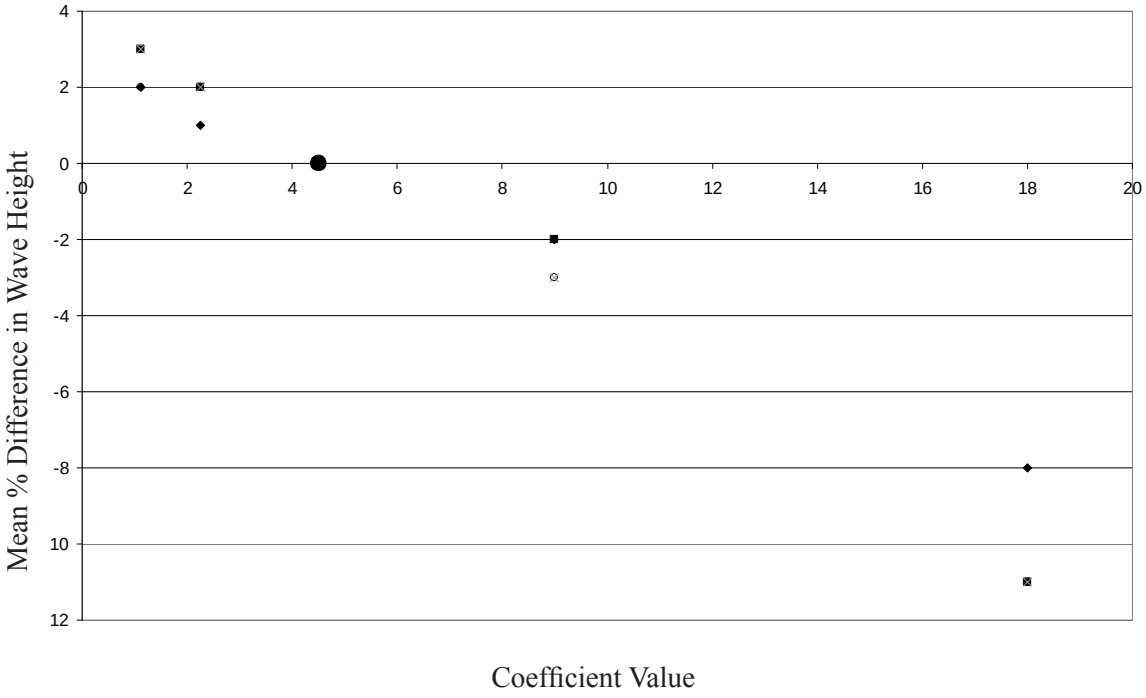

Figure 20. Using the medium wave case with a following wind, the value of the coefficient for determining rate of dissipation within the Janssen formulation for exponential wave growth produced significant change in wave height. Symbols are described in Figure 12.

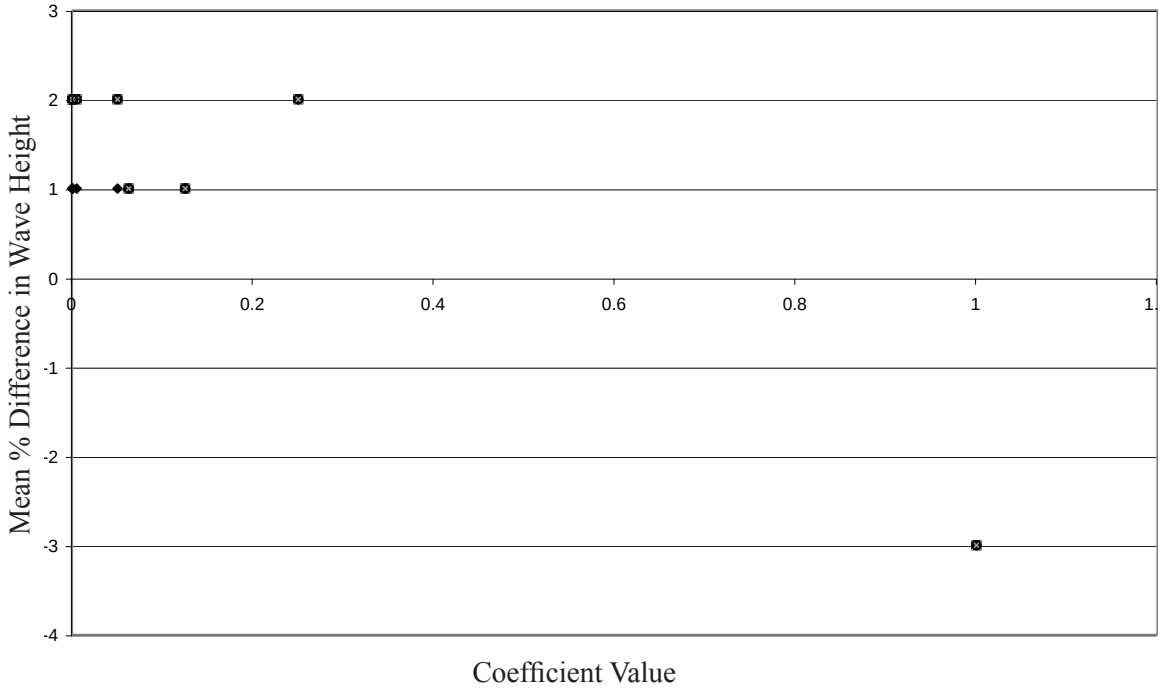

Figure 21. Varying the value of the delta within the Janssen formulation produced significant change in wave height. The small wave case and following wind were used in this model run. Wave height is inversely proportional to coefficient value. Symbols are described in Figure 12.

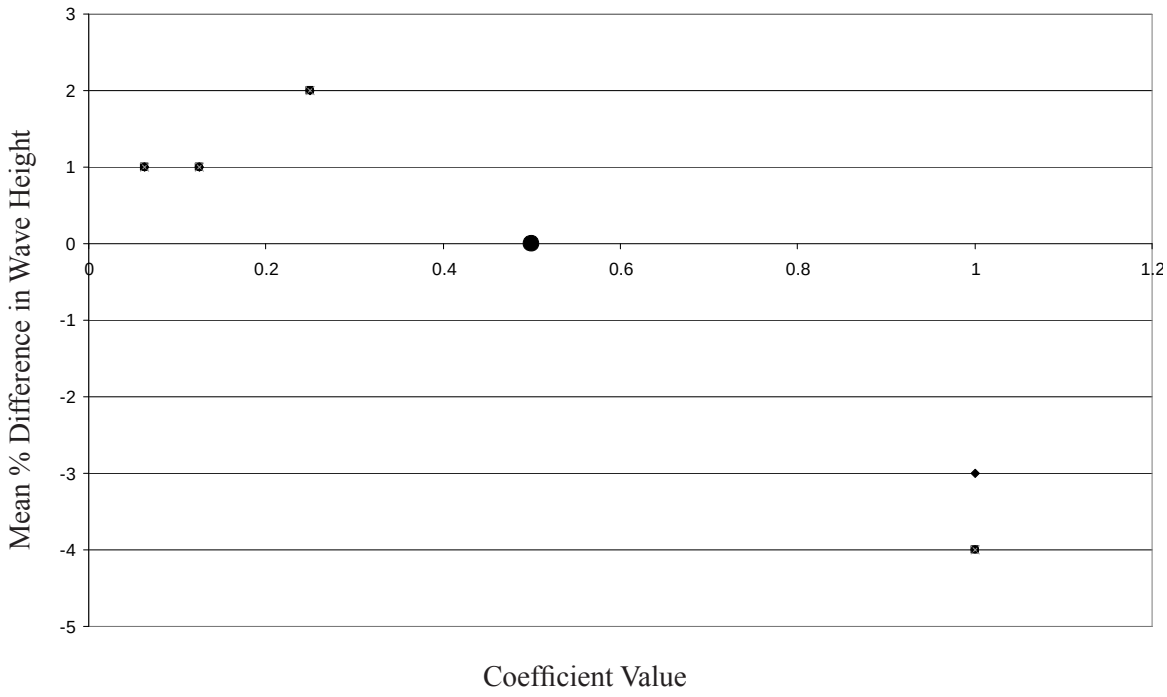

Figure 22. For the small wave case with a crossing wind, the value of delta within the Janssen formulation produced significant change in wave height. Symbols are described in Figure 12.

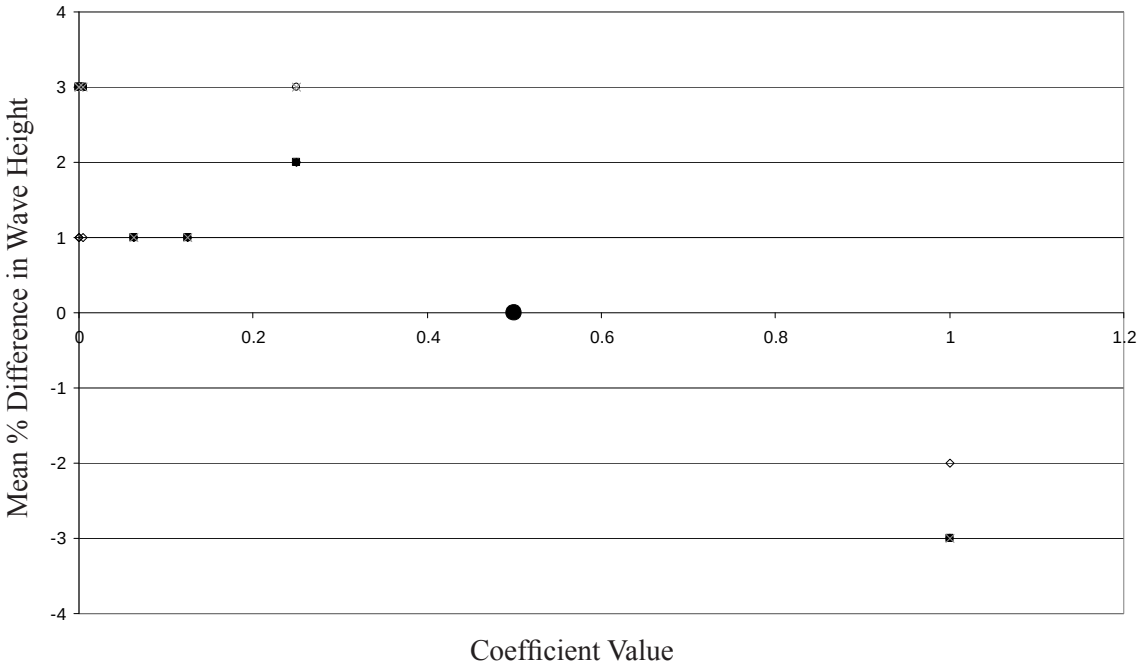

Figure 23. For the medium wave case with a following wind, using the Janssen formulation for wind input and whitecapping, wave height is inversely proportional to coefficient value. Symbols are described in Figure 12.

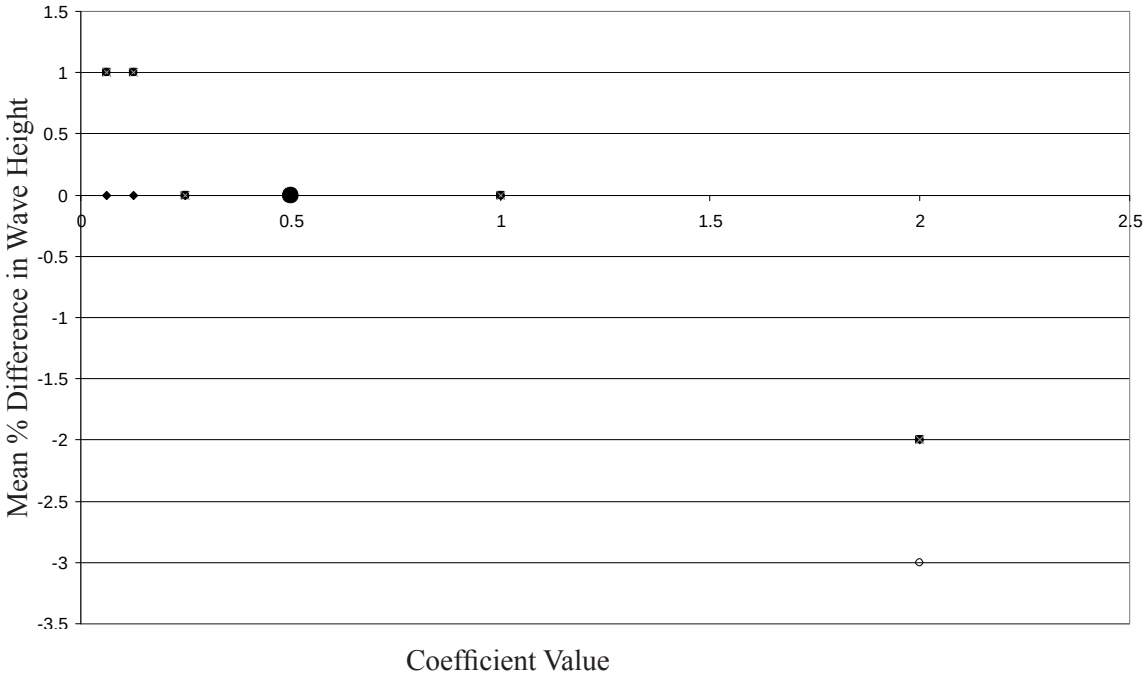

Figure 24. Using the Janssen formulation for wind input/whitecapping with the medium wave case with a crossing wind, wave height is inversely proportional to coefficient value. Symbols are described in Figure 12.

The model showed some sensitivity in the coastal areas to bottom friction formulation. The JONSWAP formulation for bottom friction was tested with two values of the coefficient c_f (0.038 and 0.067 m^2s^{-3}), Madsen bottom friction with two values of the coefficient K_N (0.02 and 0.05 m), and Collins bottom friction with one value of the coefficient c_w (0.015). The largest differences in wave height, roughly 5%, corresponded to larger waves in the Madsen (K_N = 0.05 m) case . Differences in modeled wave height become more pronounced with increasing wave height at the model boundary. Collins bottom friction produced very similar results to the JONSWAP formulation for bottom friction in all cases. Generally, the SWAN model is slightly more sensitive to the Madsen formulation for bottom friction than the JONSWAP or Collins formulations. There was negligible change in wave direction with changing bottom friction.

Madsen bottom friction is determined with the drag friction law. In this model, dissipation depends on the bottom roughness length (K_N) (Weber, 1991). Significant changes in wave height were produced when K_N was an order of magnitude larger than the default. Smaller changes in wave height occurred as K_N decreased.

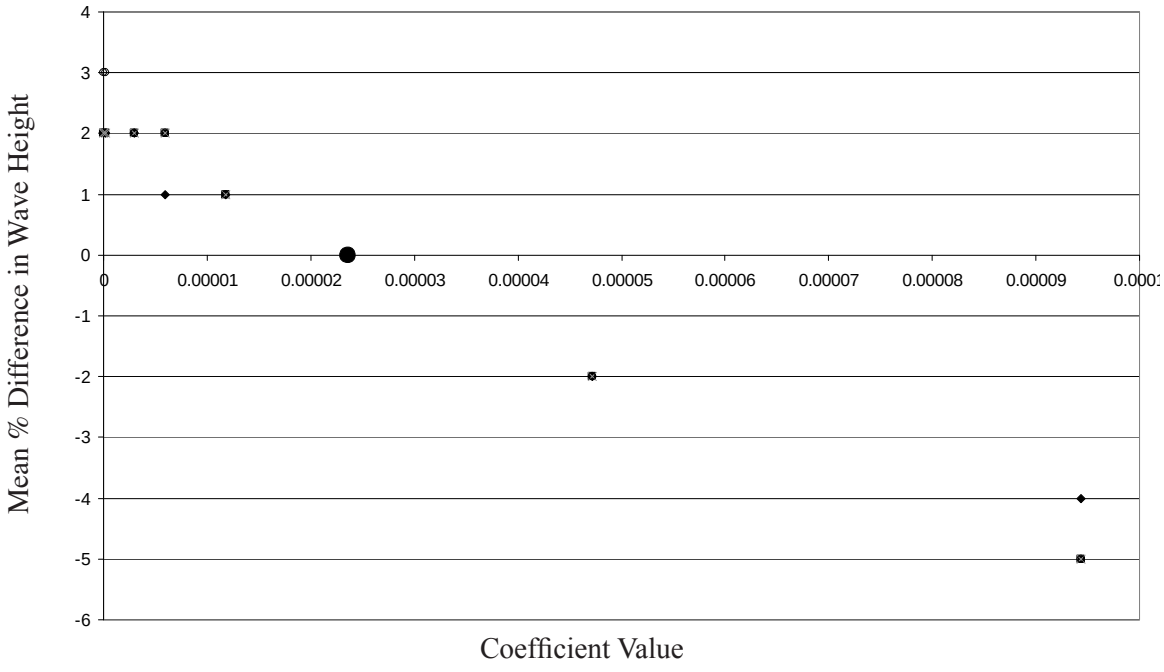

Figure 25. Using the small wave case with a following wind, wave height was significantly changed as the coefficient for determining rate of dissipation within the Komen formulation for exponential wave growth was varied. Wave height was inversely proportional to the value of the coefficient. Symbols are as in Figure 12.

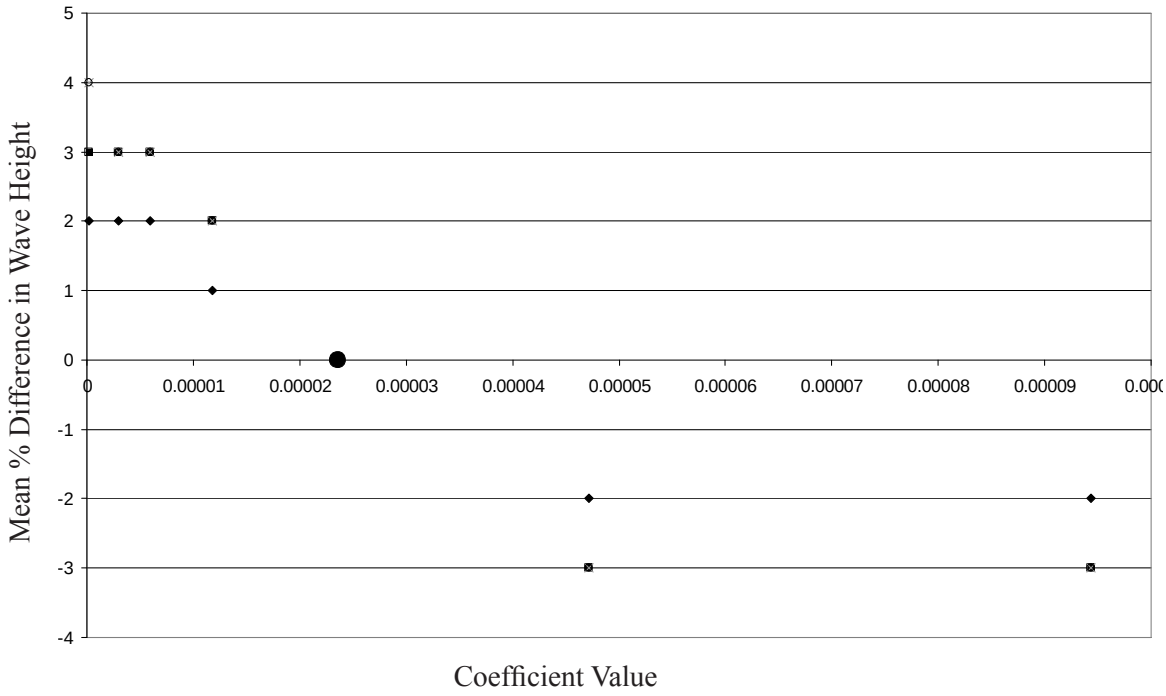

Figure 26. Using the medium wave case with a following wind, wave height was significantly changed as the coefficient for determining rate of dissipation within the Komen formulation for exponential wave growth was varied. Wave was proportional to the value of the coefficient. Symbols are as in Figure 12.

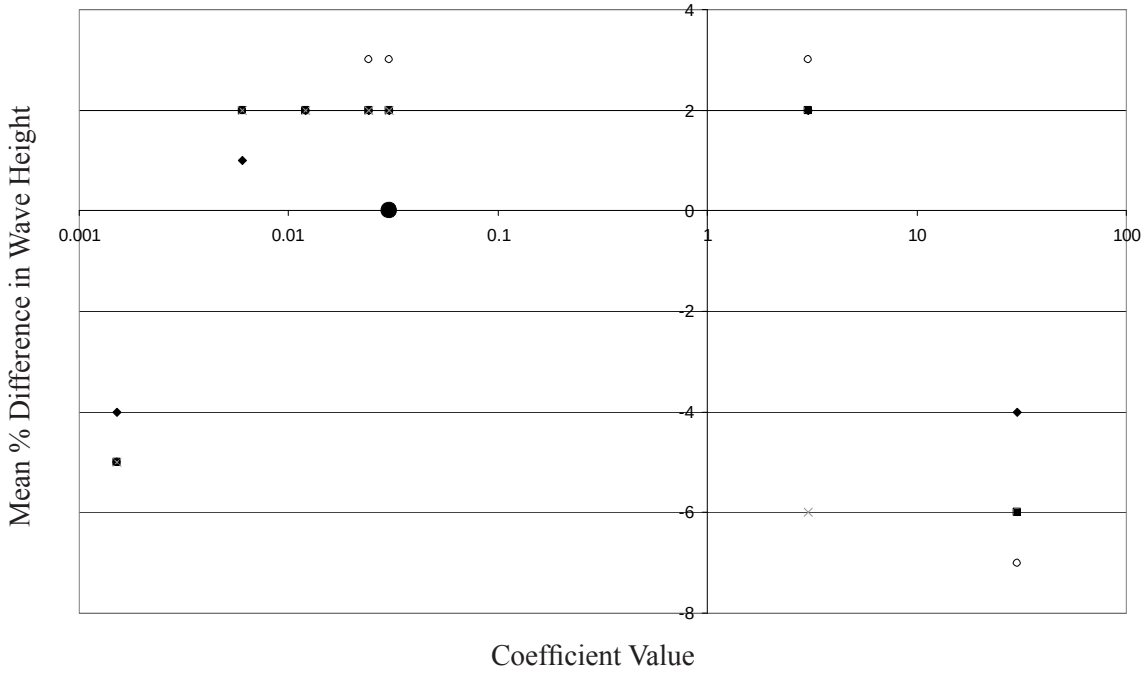

Figure 27. Using the small wave case with a following wind, wave height was significantly changed as the coefficient for $\tilde{s}_{pm}$ was increased or decreased. Symbols are as in Figure 12.

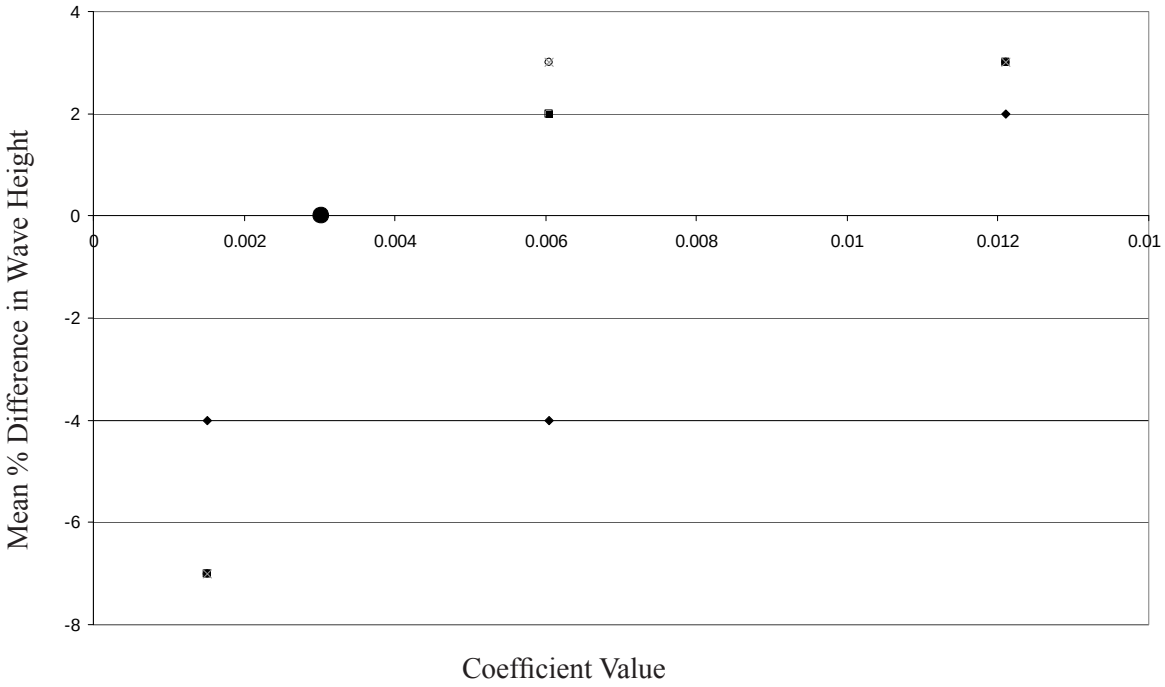

Figure 28. Using the medium wave case with a following wind, wave height varied with the coefficient for $\tilde{s}_{pm}$. Symbols are as in Figure 12.

Figures 31 and 32 show observed wave spectra used to initialize two model runs, rather than the parameterized spectra used in all other runs. Note the similarity of these spectra to the parameterized JONSWAP spectra. Little difference was noted between runs using a spectrum observed near the southwest Washington coast and a parameterized spectrum developed for waves in the North Sea . Wave direction changed little with variation in form of spectral input at the model boundary.

The SWAN model was very insensitive to the two coefficients associated with triads. The value proportionality coefficient (α_{EB}), which controls the magnitude of the triad interactions, has a default value of 0.25 (Ris, 1997). Modeled wave heights differed up to 1.3% when α_{EB} was increased by and order of magnitude and up to 0.3% when decreased by an order of magnitude. The variable controlling maximum frequency considered in the triad computations (cutfr). The value of cutfr is the ratio of maximum frequency over mean frequency. The default value is 2.5. The modeled wave height decreased 0.3% when cutfr was increased an order of magnitude and increased 0.7% when cutfr was decreased an order of magnitude. This frequency may be outside the range of frequencies considered in the body of the model (0.04 to 0.4 in the sensitivity study).

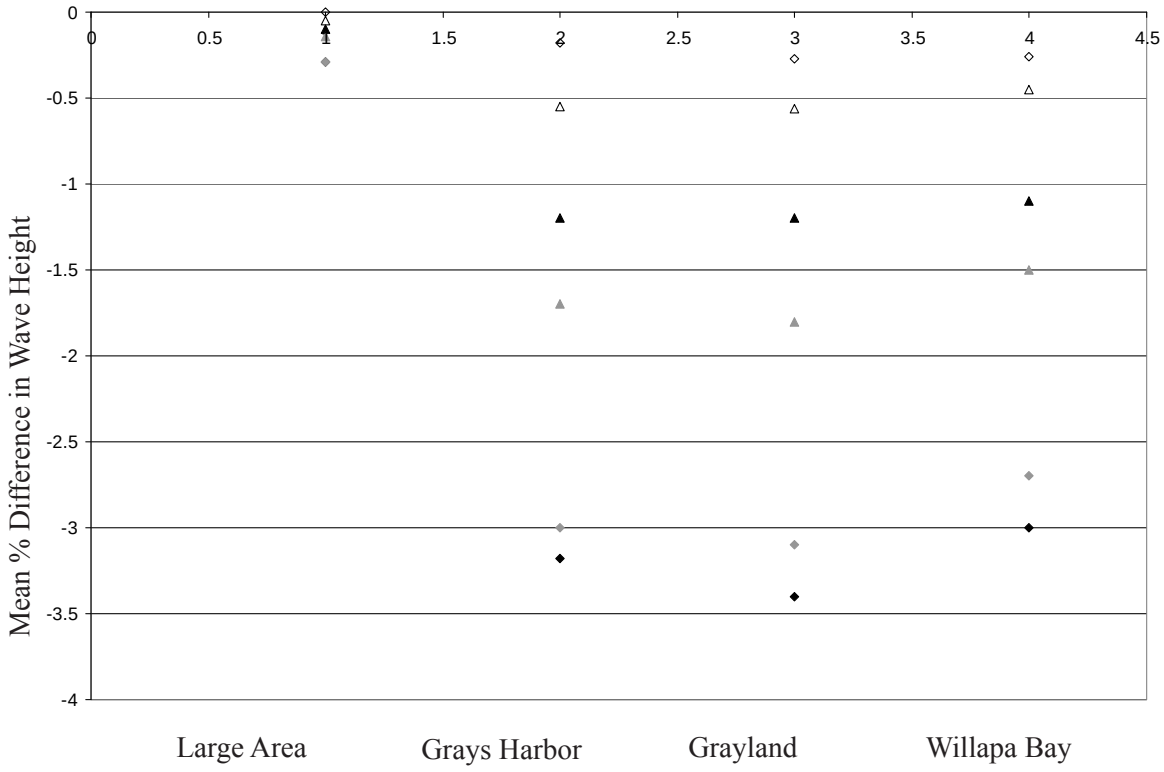

Figure 29. Graph showing wave height sensitivity to different formulations for bottom friction in the SWAN model. Each symbol represents the difference between model results using different formulations for bottom friction: JONSWAP formulation - Collins formulation, medium wave condition (◇), small wave condition (△); Madsen formulation - JONSWAP formulation, medium wave condition (◆), small wave condition (▲); Madsen formulation - Collins formulation, medium wave condition (◆), small wave condition (▲). Use of the JONSWAP or Collins formulation for bottom friction produces similar wave height results. The Madsen formulation for bottom friction produces lower wave heights than JONSWAP or Collins formulations.

The SWAN model was insensitive to two parameters. The modeler may choose to start computations with a flat ocean, allowing the linear wave growth term of Cavaleri and Malanotte to energize waves, or the wave state may be initialized with a JONSWAP spectrum at the model boundary. Wave height and direction were completely insensitive to the use of the linear wave growth term. Also, quadruplet wave-wave interactions may be computed in any of three ways. This choice did not influence the results. Therefore, one may choose the fastest method (iquad = 3) with impunity.

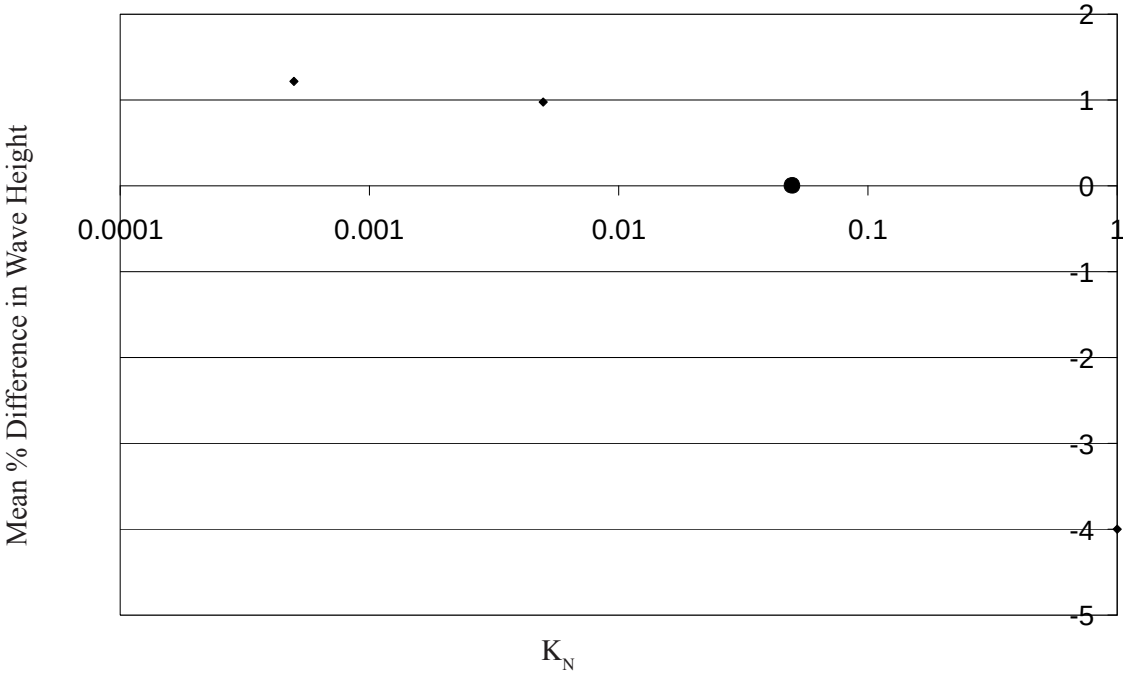

Figure 30. Graph showing wave height sensitivity to varying value of K_N in the Madsen formulation for bottom friction.

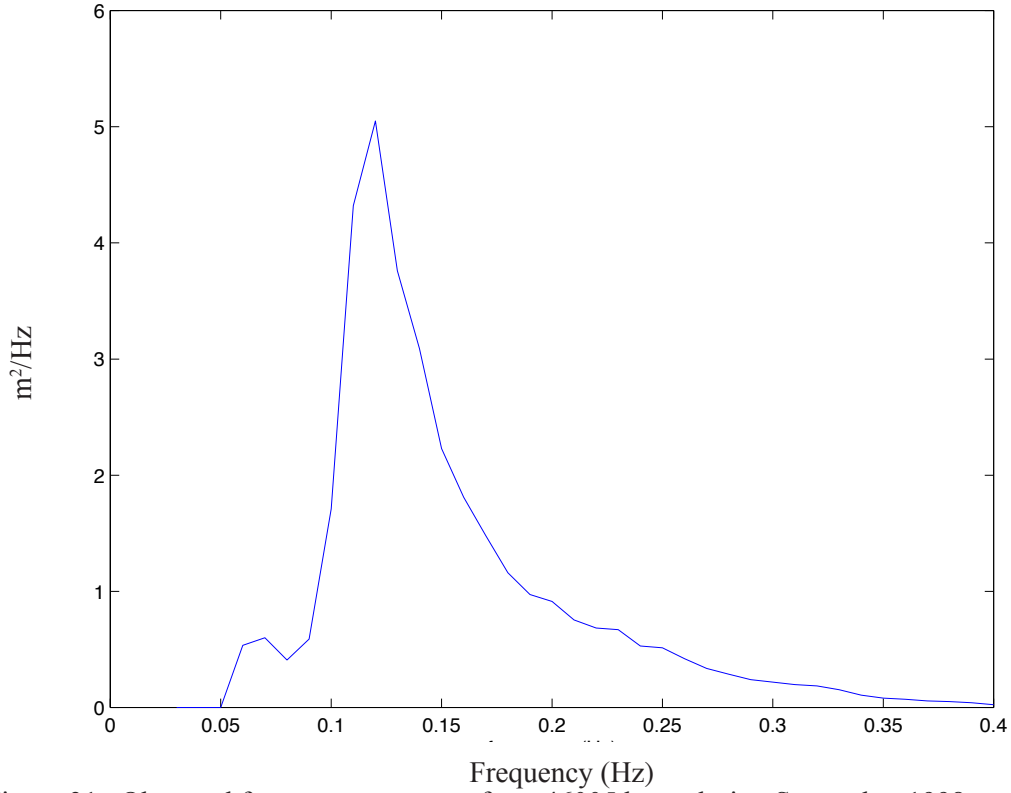

Figure 31. Observed frequency spectrum from 46005 buoy during September 1998 used to initialize the SWAN model for comparison with model results using the JONSWAP parameterized spectrum.

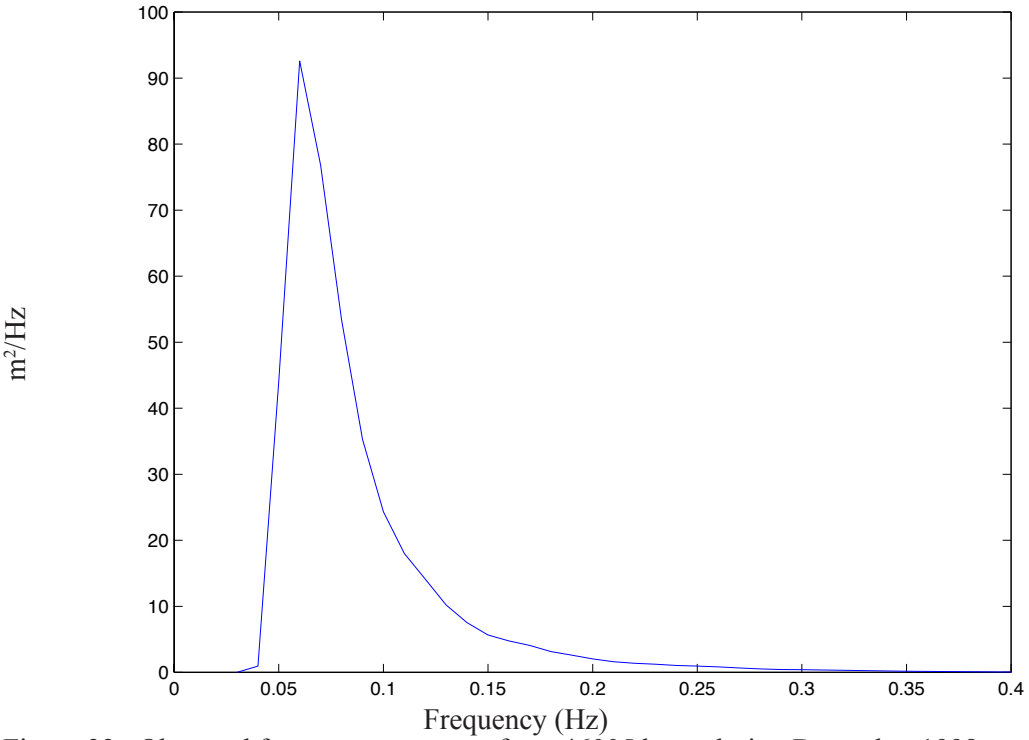

Figure 32. Observed frequency spectrum from 46005 buoy during December 1998 used to initialize the SWAN model for comparison with model results using the JONSWAP parameterized spectrum.

Pre-experiment

Prior to deploying instruments during the field experiment, a number of SWAN model runs were completed to investigate instrument location options. The object of the runs was to find locations on the north and south sides of the Grays Harbor ETD that showed the maximum influence of the delta. "Influence" was characterized by examining wave direction on an isobath and comparing the values on the delta with those on "straight" coast sections to the north and south of the ETD. We found that wave direction was much more dramatically impacted by the delta than was wave height. In some cases, a particular side of the delta may have had little influence. The cases where influence was significant are shown in Table 2. Significant wave heights and directions predicted over the model domain are shown in Figures 33-37. Isobaths are shown in white. To best identify changes over the ETD, scale bars on the figures are unique to each plot. This plan view resolves the overall influence of wave climate. In Run 1, offshore wave direction is from due west. Note the larger wave heights in shallower water on the south side of the delta. Wave direction appears to focus wave energy on the ETD. Wave height at the model boundary was 5 m for Run 2 and Run 3. Offshore wave direction in Run 2 is 20° south of west.

Significant shoaling on the south side of the ETD is evident in this run. Wave direction differs by 40^{o} between the north and south sides of the ETD. Offshore wave direction in Run 3 is 20^{o} north of west. Again the difference between wave direction is 40^{o} between north and south sides of the ETD. Offshore wave height in Run 4 is 7 m and direction is 35^{o} south of west. Note differences in wave height around the ETD. Wave direction is more strongly influenced north of the ETD than south of the ETD. Offshore wave direction in Run 6 is 20^{o} north of west as in Run 3, however wave height is 2 m higher and period is 14 s. This results in a different distribution of wave heights around the ETD. Also the difference between wave direction north and south of the ETD is less than Run 3.

Figures 38-42 show the same results along the 40 m, 35 m, 30 m, 25 m, 20 m, and 15 m isobaths. These results clearly show the decrease in wave height and wave refraction as the water shallows. When waves originate from due west or north of west, the south side of the ETD shows more influence on wave direction. Bathymetric contours on the ETD in the south deviate more from a N-S line than do those on the north side. Therefore, an instrument was located on the south side of the ETD.

Figures 43-52 display the model results as east-west profiles located north and south of the ETD. In these figures, the profiles are spaced at 2 km intervals north and south of the ETD. A profile is also included in the far north (5210 km) and in the far south (5183 km). From these figures, a difference between the ETD influence on the north and south sides is less apparent in wave height than in direction.

Figure 53 is a plot of locations of maximum influence listed in Table 2. Note in the table, the same line was derived from two different runs. Furthermore, the lines on the south side extend to deeper water. From Figure 53, tripod locations in Figure 9 were chosen.

Run Number	Hsig (m)	Peak Period (s)	Wave Direction	Wind Speed (m/s)	Wind Direction	Directional Spreading (ms)	Isobath (m)	Max change south side	Δ Degrees coast - ETD	Max change north side	Δ Degrees coast - ETD
1	3.5	12	270	13.5	285	30	15	5194000	10.2	5201000	6.5
							20	5193000	7	5200000	3.9
							25	5193000	4.2		
2	5.1	13	250	13.5	285	30	15	5194500	11.9	5201000	7.7
							20	5193500	7.9	5200000	4.6
							25	5193000	5.1		
3	5.1	13	290	13.5	255	30	15	5194000	15.1	5201000	9.6
							20	5193000	11.5	5200000	5.9
							25	5192500	7.6	5203500	4.2
							30	5193000	5.6		
							35	5193000	4.1		
4	7.1	14	235	13	290	30	15	5194000	13.2	5202000	7.8
							20	5193500	8.6	5200000	5.5
							25	5193500	6.1		
6	7.1	14	290	13	290	30	15	5194000	12.4	5200000	8.1
							20	5193000	9.3	5200000	5.1
							25	5192500	6.5		
							30	5193000	5.3		
							35	5193000	4.2		

Table 2 . Significant pre-experiment runs are described. Boundary conditions for each run is given in columns 2 - 6. Locations of maximum change are specified in columns 9 and ll. The amount of change is given in degrees in columns 10 and 12.

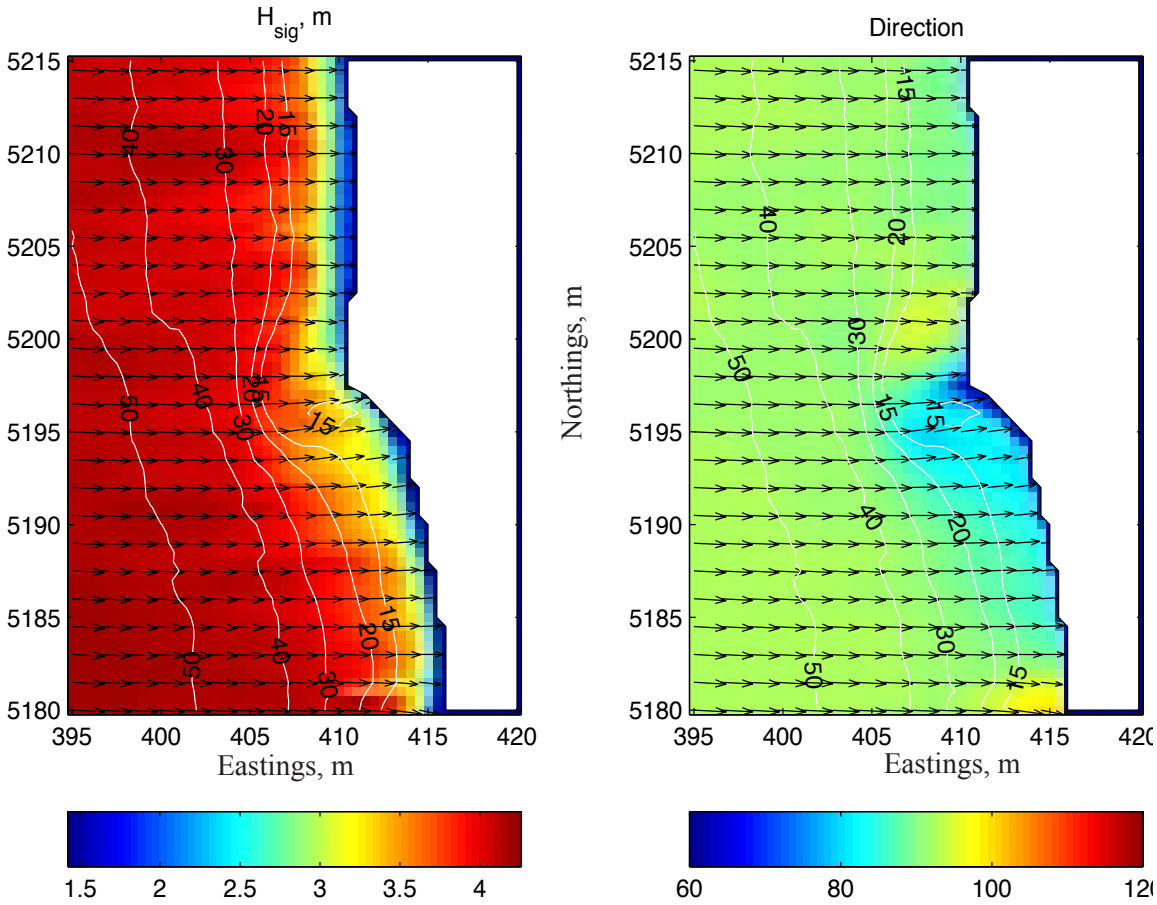

Figure 33. Wave height and direction with wave direction for Run 1 plotted as vectors and bathymetry contours shown. Offshore wave height was 3.5 m, peak period was 12 s, wave direction was 270°.

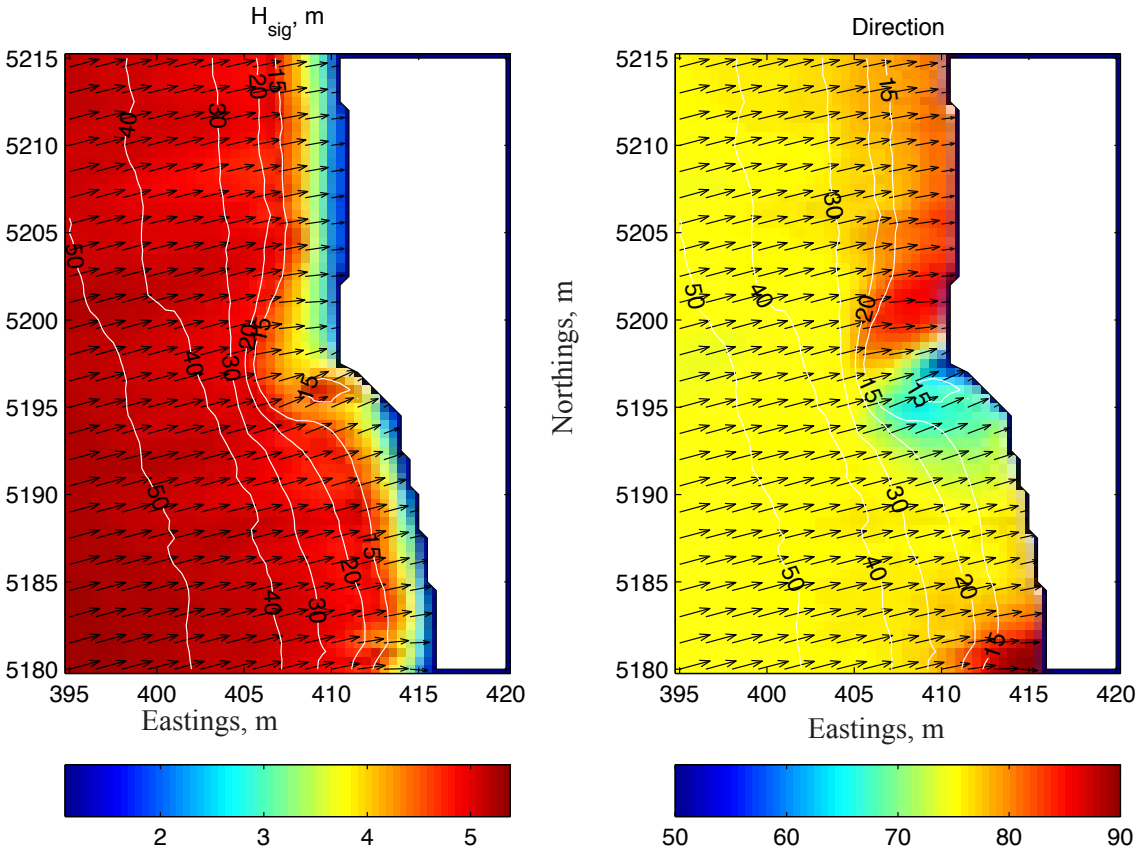

Figure 34. Wave height and direction with wave direction for Run 2 plotted as vectors and bathymetry contours shown. Offshore wave height was 5.1 m, peak period was 13 s, peak wave direction was 250°.

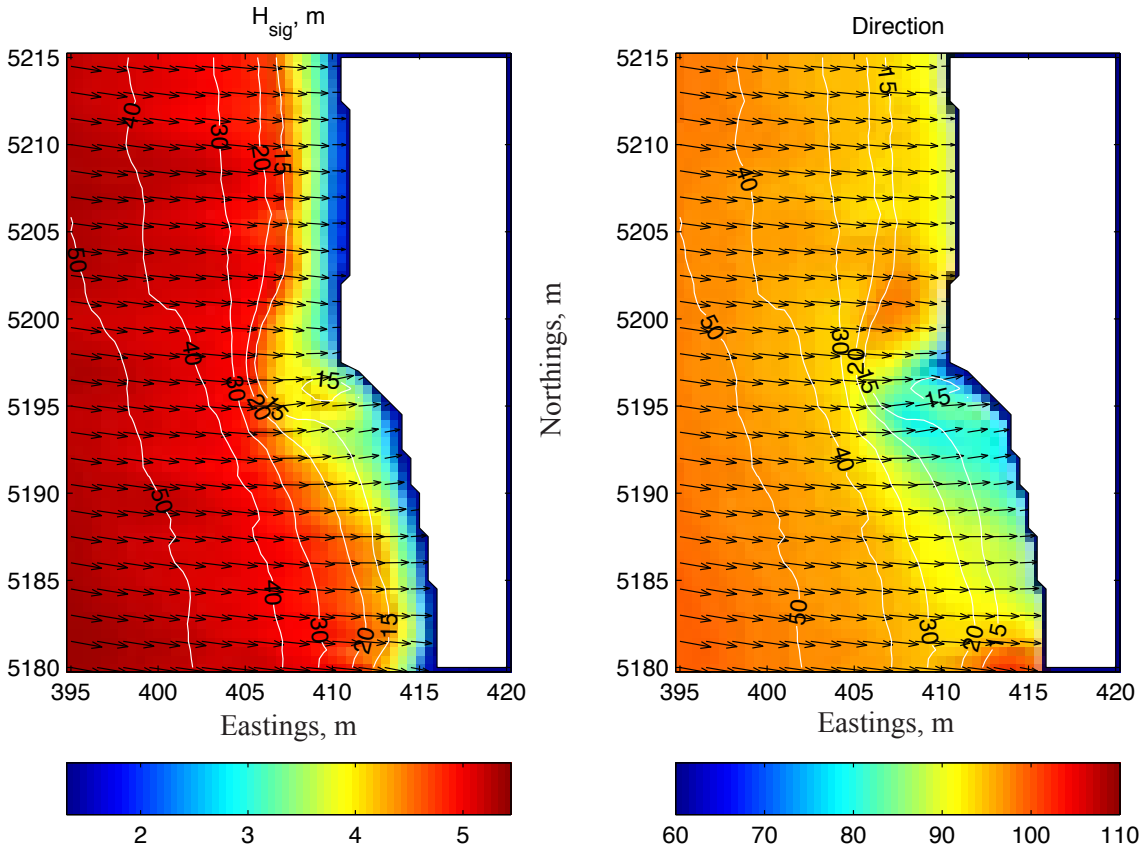

Figure 35. Wave height and direction with wave direction for Run 3 plotted as vectors and bathymetry contours shown. Wave height at the boundary was 5.1 m, and peak period was 13°, as in Run 2. Peak wave direction was from 290°.

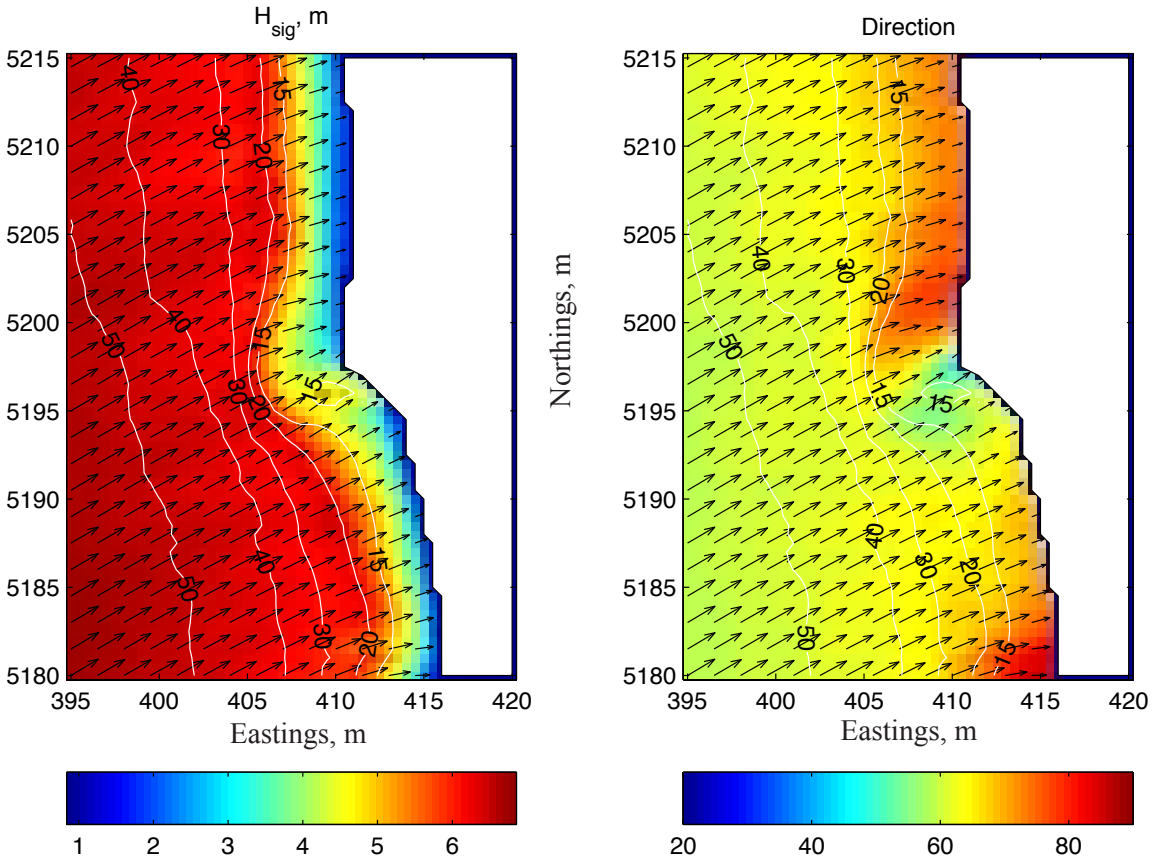

Figure 36. Wave height and direction with wave direction for Run 4 plotted as vectors and bathymetry contours shown. Wave height at the model boundary was 7.1 m, peak wave period was 14 s, and peak wave direction was 235°.

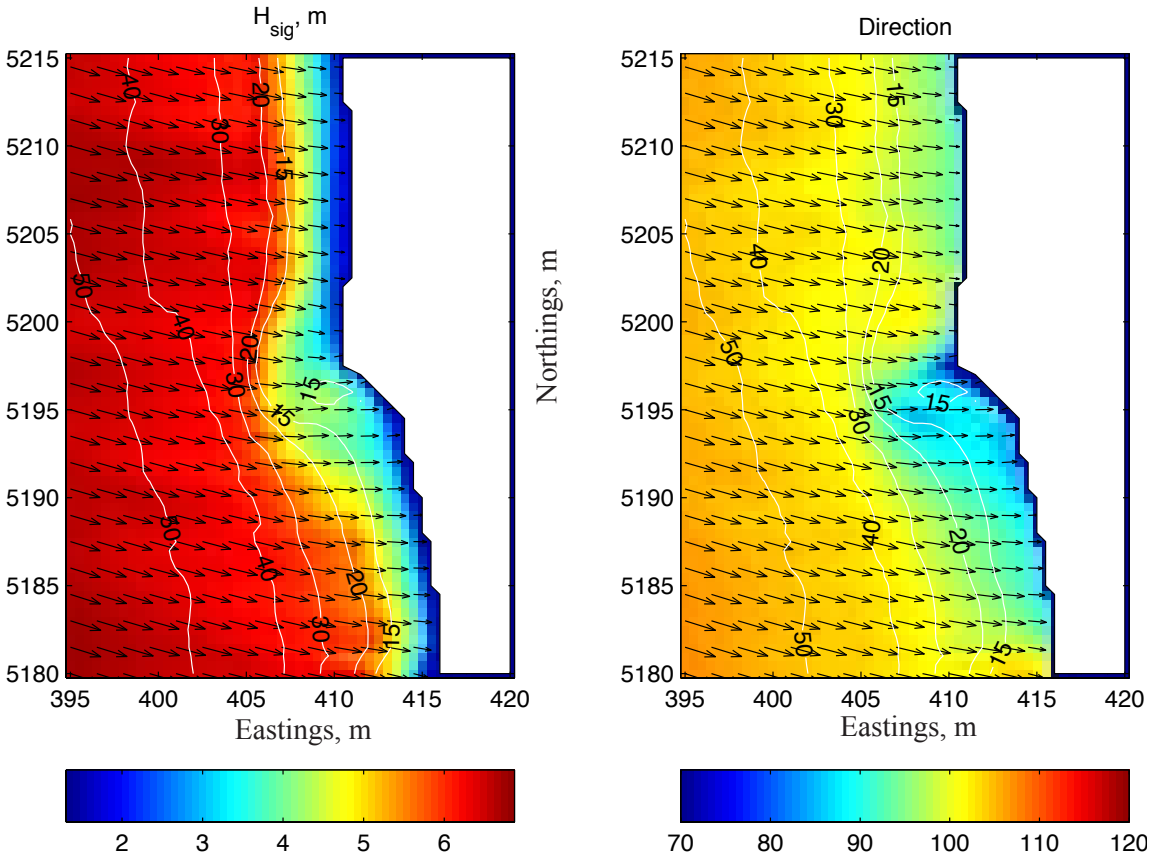

Figure 37. Wave height and direction with wave direction for Run 6 plotted as vectors and bathymetry contours shown. Wave direction at the offshore boundary was 7.1 and peak period was 14 s, as in Run 5. Peak wave direction was from 290°.

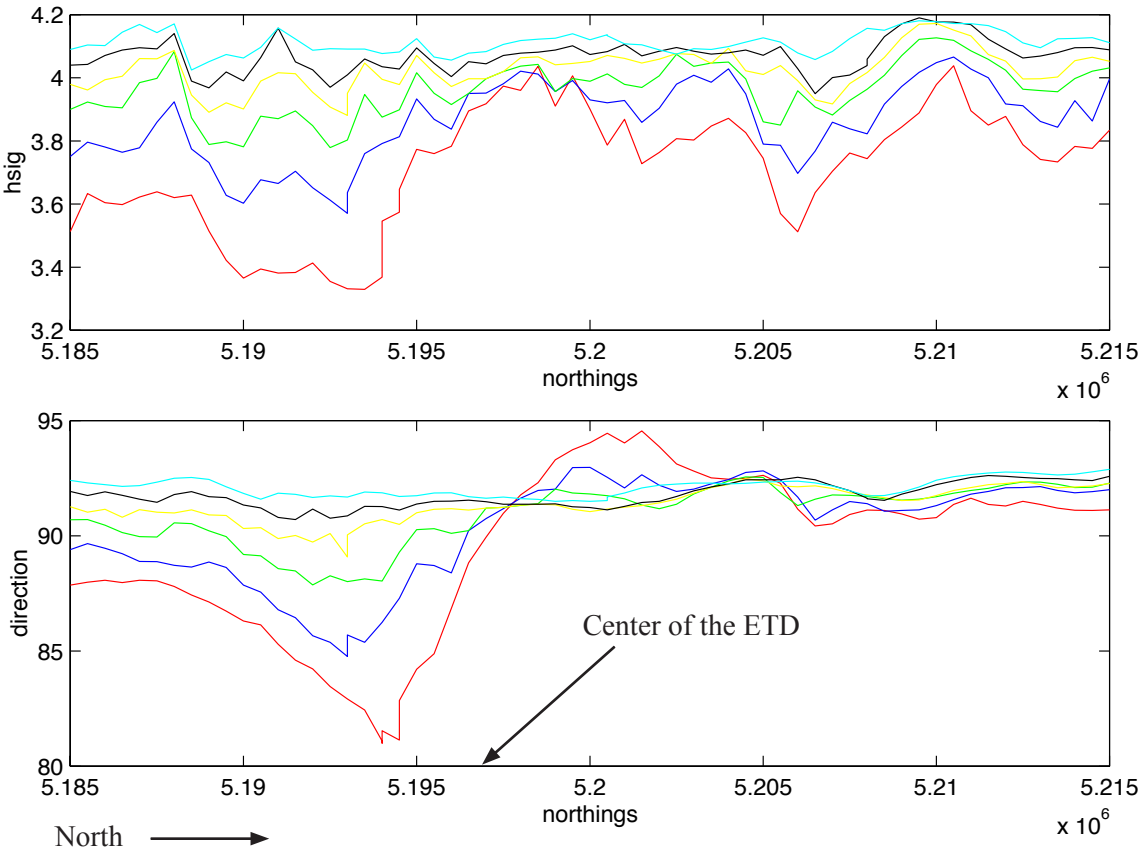

Figure 38. Wave height and direction for Run 1 plotted along isobaths. Red (15 m), blue (20 m), green (25 m), yellow (30 m), black (35 m), cyan (40 m). The ETD is located between approximately 5.193 x 10^6 northings and 5.203 x 10^6 northings. Center of the ETD is located near 5.197 x 10^6 northings. Notice the change in modeled wave height and direction as the model propagates over the ETD.

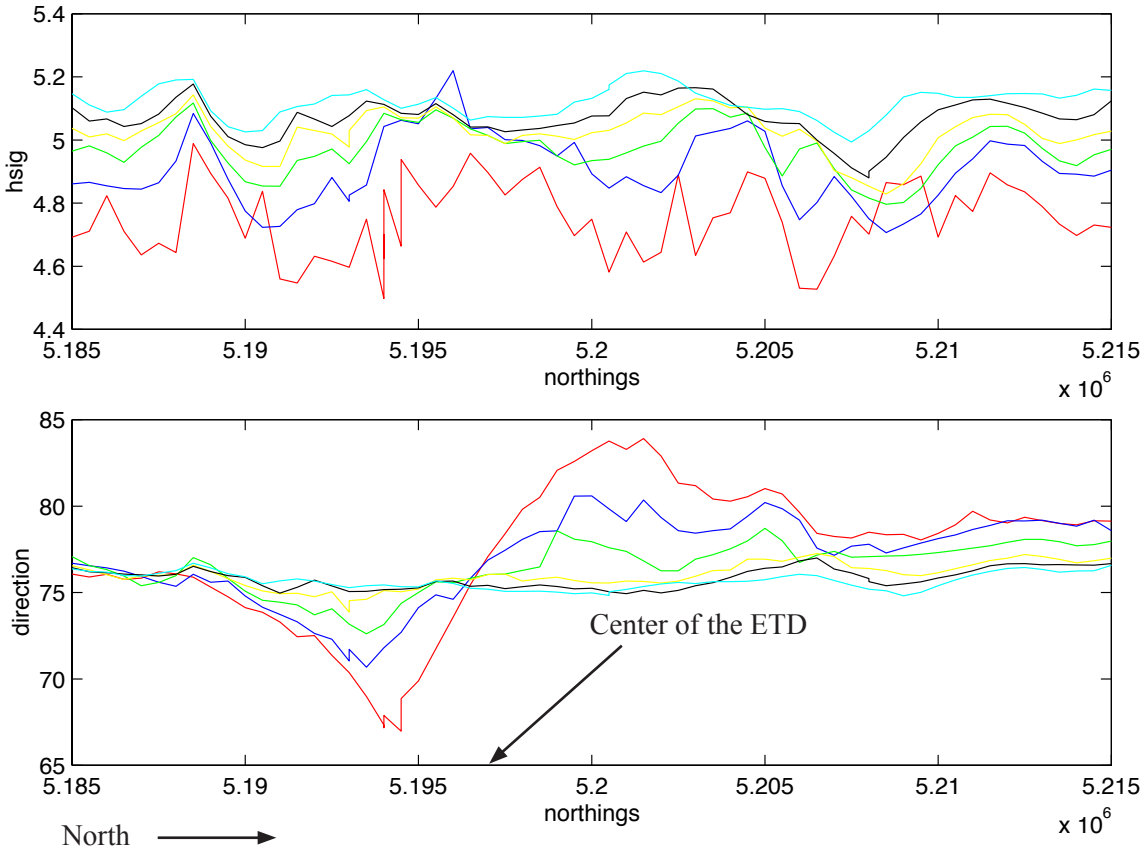

Figure 39. Wave height and direction for Run 2 plotted along isobaths. Red (15 m), blue (20 m), green (25 m), yellow (30 m), black (35 m), cyan (40 m). The ETD is located between approximately 5.193 x 10^6 northings and 5.203 x 10^6 northings. Center of the ETD is located near 5.197 x 10^6 northings. Notice the change in modeled wave height and direction as the model propagates over the ETD.

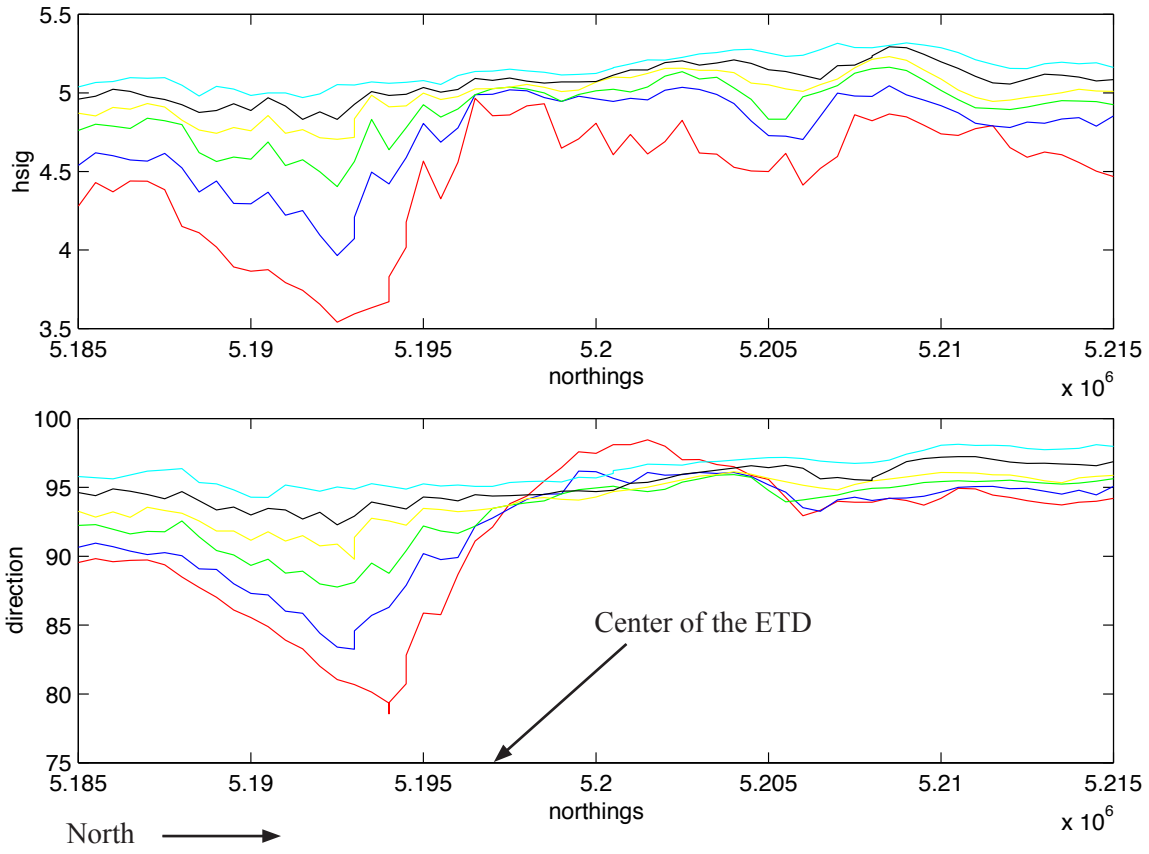

Figure 40. Wave height and direction for Run 3 plotted along isobaths. Red (15 m), blue (20 m), green (25 m), yellow (30 m), black (35 m), cyan (40 m). The ETD is located between approximately 5.193 x 10^6 northings and 5.203 x 10^6 northings. Center of the ETD is located near 5.197 x 10^6 northings. Notice the change in modeled wave height and direction as the model propagates over the ETD.

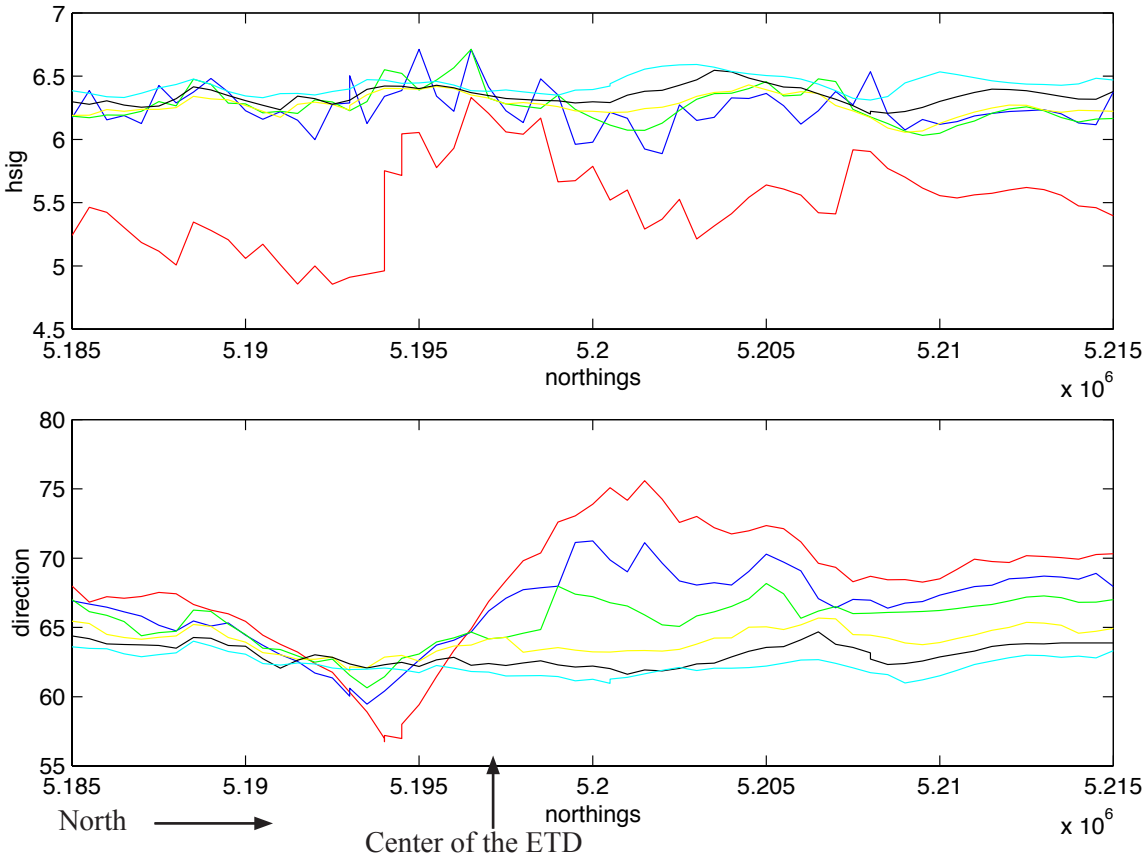

Figure 41. Wave height and direction for Run 4 plotted along isobaths. Red (15 m), blue (20 m), green (25 m), yellow (30 m), black (35 m), cyan (40 m). The ETD is located between approximately 5.193 x 10^6 northings and 5.203 x 10^6 northings. Center of the ETD is located near 5.197 x 10^6 northings. Notice the change in modeled wave height and direction as the model propagates over the ETD.

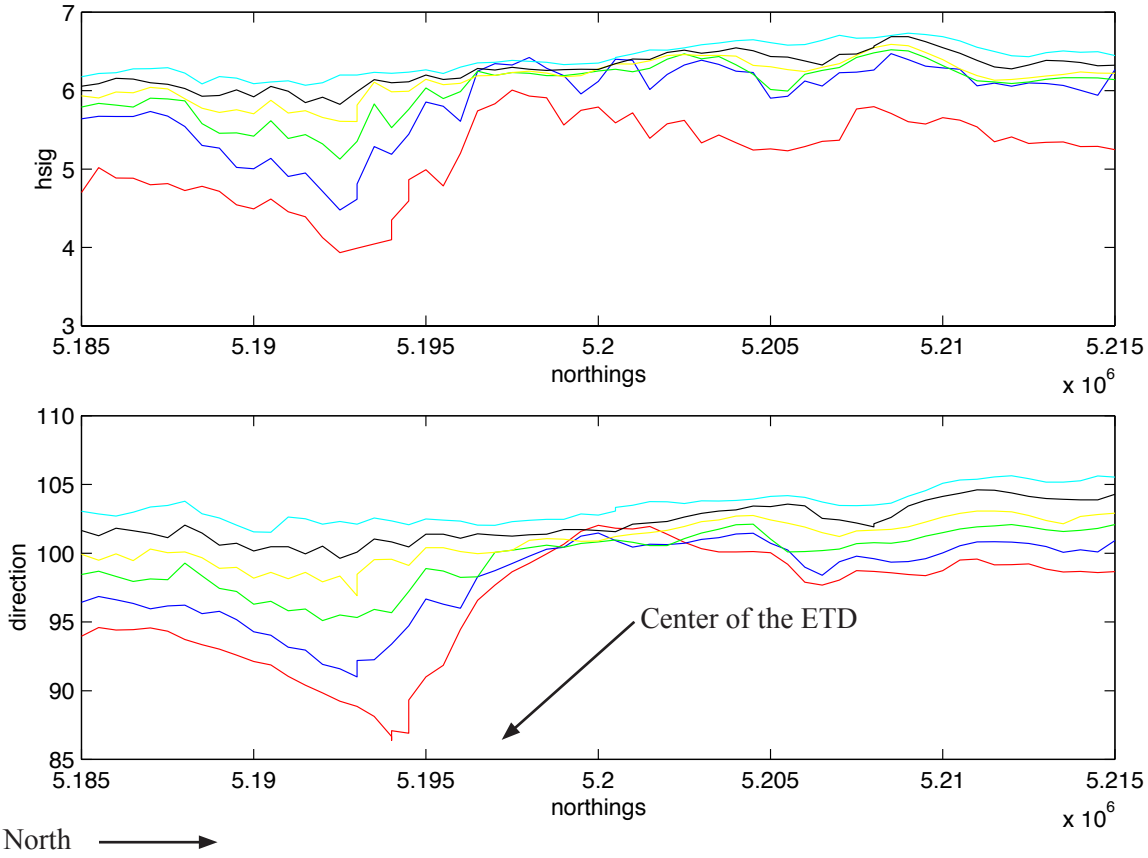

Figure 42. Wave height and direction for Run 6 plotted along isobaths. Red (15 m), blue (20 m), green (25 m), yellow (30 m), black (35 m), cyan (40 m). The ETD is located between approximately 5.193 x 10^6 northings and 5.203 x 10^6 northings. Center of the ETD is located near 5.197 x 10^6 northings. Notice the change in modeled wave height and direction as the model propagates over the ETD.

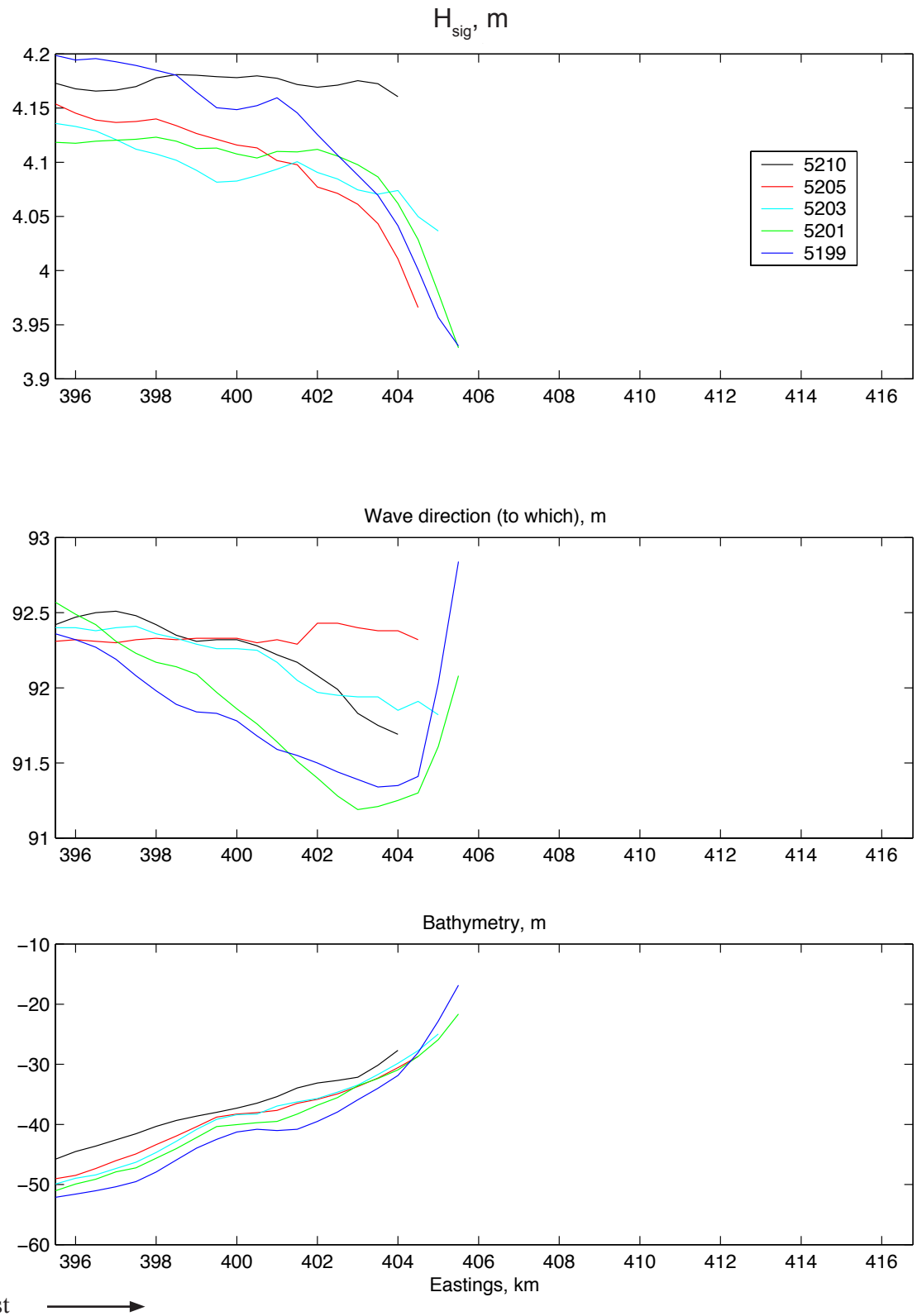

Figure 43. Profiles of wave height and direction plotted against water depth in the east-west direction for Run 1 for the north side of the ETD.

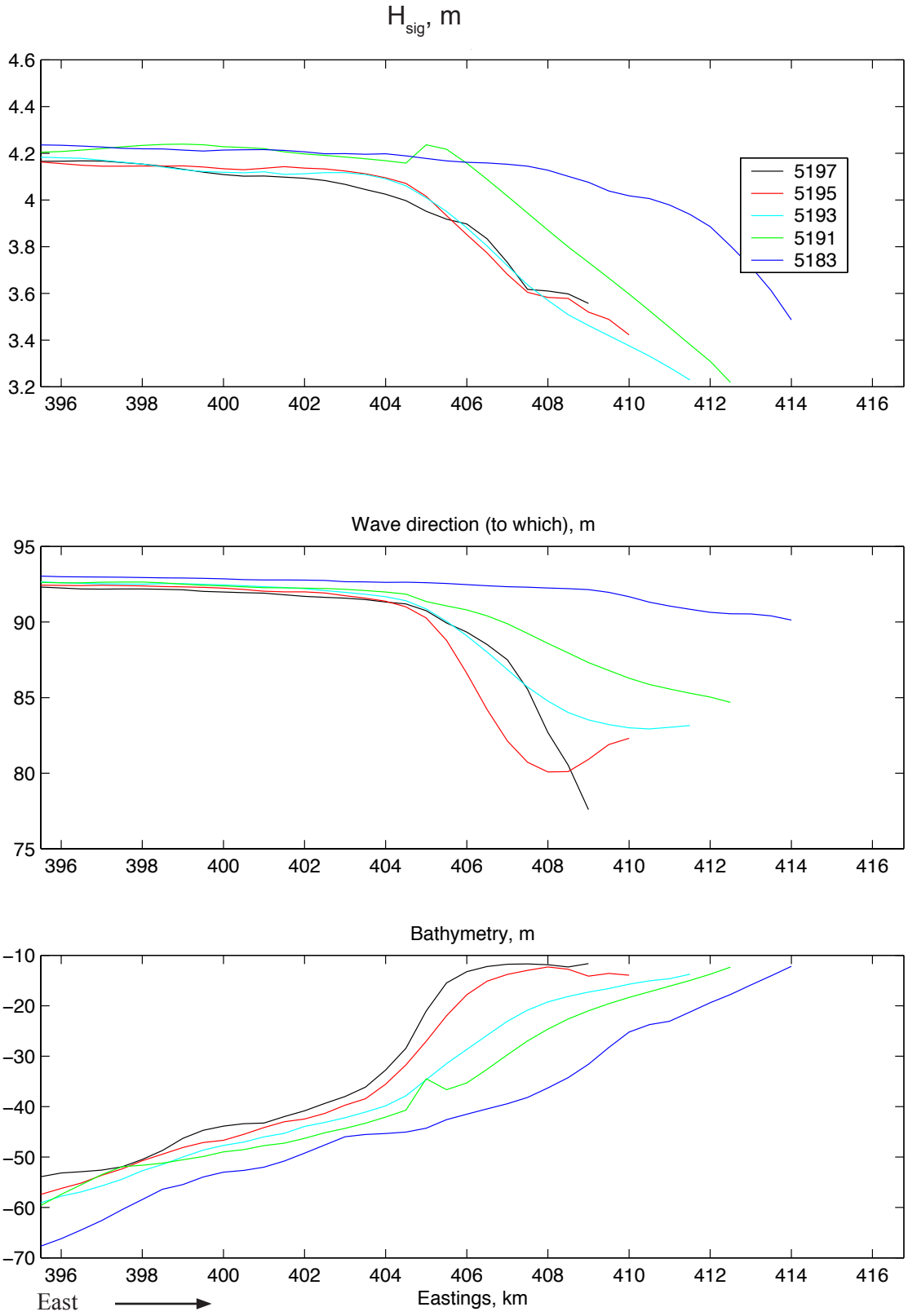

Figure 44. Profiles of wave height and direction from Run 1 plotted against water depth in the east-west direction for the south side of the ETD.

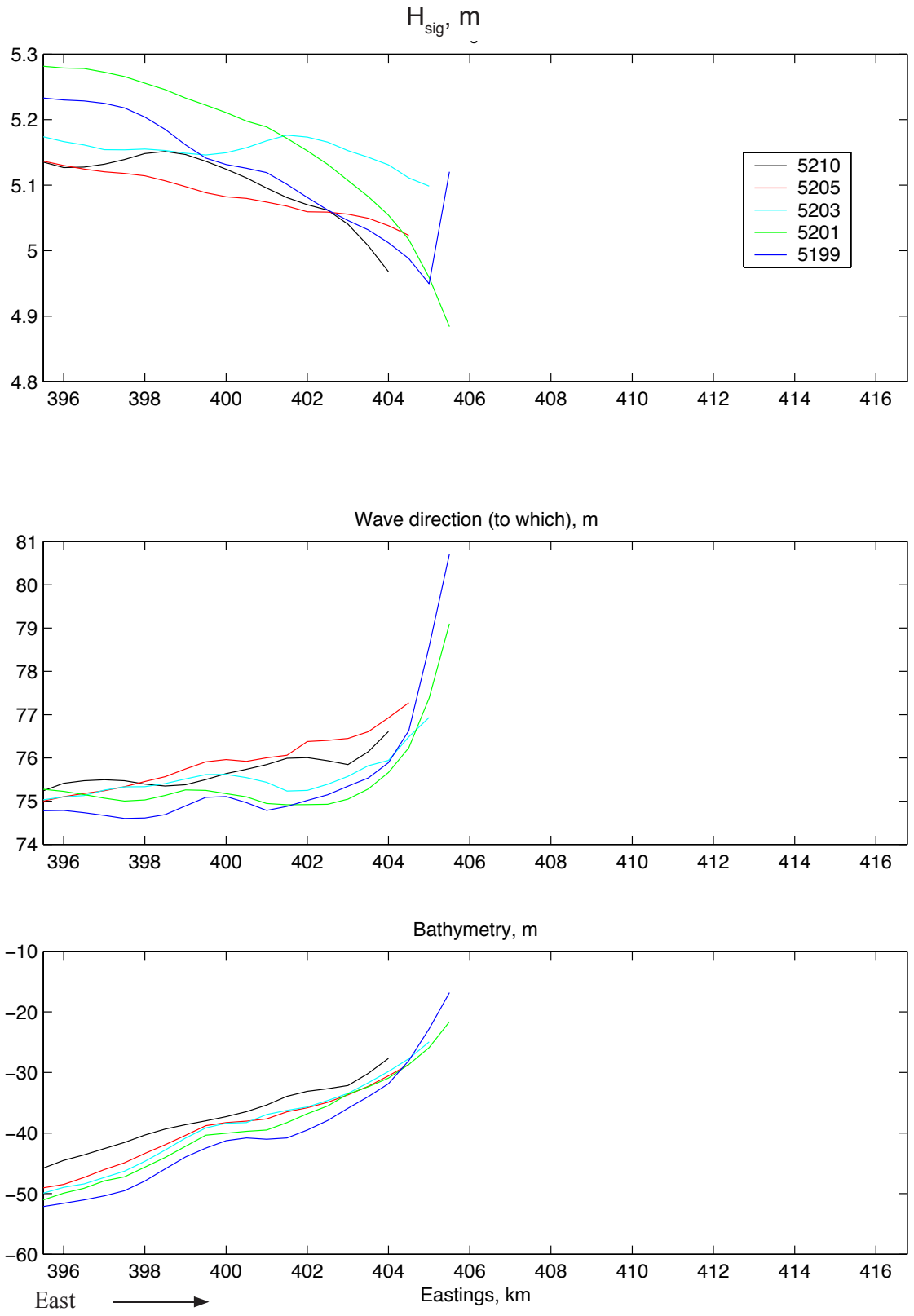

Figure 45. Profiles of wave height and direction from Run 2 plotted against water depth in the east-west direction for the north side of the ETD.

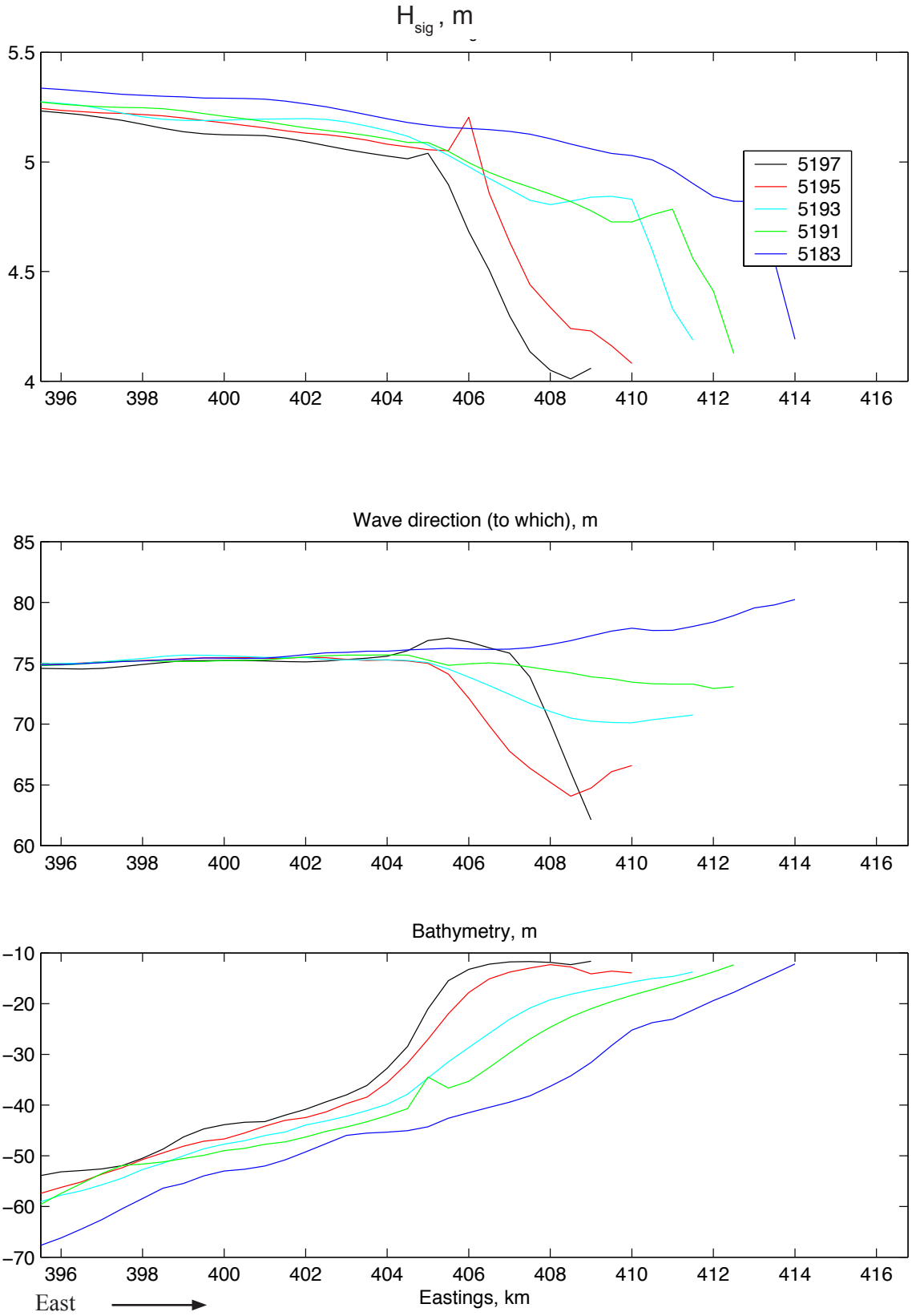

Figure 46. Profiles of wave height and direction from Run 2 plotted against water depth in the east-west direction for the south side of the ETD.

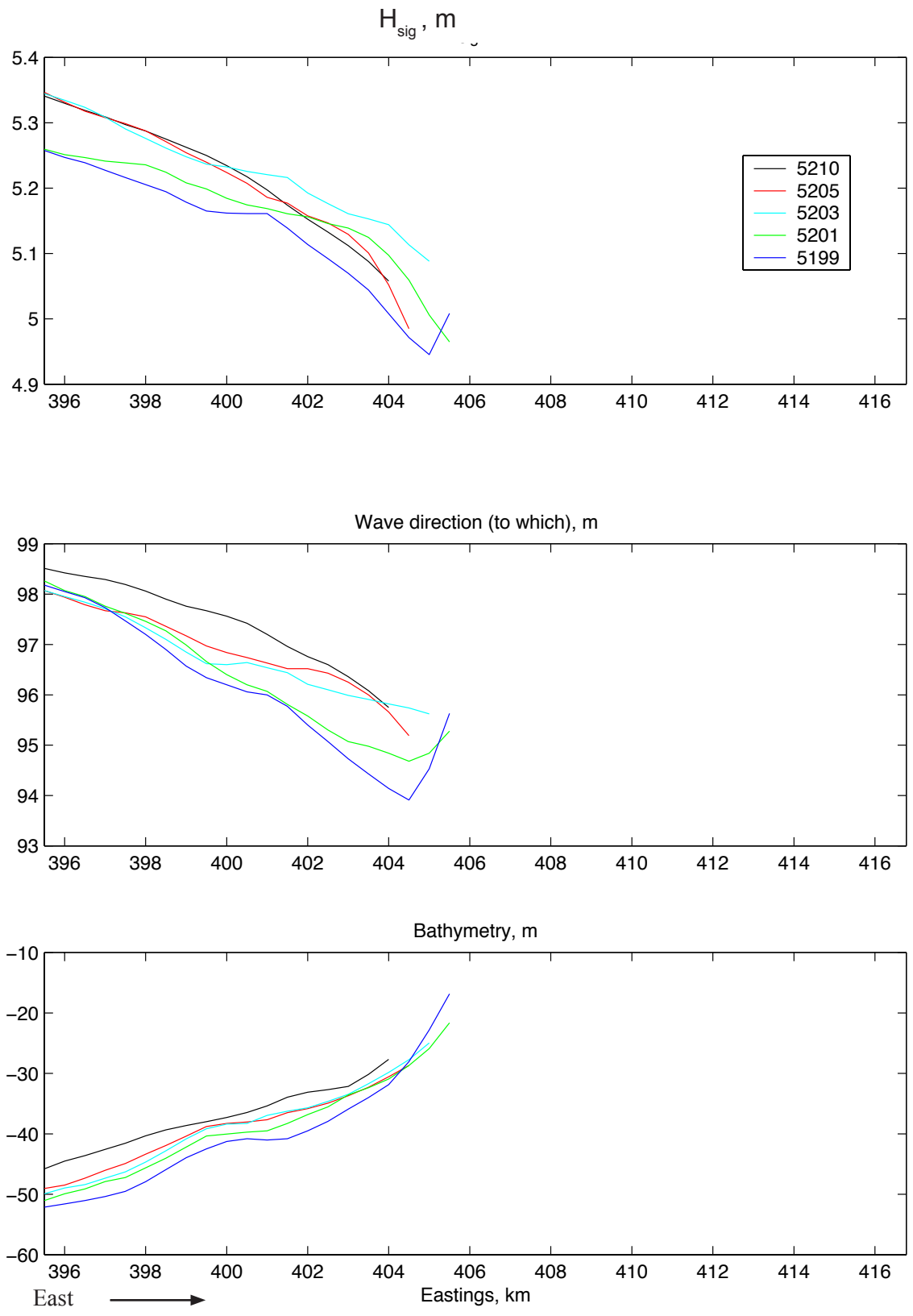

Figure 47. Profiles of wave height and direction from Run 3 plotted against water depth in the east-west direction for the north side of the ETD.

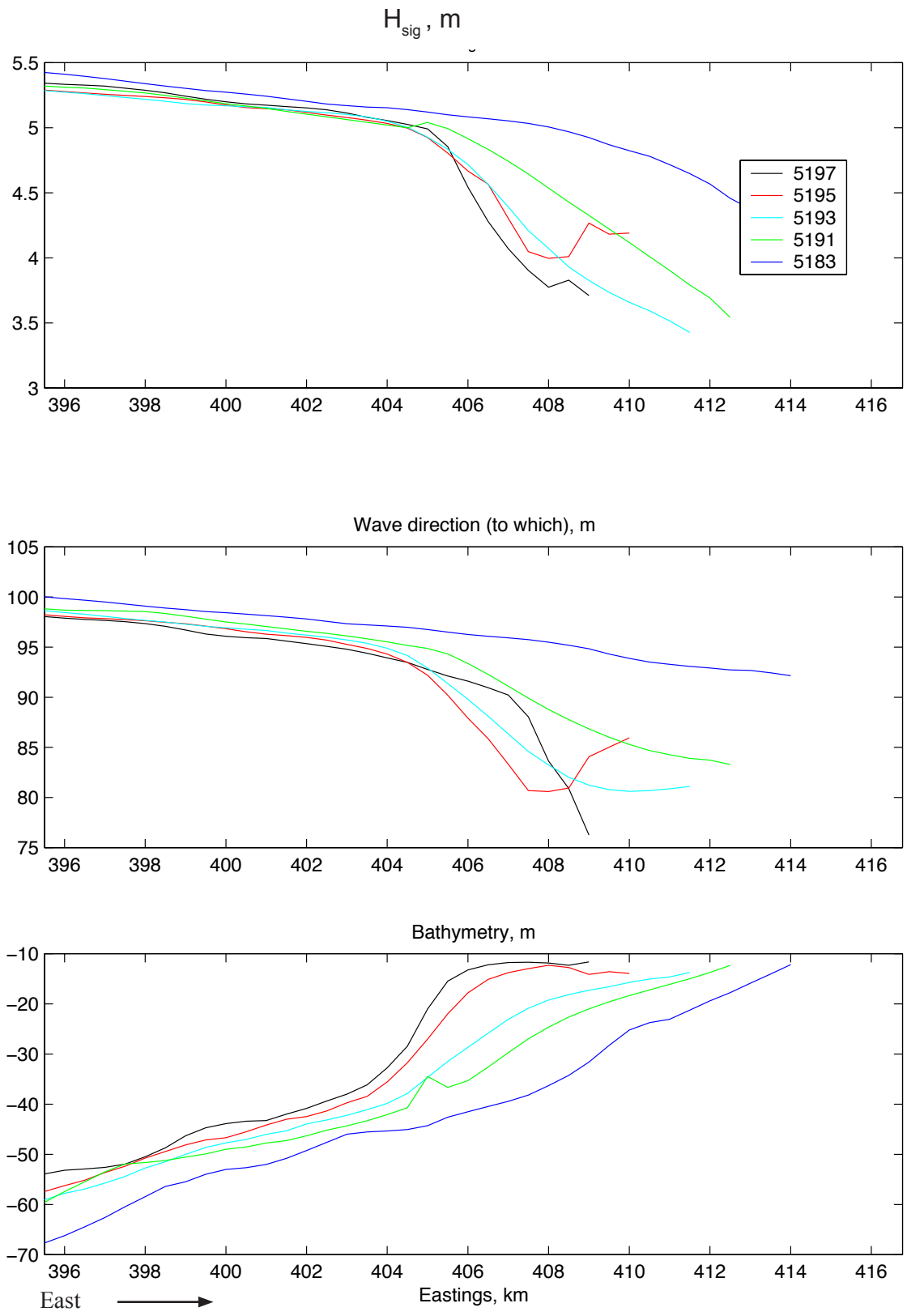

Figure 48. Profiles of wave height and direction from Run 3 plotted against water depth in the east-west direction for the south side of the ETD.

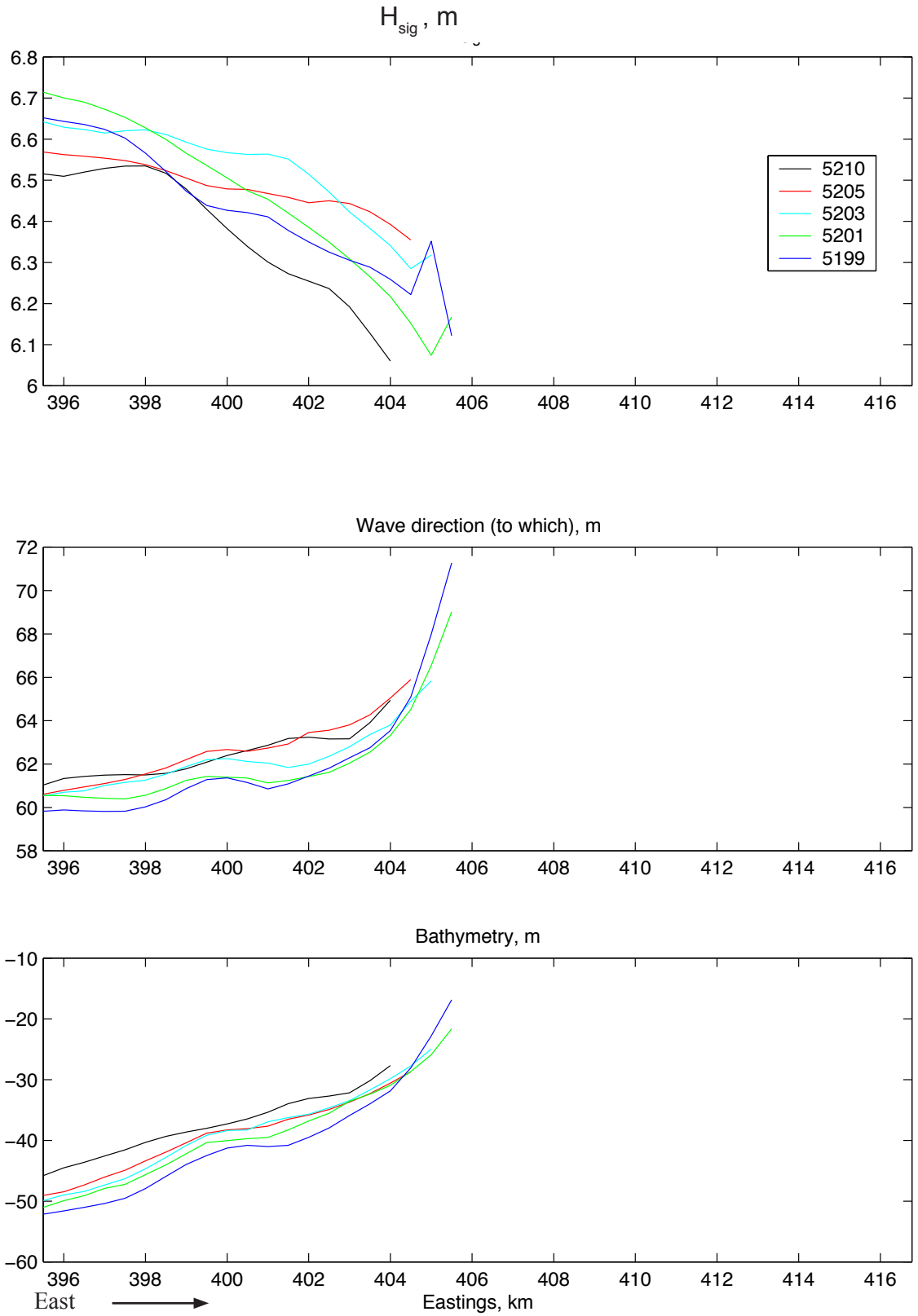

Figure 49. Profiles of wave height and direction from Run 4 plotted against water depth in the east-west direction for the north side of the ETD.

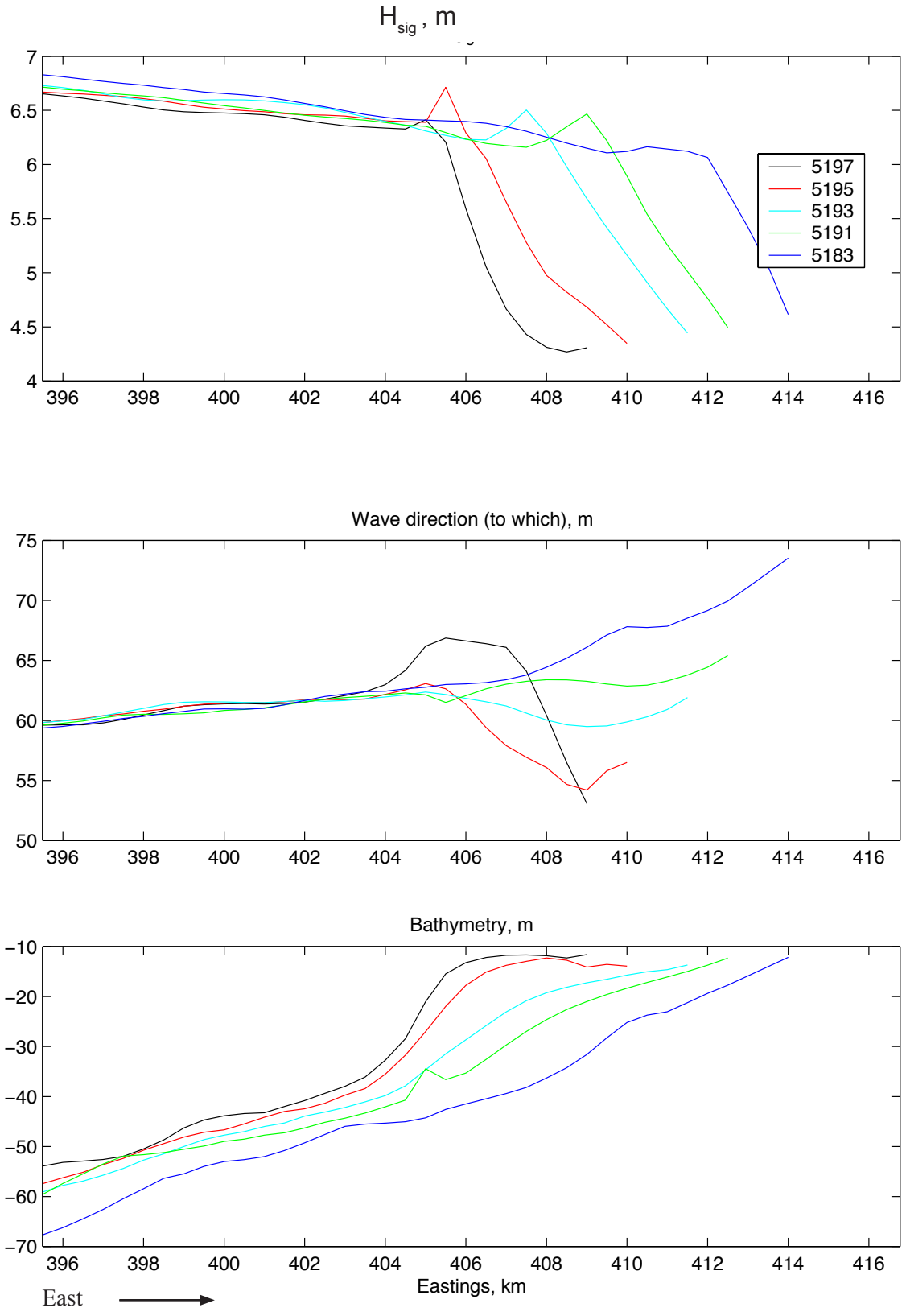

Figure 50. Profiles of wave height and direction from Run 4 plotted against water depth in the east-west direction for the south side of the ETD.

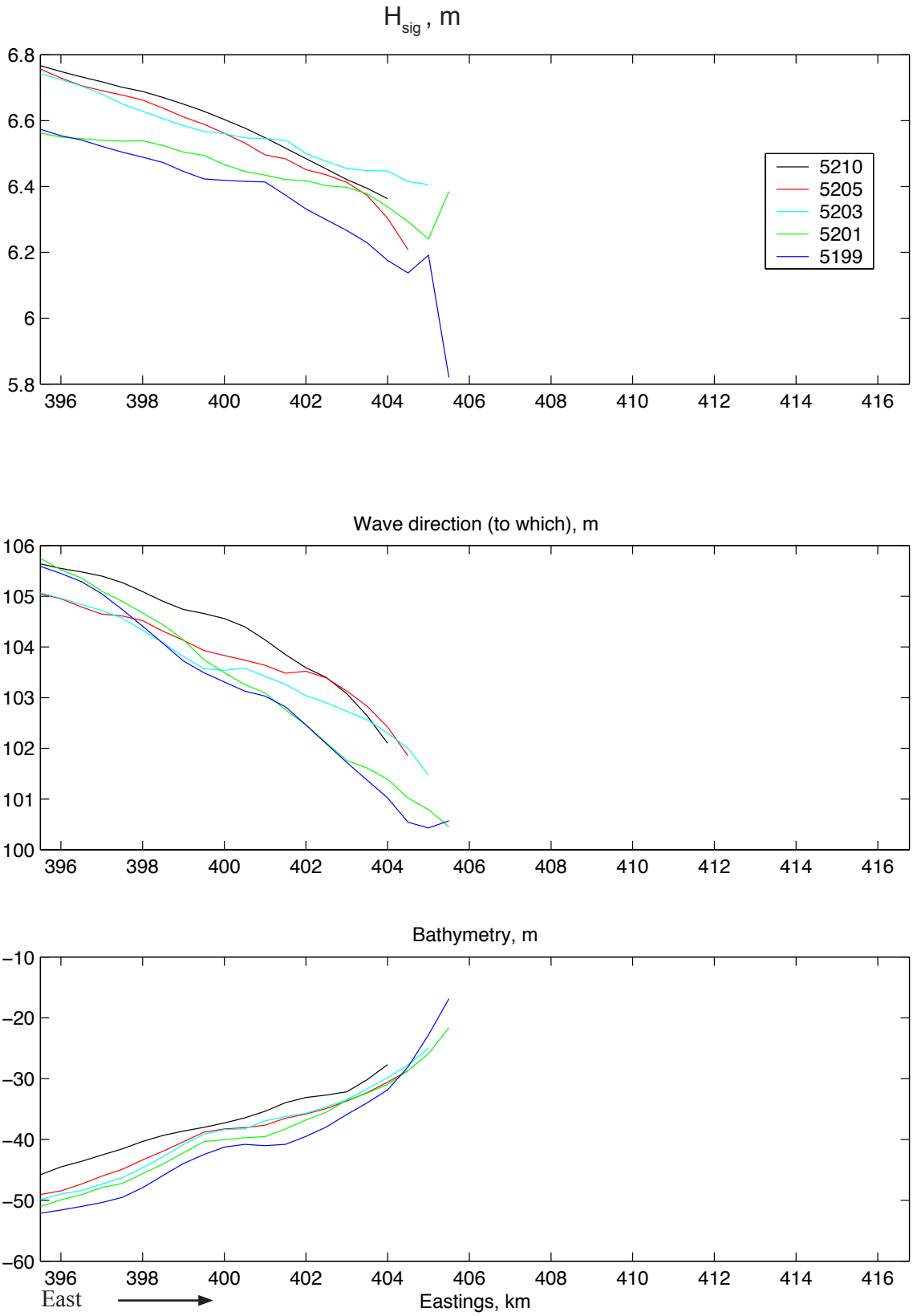

Figure 51. Profiles of wave height and direction from Run 6 plotted against water depth in the east-west direction for the north side of the ETD.

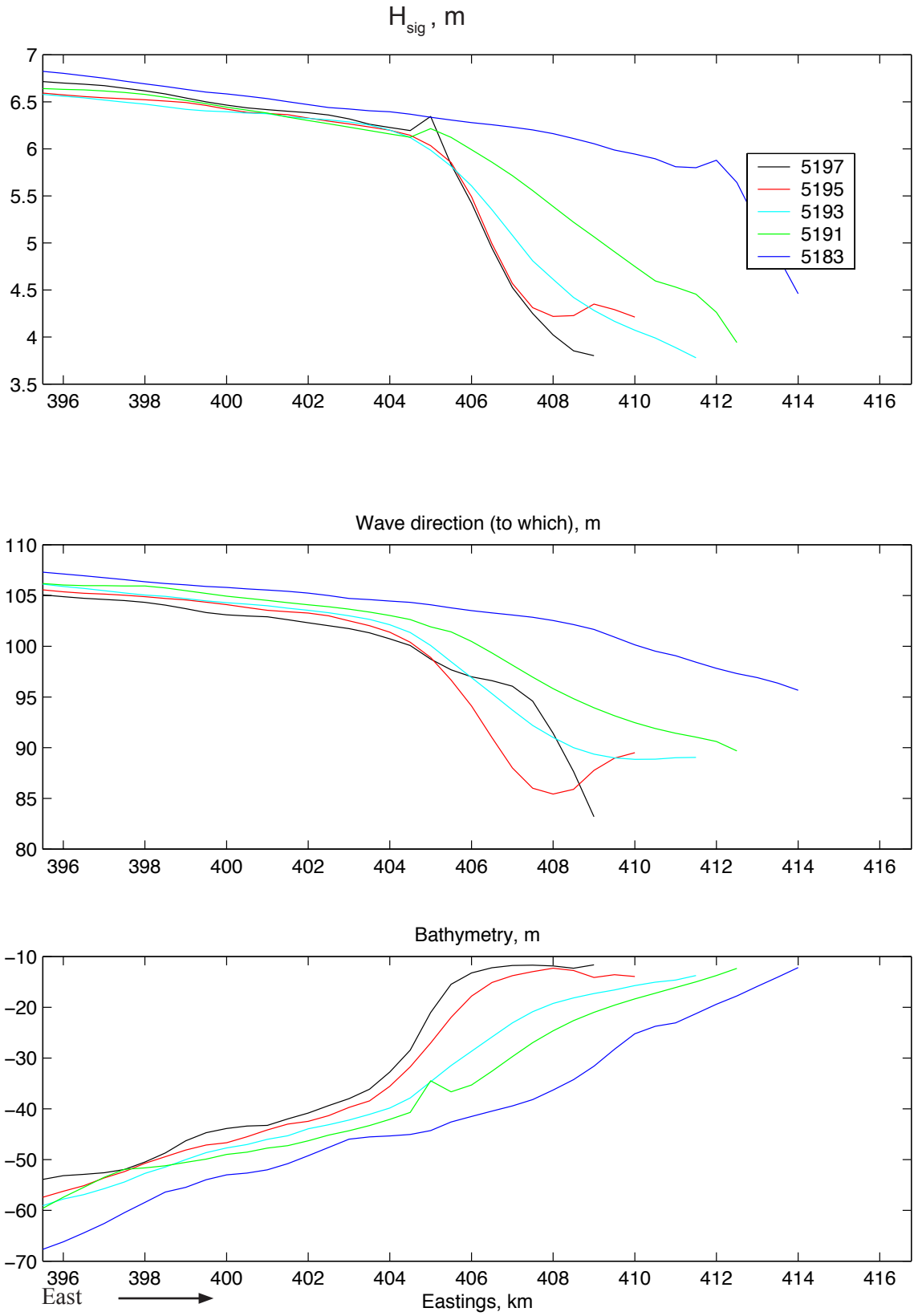

Figure 52. Profiles of wave height and direction from Run 6 plotted against water depth in the east-west direction for the north side of the ETD.

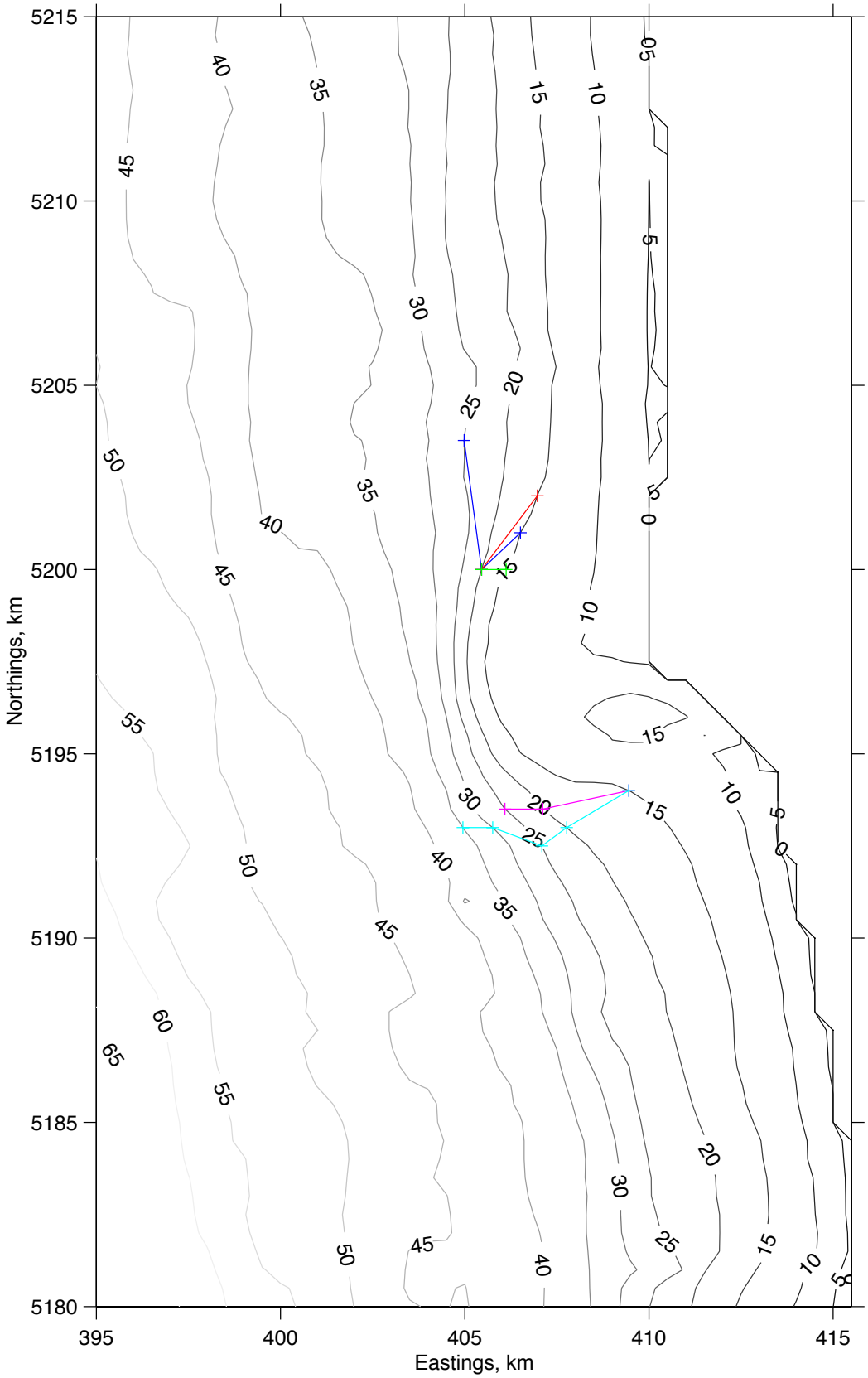

Figure 53. Locations of maximum influence of the ETD on wave direction.

Field Experiment

Wave data collected during the field deployment were of exceptionally high quality. The results of several data quality checks are shown. Mean signal strength and standard deviation of signal strength were examined at each receiver per data burst for the ADVs. Signal strength was high throughout the experiment. Mean correlation between signals, and standard deviation of correlation per burst gave quality estimates of ADV measurements. Correlation between signals was acceptable. Instances of poor velocity measurements never extended more than ten continuous data points (5 seconds). Examination of compass heading (Figure 54) showed several occasions where a tripod was reoriented during or between a data burst. These instances were investigated, resulting in several bursts removed from the data set because of unusual circumstances. A fishing trawler raised the SS tripod to the surface during recording data period. Several days of pressure data at the ND tripod were discarded due to attenuated pressure sensor

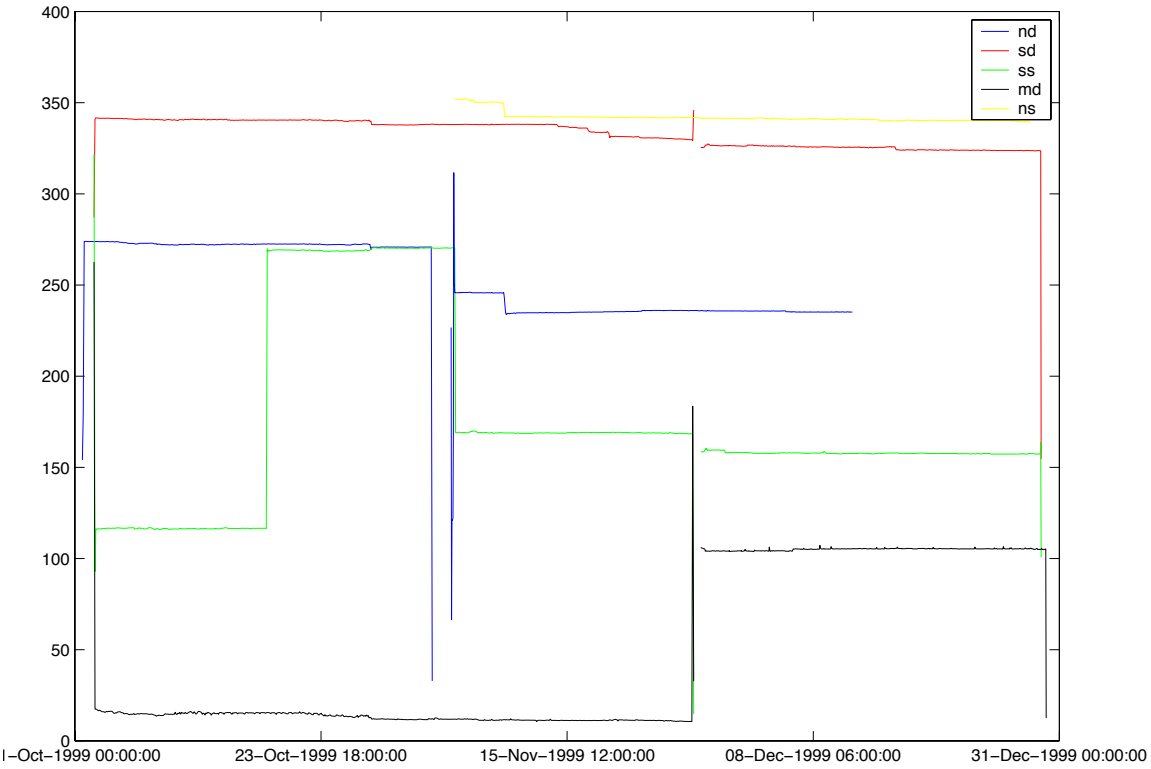

Figure 54. Compass heading for tripods during the field experiment. Notice reorientation of the tripods throughout the experiment.

readings. The compass on MD was not properly calibrated during the second deployment resulting in poor-quality wave directional measurements.

Data were processed to remove and interpolate over points of poor quality. The deglitched data were plotted in the same format as raw data. Wave energy spectra and wave directional spectra for each burst were calculated and plotted. The deglitched data were processed to produce bulk averaged statistics including horizontal velocities, wave height, peak direction, and peak period (Figure 55). These statistics will be used to determine conditions for use in the model calibration and validation study.

Figure 55 shows burst averaged wave statistics including horizontal velocities, significant wave height, peak direction, and peak period at every station during the field experiment. During October 1999 waves were fairly quiescent with significant wave heights near 3 m. Peak wave direction was generally from WNW with periods near 12 s. On several occasions during this low wave period, peak direction changed to WSW with a corresponding shift to higher peak periods (15 s-17 s). A large wave event occurred on October 29, 1999. Significant wave height reached 6 m at the tripods. Peak period was 15-17 s and peak direction was from the WSW. This first storm was followed by 13 events where wave height was greater than 4 m. Each event followed the characteristic pattern of a change in peak wave direction to the WSW and an increase in peak period.

From the three-month time series of data, time periods were chosen for modeling runs. All times are reported as GMT. Criteria for chosen time periods were: 1) stable conditions over wave travel time from 46005 to the moorings at Grays Harbor, 2) significant wave height must be constant at each mooring, 3) wind speed must be constant at 46005, 4) wave direction and wind direction must be constant through out the time period at each mooring, 5) peak period must be constant for all moorings to show that locally generated wind waves were not being compared with ocean swell.

Plots of wave statistics from the time period between 10/13/99 02:00 and 10/13/99 22:00 area shown in Figure 56. Wave height is constant near 2.7 m at 46005 and slightly lower at the Grays Harbor moorings. Wave height at SS is several cm lower at SS than at other moorings. Wind speed was fairly steady between 5 ms^{-1} and 10 ms^{-1}. Wind direction shifted from slightly south of west to slightly north of west over the 20 hour time period. Similarly wave direction

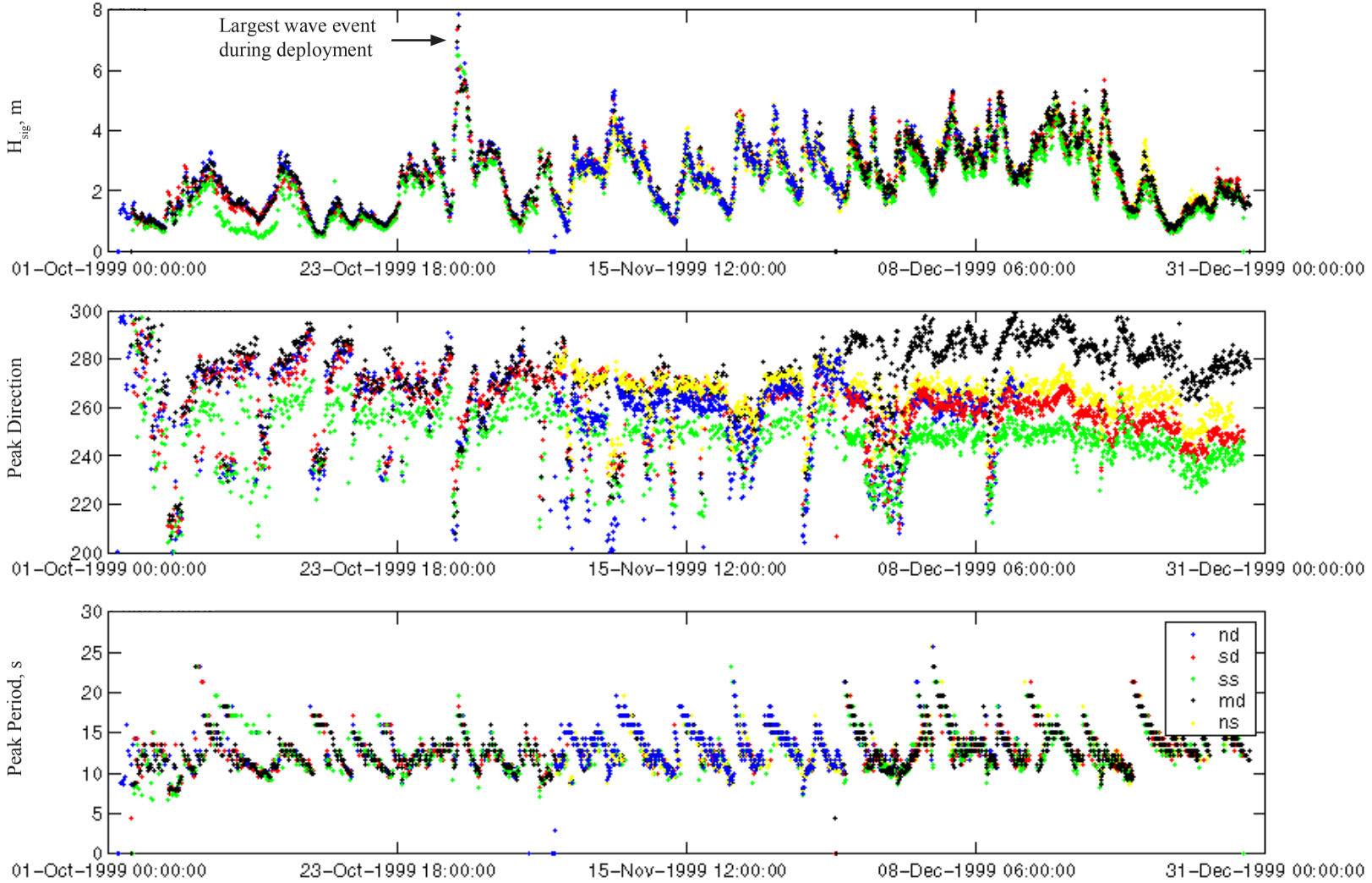

Figure 55. Plot of burst averaged wave statistics including horizontal velocities, significant wave height, peak wave direction and peak period at every station during the field experiment. x-axis represents dates of the deployment. Direction in degrees is increasing clockwise with 0 to the north. Each symbol represents a tripod.

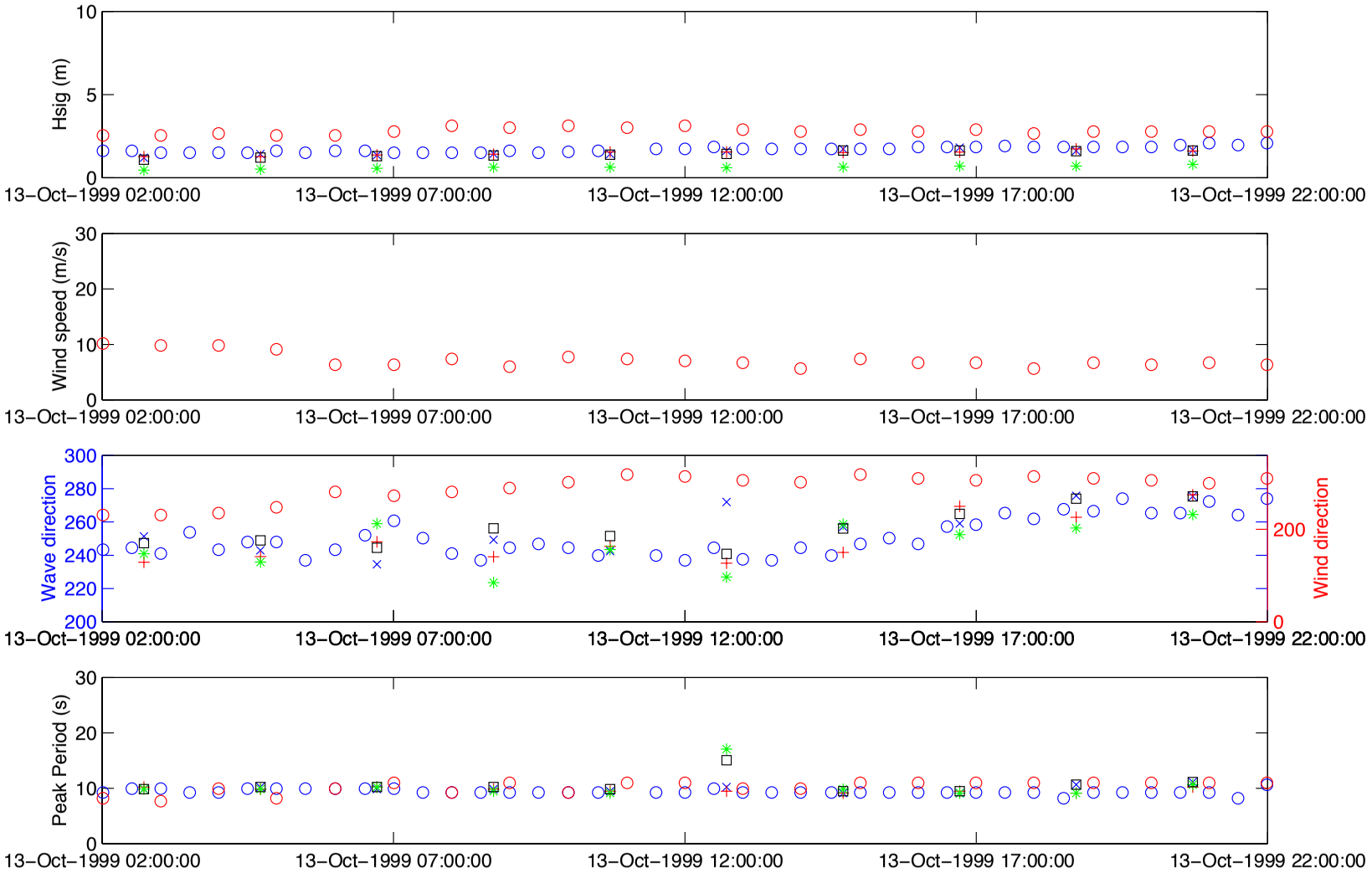

Figure 56. Plot of wave statistics and wind information between 10/13/99 02:00 and 10/13/00 22:00 at 46005 (o), CDIP (o), ND (×), SD (+), SS (*), MD (□), NS (◇)

shifted from south of west to north of west during this time period. Peak period was constant near 10 s over the deployment, except at SS and MD during the 10/13/99 13:00 burst.

Figure 57 shows burst mean statistics for the time period between 10/28/99 14:00 and 10/29/99 02:00. Conditions at the tripods and the CDIP buoy are very similar through out the time period. Wind slackens during the time period and wave height decreases offshore. However wave height at the tripods remains constant. The decreasing wave height offshore may introduce error in the boundary conditions. The change in wind speed is expected to decrease the amount of whitecapping as well. Wind direction rotates from north of west to south of west, the direction from which the waves are coming. The rotation of wind direction will influence the amount of energy added to the waves. This variation in energy addition will not be reflected in the model, where an average value for wind will be used. Wave direction is steady from the southwest throughout the time period. This stability provides confidence in wave direction at the model boundary and in measured wave direction. Peak period is similar at all tripods and buoys between 10/28/99 14:00 and 10/29/99 02:00, providing evidence that wave conditions are stable during the time period to be modeled. From wave group travel time based on a wave period of 15 s, waves present at 46005 at 10/28/99 14:00 have traveled to the study area at Grays Harbor by 10/29/99 02:00. Based on the analysis of this time period, some error is expected due to variability of conditions offshore. However, accurate model results may still be produced.

The time period between 11/15/99 03:00 and 11/15/99 14:00 (Figure 58) was characterized by a mean offshore significant wave height of 4.2 m. Wave height at 46005 decreases very little over this time period. Wave direction was from 275^{o}. Wave direction is very constant at 46005 and very similar to wave height at the tripods. Accurate directional results would be expected from the model. Peak period was 15.3 s at 46005 and 16.2 at Grays Harbor. This stability is expected to result in accurate wave height at the model boundary. Significant wave height at the Grays Harbor moorings was near 2.9 m. Wave conditions at the tripod are stable, ensuring accurate wave height for comparison with the modeled results. Wind speed was constant near 11.2 ms^{-1} and direction was nearly 125^{o} south of wave direction, making this an excellent test of model ability to produce accurate results when wind direction does not coincide with wave direction.

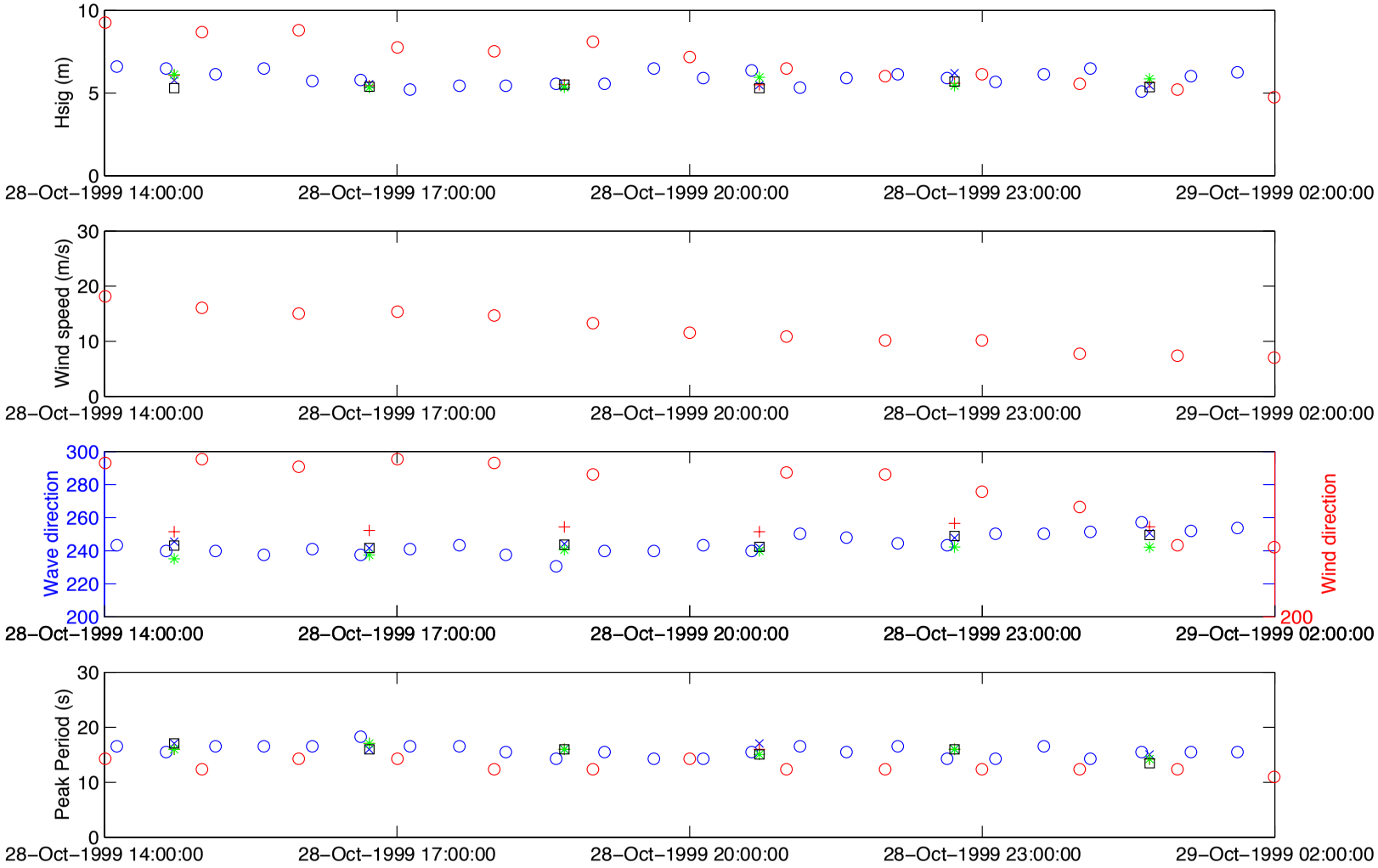

Figure 57. Plot of wave statistics and wind information between 10/28/99 14:00 and 10/29/00 02:00.at 46005 (o), CDIP (o), ND (x), SD (+), SS (*), MD (□), NS (◇)

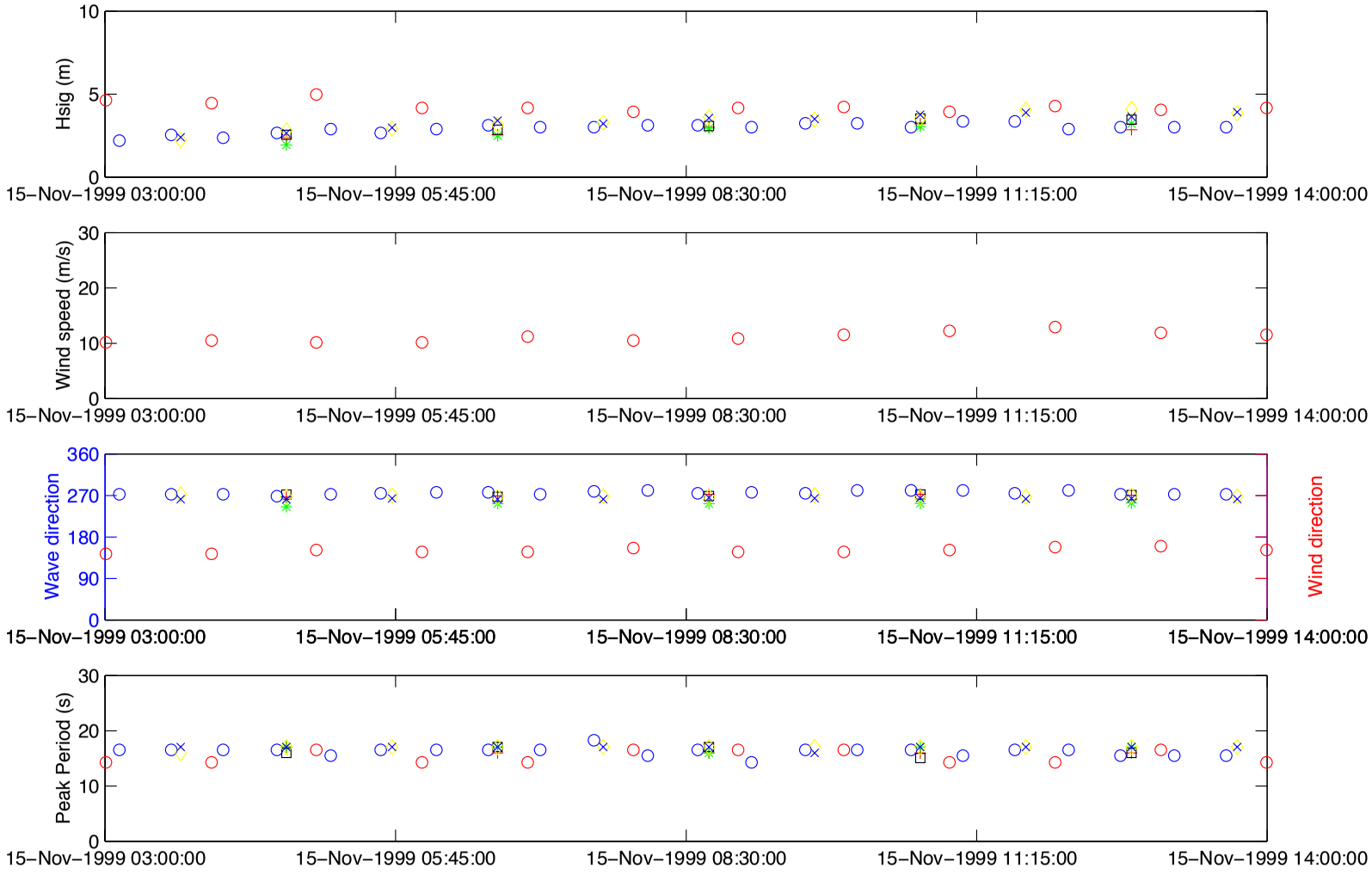

Figure 58. Plot of wave statistics and wind information between 11/15/99 03:00 and11/15/99 14:00.at 46005 ( ), CDIP ( ), ND ( ), SD ( ), SS (*), MD ( ), NS ( )

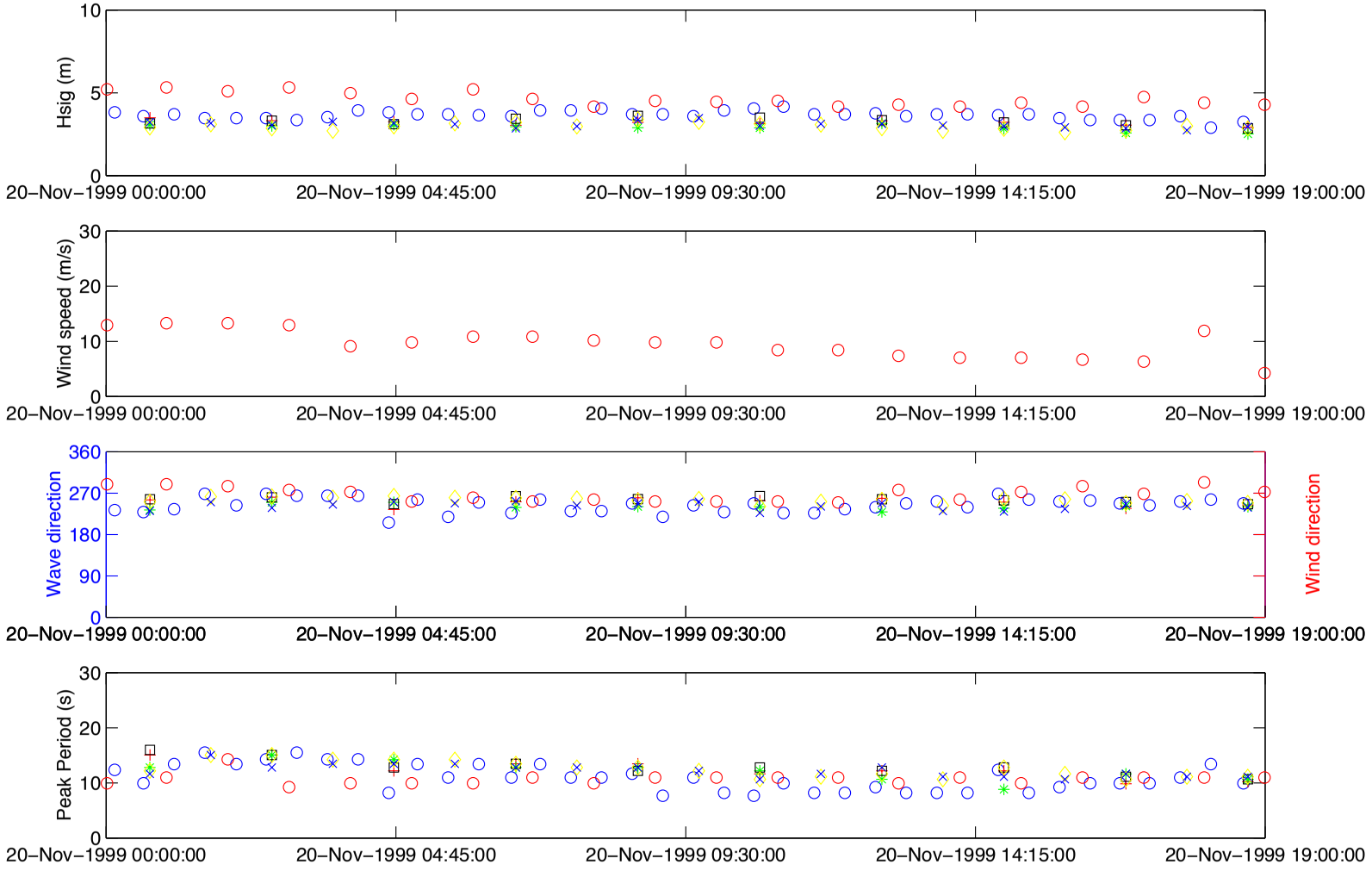

Figure 59. Plot of wave statistics and wind information etween 11/20/99 00:00 and11/20/99 19:00.at 46005 ( ), CDIP ( ), ND ( ), SD ( ), SS ( ), MD ( ), NS ( ).

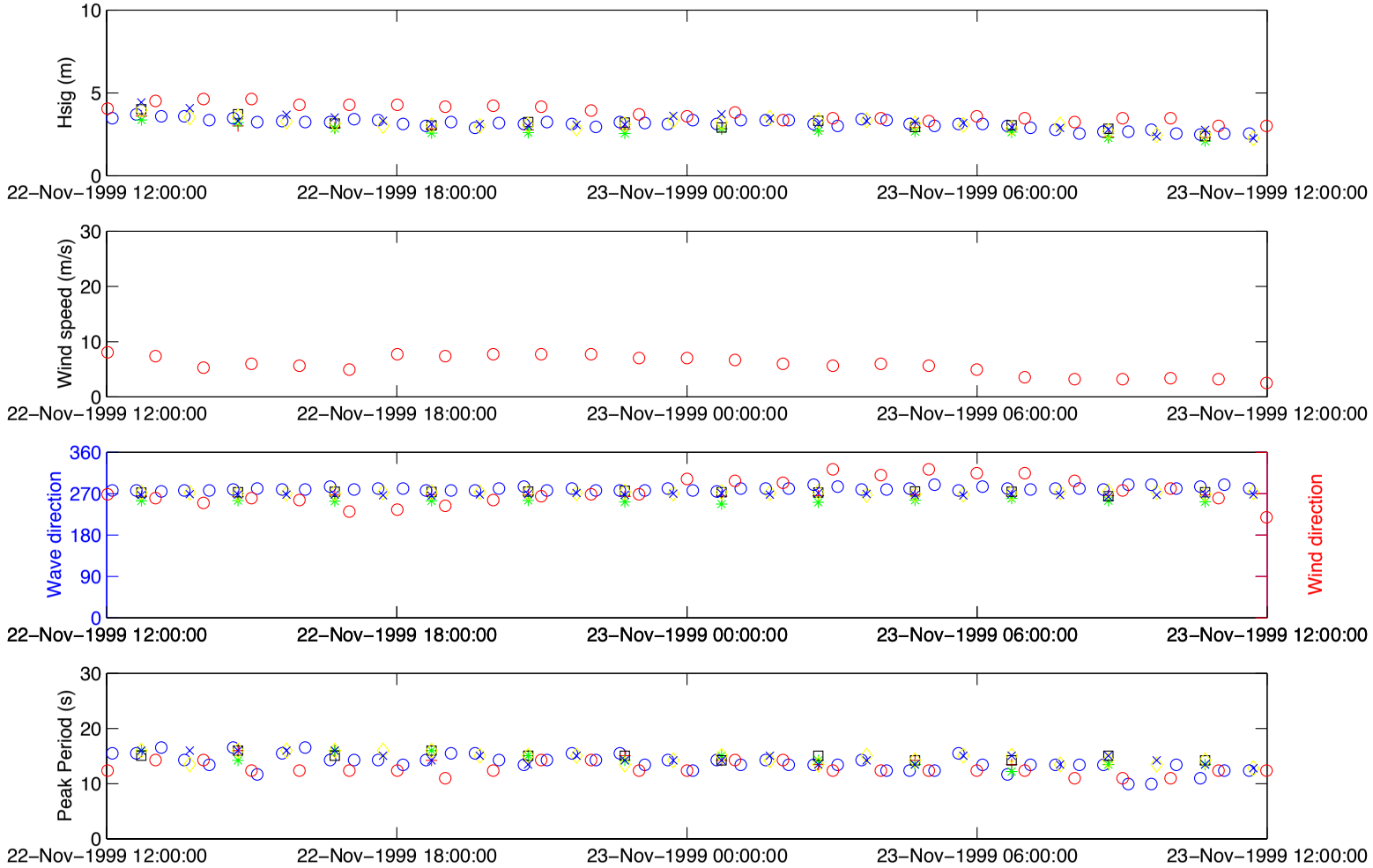

Figure 60. Plot of wave statistics and wind information) between 11/22/99 12:00 and11/23/99 12:00.at 46005 ( ), CDIP ( ), ND ( ), SD ( ), SS ( ), MD ( ), NS ( ).

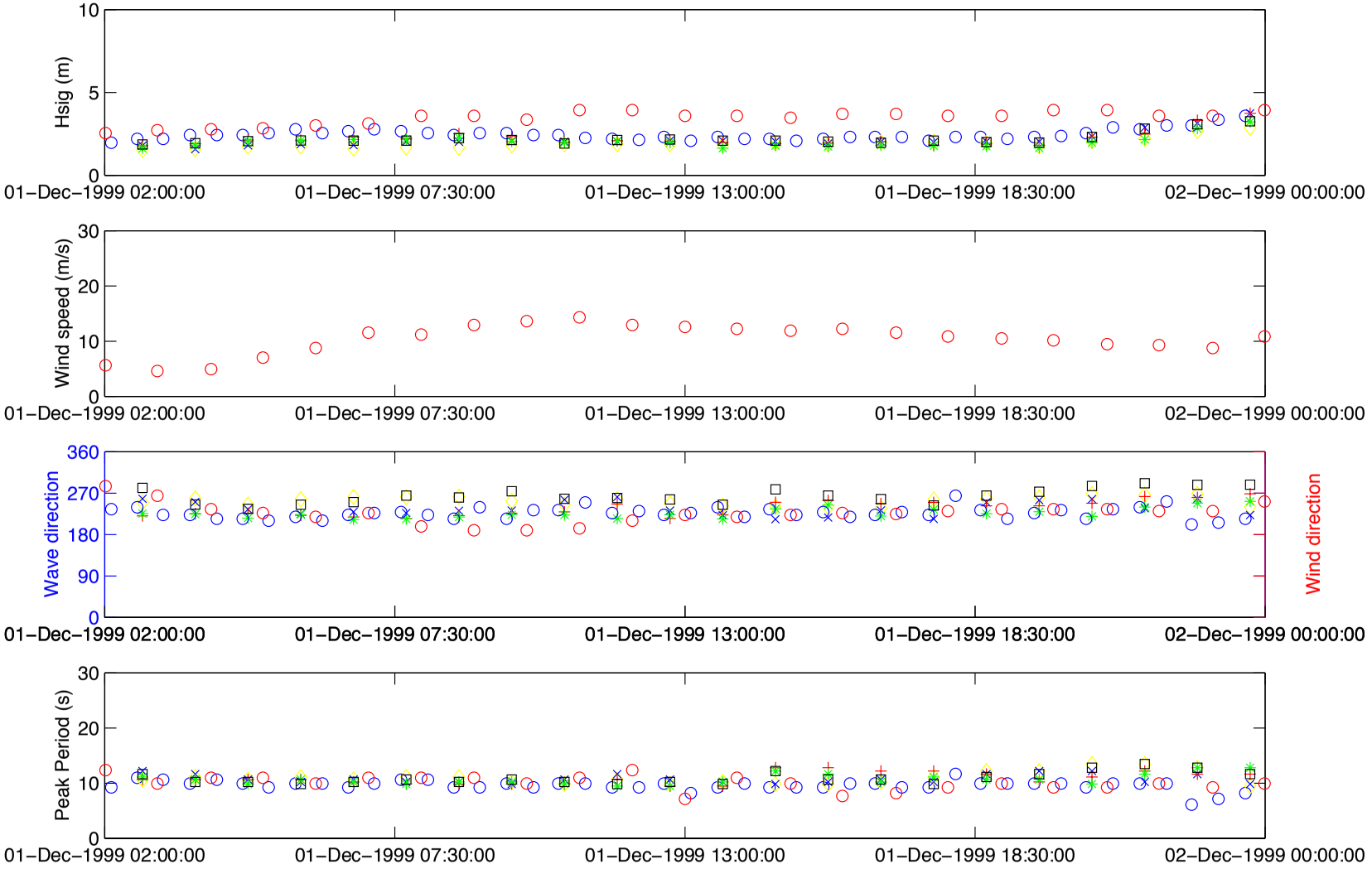

Figure 61. Plot of wave statistics and wind information between 12/01/99 02:00 and12/02/99 00:00.at 46005 ( ), CDIP ( ), ND ( ), SD ( ), SS ( ), MD ( ), NS ( )

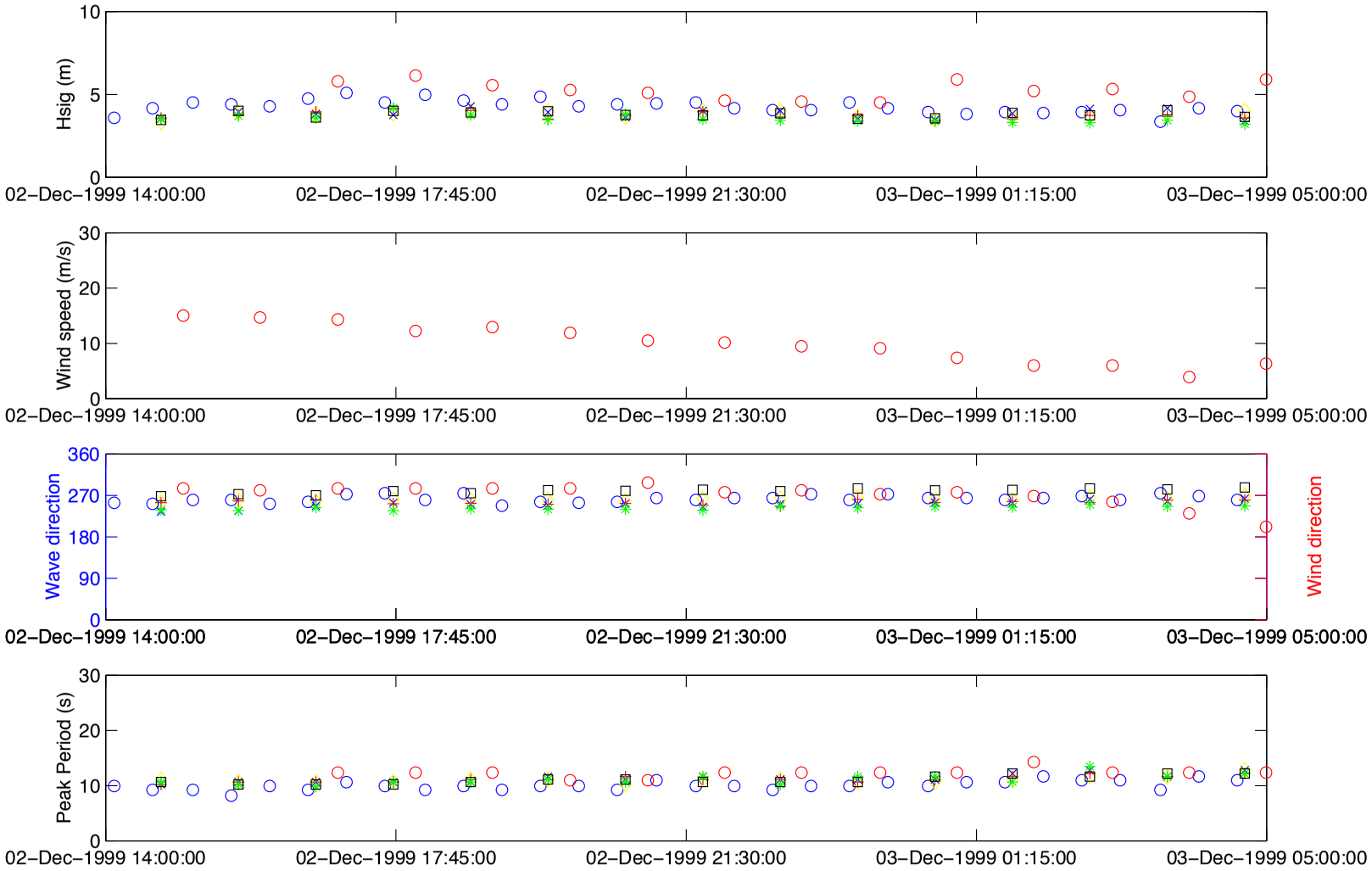

Figure 62. Plot of wave statistics and wind information between 12/02/99 14:00 and12/03/99 06:00.at 46005 ( ), CDIP ( ), ND ( ), SD (+), SS (*), MD ( ), NS ( )

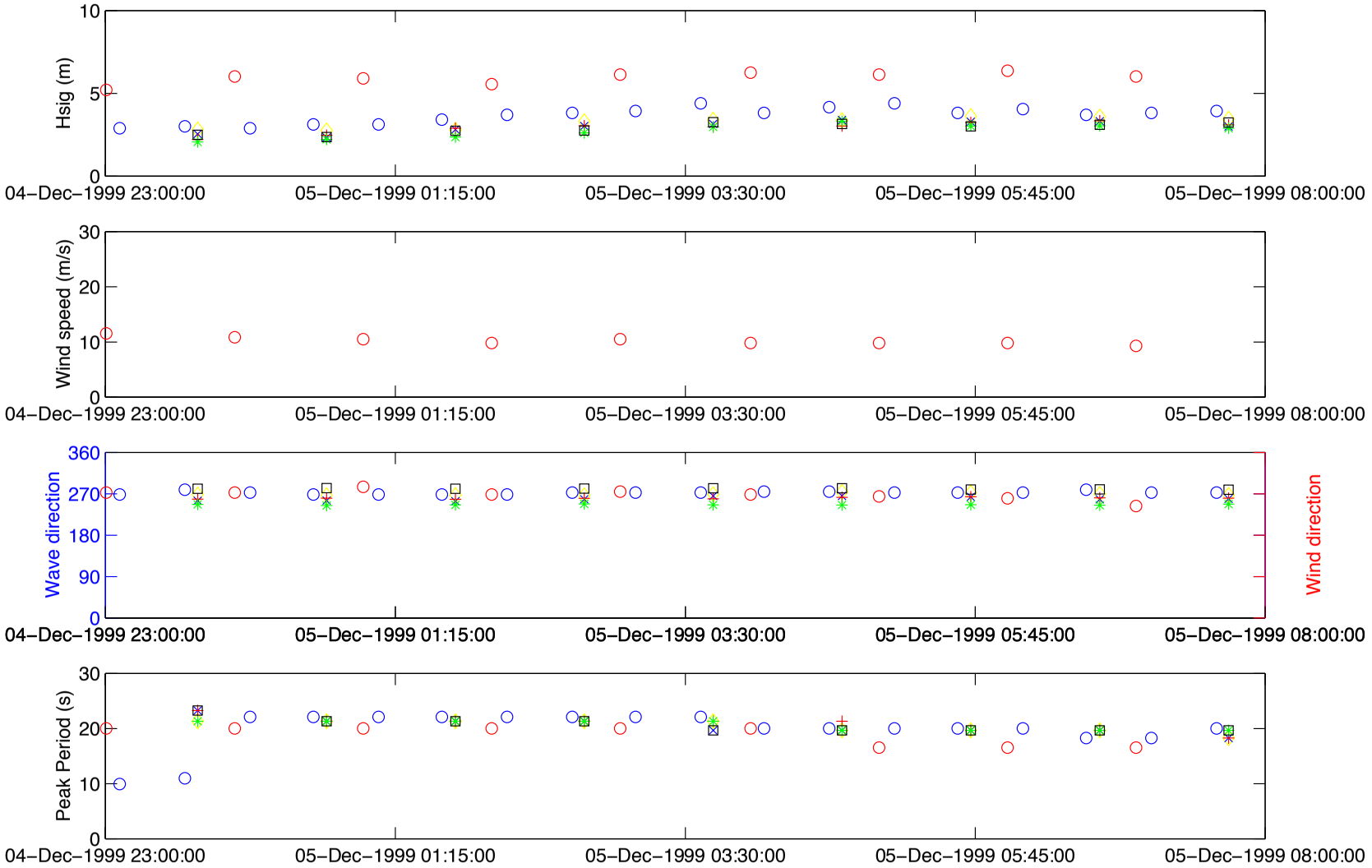

Figure 63. Plot of wave statistics and wind information between 12/04/99 23:00 and12/05/99 08:00. at 46005 (o), CDIP (o), ND (x), SD (+), SS (*), MD (□), NS (◇)

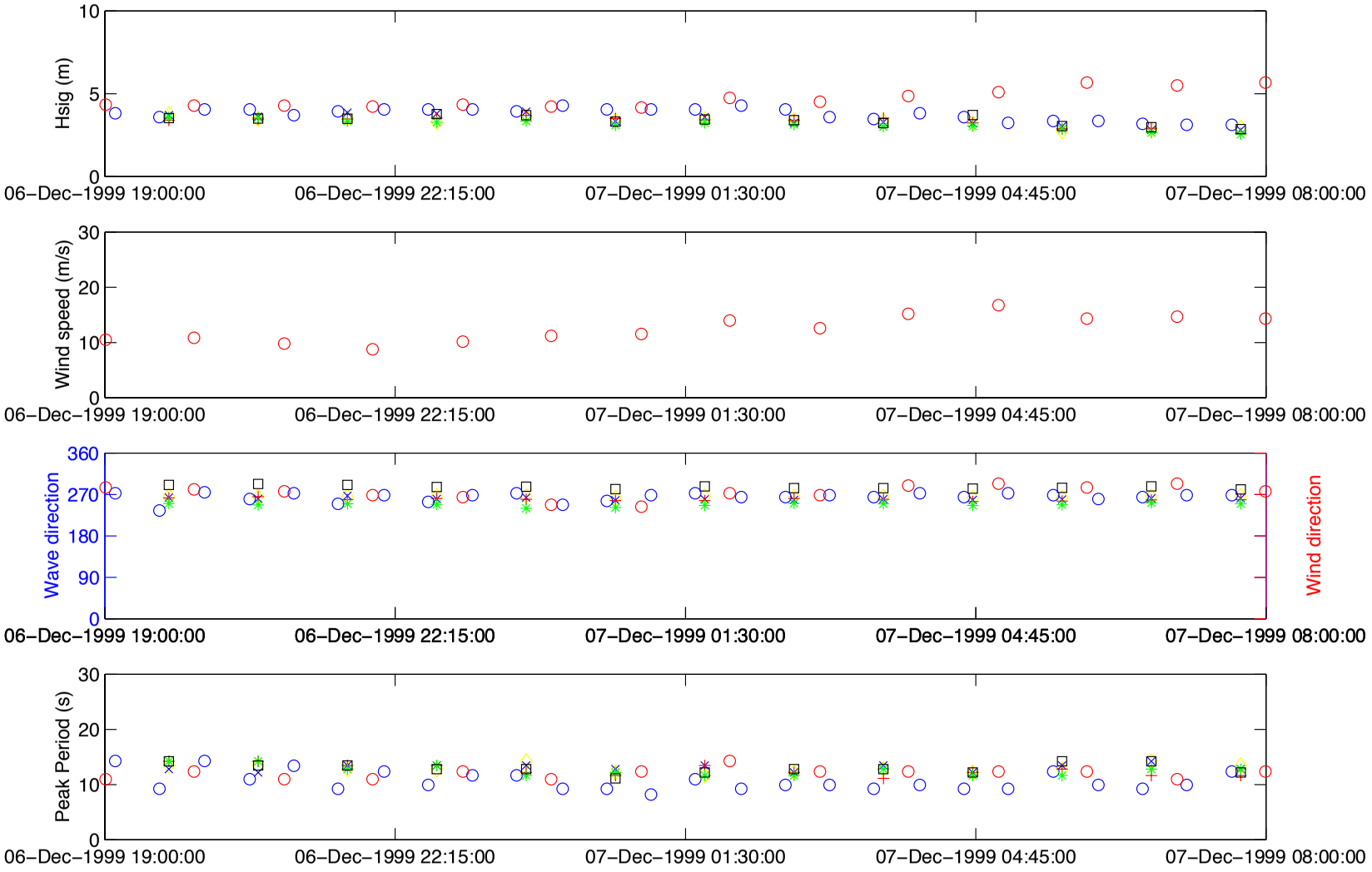

Figure 64. Plot of wave statistics and wind information between 12/06/99 19:00 and12/07/99 08:00.at 46005 ( ), CDIP ( ), ND ( ), SD ( ), SS ( ), MD ( ), NS ( )

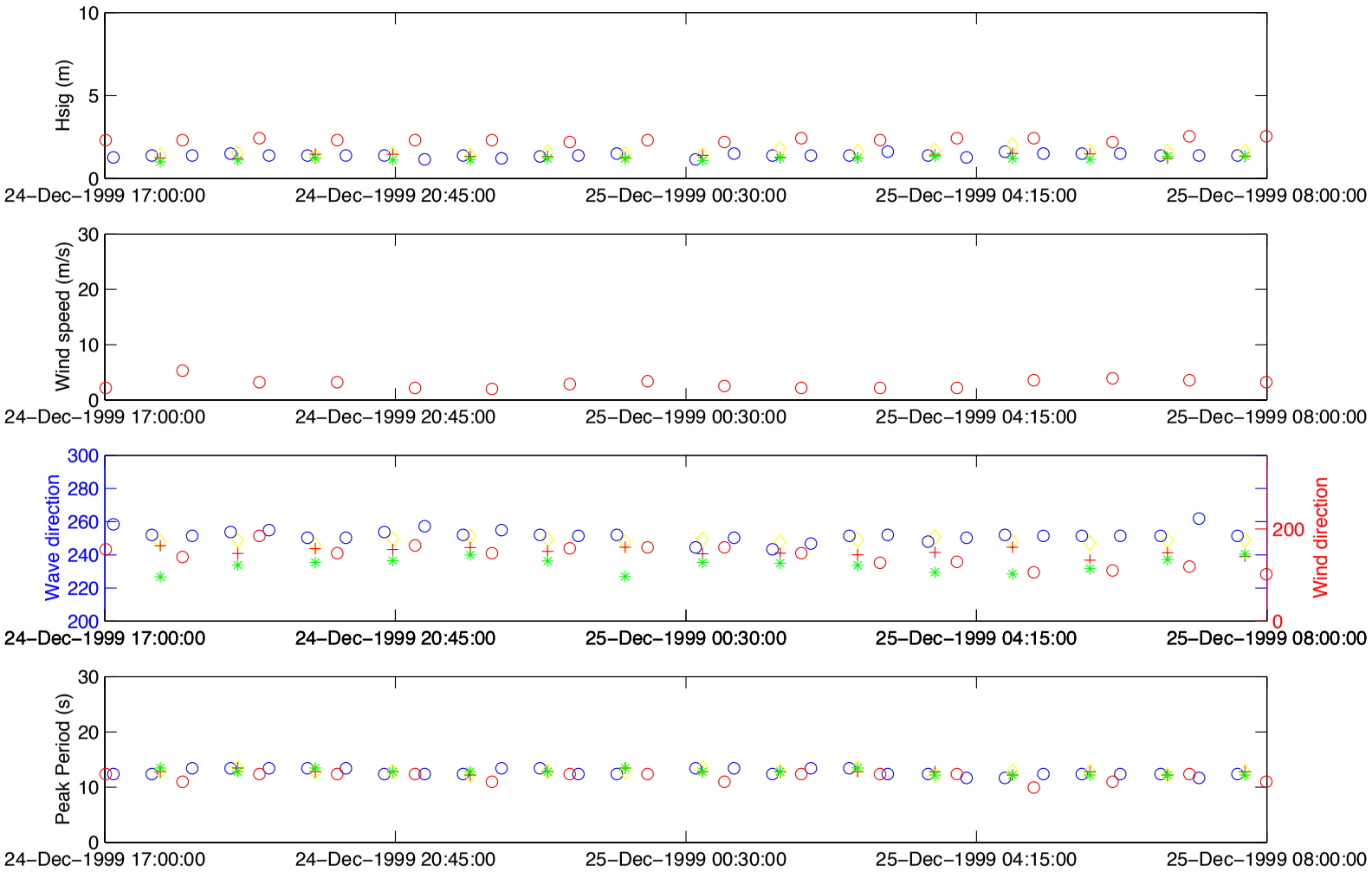

Figure 65. Plot of wave statistics and wind information between 12/24/99 17:00 and 12/25/99 08:00 at 46005 (o), CDIP (o), ND (×), SD (+), SS (*), MD (□), NS (◇)

Several sources of variability are evident in the time period between 11/20/99 00:00 and 11/20/99 19:00 shown in Figure 59. Significant wave height at 46005 was 4.6 m over the time period. Wave height at the offshore boundary decreases slightly over the time period to be modeled. This decrease in wave height will introduce some error into the average wave height used at the boundary condition. Wave height at the Grays Harbor moorings was near 3.7 m. Wave height at the tripods is relatively constant over the modeled time period. Therefore, little error would be expected by averaging field data over this time period. Mean wind speed was 9.9 ms^{-1}, although it varied slowly over 10 ms^{-1} during this time period, introducing some error into wind input for the model. Average wave direction at 46005 was 268^{o} and varied slightly over the time period modeled. This is expected to produce some error in wave direction at the model boundary. Peak period varies over several seconds at 46005 and at the tripods. This indicates that conditions are slightly usable over the time period to be modeled. Model results from this time period will provide an estimate of the amount of instability allowable in the boundary conditions before model error becomes great.

Figure 60 shows wave and wind conditions for the period between 11/22/99 12:00 and 11/23/99 12:00. Average wave height at 46005 over this time period was 3.67 m. Wave height decreased at the offshore buoy throughout this time period. This will introduce some error into input at the model boundary. A similar decrease in wave height was also evident at the tripods. The decrease in wave height may be the result of slackening wind during the time period. Average wind speed at 46005 was 5.75 ms^{-1} with a variable wind direction with a mean value of 275^{o}. This variation may result in some error in modeled wave direction. Wave height in the study area was near 3.1 m and wave direction varied slightly around 279^{o}. Peak period offshore was 12.7 s and near Grays Harbor it was 13.7 s. This variation in peak period may introduce some error into model input for peak frequency as well as peak direction.

Plots of burst averaged wave statistics from 12/01/99 02:00 to 12/02/99 00:00 are shown in Figure 61. Average significant wave height offshore was 3.4 m. Average significant wave height near the Grays Harbor study area was 2.5 m. Wave height offshore increased as a result of increasing wind speed. Similarly, wave height at the tripods also increased several hours after offshore wave height increased. This non-stationarity may decrease accuracy of model results. Average wind speed at 46005 10.4 ms^{-1} and wind direction was 226^{o}. Wind direction was

relatively constant throughout the time period. Peak wave direction at the CDIP buoy was 226°. Peak period was 10.1 s at 46005 and 9.6 s at the CDIP buoy. Wave direction varied slightly during this time period, most likely as a result of fluctuations in peak period. This variation in peak direction and peak period will increase error in model results.

Figure 62 shows wave and wind conditions between 12/02/99 14:00 and 12/03/99 05:00. Average significant wave height was relatively steady at 46005 during this period 4.5 m and 4.2 m at all moorings near Grays Harbor. In contrast, wind speed decreased throughout the time period, which may introduce some error into model results. Average wind speed at 46005 was 9.2 ms^{-1} and wind direction was 270°. Wave direction at the CDIP buoy was 262°. Wave and wind directions were relatively constant during the time period. Peak period at the offshore buoy was 12.4 s, while it was 10.1 s at the CDIP buoy. The disparity in peak period between offshore and near Grays Harbor may be a source of error model/data comparison. However, due to the low amount of variability during this time period, model results would be expected to be quite accurate.

Conditions between 12/04/99 23:00 and 12/05/99 08:00 are shown in Figure 63. Significant wave height at the offshore buoy was 5.9 m. Significant wave height at the Grays Harbor study location was 3.7 m and wave direction was 272°. Wave height is relatively constant offshore and near Grays Harbor. This will result in accurate input at the model boundary and

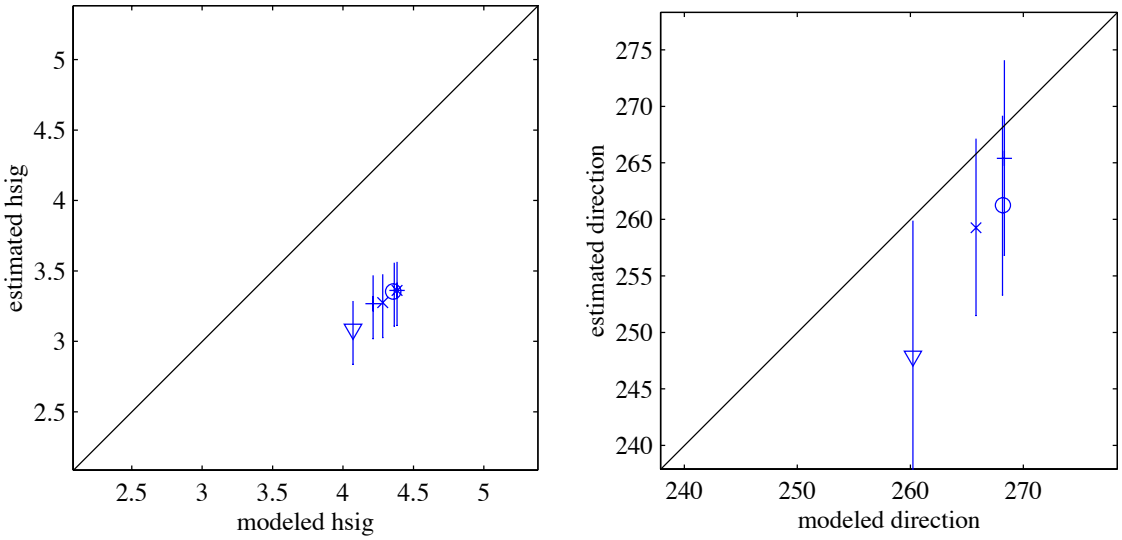

Figure 66. Model results from CR1 compared with field data.

Calibration Run Number	Whitecapping Formulation	Bottom Friction Formulation	Comments
1	Komen	JONSWAP	Default Values in the SWAN Model
	C_{DS2} = 2.36 x 10^{-5} s_{pm} = 3.02 x 10^{-5}	C_j = 0.038	
2	Komen	Madsen	Bottom friction formulation varied from JONSWAP formulation to Madsen formulation using default value for K_N
	C_{DS2} = 2.36 x 10^{-5} s_{pm} = 3.02 x 10^{-5}	K_N = 0.05 m	
3	Komen	Madsen	Value of K_N increased an order of magnitude from the default value
	C_{DS2} = 2.36 x 10^{-5} s_{pm} = 3.02 x 10^{-5}	K_N = 0.5 m	
4	Komen	Madsen	Whitecapping/wind input coefficient for dissipation increased according to Bender (1996)
	C_{DS2} = 2.95 x 10^{-5} s_{pm} = 3.02 x 10^{-5}	K_N = 0.05 m	
5	Komen	Madsen	Whitecapping/wind input coefficient for dissipation increased according to Komen (1984)
	C_{DS2} = 3.33 x 10^{-5} s_{pm} = 3.02 x 10^{-5}	K_N = 0.05 m	
6	Komen	Madsen	Whitecapping/wind input coefficient for dissipation increased according to Bender (1996)
	C_{DS2} = 5.0 x 10^{-5} s_{pm} = 3.02 x 10^{-5}	K_N = 0.05 m	
7	Komen	Madsen	Increase the value of wave steepness in the Komen formulation for whitecapping/wind input from the default according to Bender (1996)
	C_{DS2} = 2.36 x 10^{-5} s_{pm} = 4.57 x 10^{-5}	K_N = 0.05 m	
8	Janssen	JONSWAP	Whitecapping/wind input formulation varied from the default Komen formulation to the Janssen formulation
	C_{DS1} = 4.5 δ = 0.5	C_j = 0.038	
9	Janssen	Madsen	Whitecapping/wind input formulation varied from the default Komen formulation to the Janssen formulation and the bottom friction formulation is varied from the default to the Madsen formulation
	C_{DS1} = 4.5 δ = 0.5	K_N = 0.05 m	

Table 3. Description of calibration runs.

Calibration Run Number	Whitecapping Formulation		Bottom Friction Formulation	Comments
10	Janssen		Madsen	Whitecapping/wind input formulation varied from the default Komen formulation to the Janssen formulation with a value of 2.25 and the bottom friction formulation is varied from the default to the Madsen formulation
	C_{ds1} = 2.25	δ = 0.5	K_N = 0.05 m	
11	Janssen		JONSWAP	Whitecapping/wind input formulation varied from the default Komen formulation to the Janssen formulation with a value of 2.25
	C_{ds1} = 2.25	δ = 0.5	C_j = 0.038	
12	Komen		Madsen	Decrease the value of wave steepness in the Komen formulation for whitecapping/wind input from the default to test effect on wave height (optimization)
	$C_{ds2} = 2.36 \times 10^{-5}$	$s_{pm} = 1.47 \times 10^{-5}$	K_N = 0.05 m	
13	Komen		Madsen	Value of K_n decreased an order of magnitude from the default value
	$C_{ds2} = 2.36 \times 10^{-5}$	$s_{pm} = 3.02 \times 10^{-5}$	K_N = 0.005 m	
14	Komen		Madsen	Whitecapping/wind input coefficient for dissipation decreased to test effect on wave height (optimization)
	$C_{ds2} = 1.3 \times 10^{-5}$	$s_{pm} = 3.02 \times 10^{-5}$	K_N = 0.05 m	
15	Janssen		Madsen	Whitecapping/wind input formulation varied from the default Komen formulation to the Janssen formulation with a value of 6.0 and the bottom friction formulation is varied from the default to the Madsen formulation
	C_{ds1} = 6.0	δ = 0.5	K_N = 0.05 m	
16	Janssen		Madsen	Whitecapping/wind input formulation varied from the default Komen formulation to the Janssen formulation with a value of 9 and the bottom friction formulation is varied from the default to the Madsen formulation
	C_{ds1} = 9.0	δ = 0.5	K_N = 0.05 m	

Table 3 (cont'd). Description of calibration runs.

Calibration Run Number	Whitecapping Formulation		Bottom Friction Formulation	Comments
17	Janssen		Madsen	Whitecapping/wind input formulation varied from the default Komen formulation to the Janssen formulation with a value of 12 and the bottom friction formulation is varied from the default to the Madsen formulation
	C_{ds1} = 12.0	δ = 0.5	K_N = 0.05 m	
18	Janssen		Madsen	Same as CR 8, however a measured wave spectra (0.03-0.40 Hz) was used with directional spreading using the Donnelan-Banner method
	C_{ds1} = 4.5	δ = 0.5	K_N = 0.05 m	
19	Janssen		Madsen	Same as CR 8, however a measured wave spectra (0.03-0.40 Hz) was used with a constant directional spreading, ms = 7
	C_{ds1} = 4.5	δ = 0.5	K_N = 0.05 m	
20	Janssen		Madsen	Whitecapping/wind input formulation varied from the default Komen formulation to the Janssen formulation with a value of 12 and the bottom friction formulation is varied from the default to the Madsen formulation
	C_{ds1} = 20.0	δ = 0.5	K_N = 0.05 m	
21	Komen		Madsen	Decrease the value of wave steepness in the Komen formulation for whitecapping/wind input from the default to test effect on wave height (optimization)
	$C_{ds2} = 2.36 \times 10^{-5}$	$s_{pm} = 0.5 \times 10^{-5}$	K_N = 0.05 m	
22	Komen		Madsen	Decrease the value of wave steepness in the Komen formulation for whitecapping/wind input from the default to test effect on wave height (optimization)
	$C_{ds2} = 5.0 \times 10^{-5}$	$s_{pm} = 0.5 \times 10^{-5}$	K_N = 0.05 m	
23	Janssen		Madsen	Same as CR 8, however a constant directional spreading of ms = 1 was used
	C_{ds1} = 4.5	δ = 0.5	K_N = 0.05 m	
24	Janssen		Madsen	Same as CR 8, however a constant directional spreading of ms = 14 was used
	C_{ds1} = 4.5	δ = 0.5	K_N = 0.05 m	

Table 3 (cont'd). Description of calibration runs.

Calibration Run Number	Rms	SI	MPI	OPI
1	0.99	0.30	0.28	0.21
2	0.87	0.27	0.37	0.19
3	0.32	0.10	0.77	0.07
4	0.80	0.24	0.42	0.17
5	0.76	0.23	0.45	0.16
6	0.66	0.20	0.52	0.14
7	1.14	0.35	0.17	0.24
8	0.42	0.13	0.69	0.09
9	0.61	0.19	0.56	0.13
10	0.56	0.17	0.59	0.12
11	0.71	0.22	0.49	0.15
12	0.39	0.12	0.72	0.08
13	0.99	0.30	0.28	0.21
14	0.93	0.28	0.00	0.22
15	0.36	0.11	0.74	0.08
16	0.24	0.07	0.82	0.05
17	0.15	0.05	0.89	0.03
18	0.89	0.27	0.35	0.19
19	0.53	0.16	0.61	0.11
20	0.00	0.00	1.00	0.00
21	-0.50	-0.15	1.37	-0.11
22	-0.27	-0.08	1.20	-0.06
23	0.17	0.05	0.89	0.04
24	0.43	0.13	0.69	0.09

Table 4. Error statistics from calibration model runs.

for comparison with model results. Wave direction is constant throughout the modeled time period, providing accurate conditions at the boundary and for model comparison. Wind speed and direction at this location were 10.2 ms^{-1} and 268^{o}, respectively. Wind speed is constant and in the same direction as wave direction, indicating those boundary conditions should be accurate. Average peak period at 46005 was 18.9 s while peak period was 19.8 s. However, wave period is nearly 10 s shorter at 46005 during the first two hours of the experiment. This will decrease the average peak period for the time period modeled and induce some error into the model.

Figure 64 shows plots of wave and wind conditions from 12/06/99 19:00 to 12/07/99 08:00. Average significant wave height at the offshore buoy was 4.6 m while wave height at the CDIP buoy was 3.7 m. Average wind speed and direction at 46005 were 12.3 ms^{-1} and 275^{o}, respectively. Wave height increased during the second half of the time period due to increasing wind speed. This increase in wave height and wind speed at the model boundary will introduce error into the model run. Wave direction at the CDIP buoy was 268^{o}. Wave and wind directions

were relatively aligned and constant throughout the deployment. Peak period at 46005 was 12.2 s and 11.2 s at the CDIP buoy. Peak period at the model boundary may be inaccurate because peak period was slightly variable offshore and lower at Grays Harbor.

Wave and wind conditions between 12/24/99 17:00 and 12/25/99 08:00 are shown in Figure 65. Wave height at 46005 is constant near 2.3 m though out the time period. Wave height in the Grays Harbor study area is near 1.4 m and constant throughout the experiment. Steady boundary conditions are expected to produce accurate model results. Steady conditions at the tripods also provide good data for comparison with model results. Offshore wind direction was constant and blowing from the southeast. Wind speed at 46005 was 3.0 ms^{-1}. Wave direction varied between the moorings at Grays Harbor. Wave direction was somewhat variable during the time period and wave direction was variable and different from wave direction. The variability of wave and wind direction is expected to introduce error at the boundary condition and at the tripods. Peak period was constant near 12 s throughout the time period indicating accurate peak period at the model boundary and accurate peak period at Grays Harbor for comparison with model results.

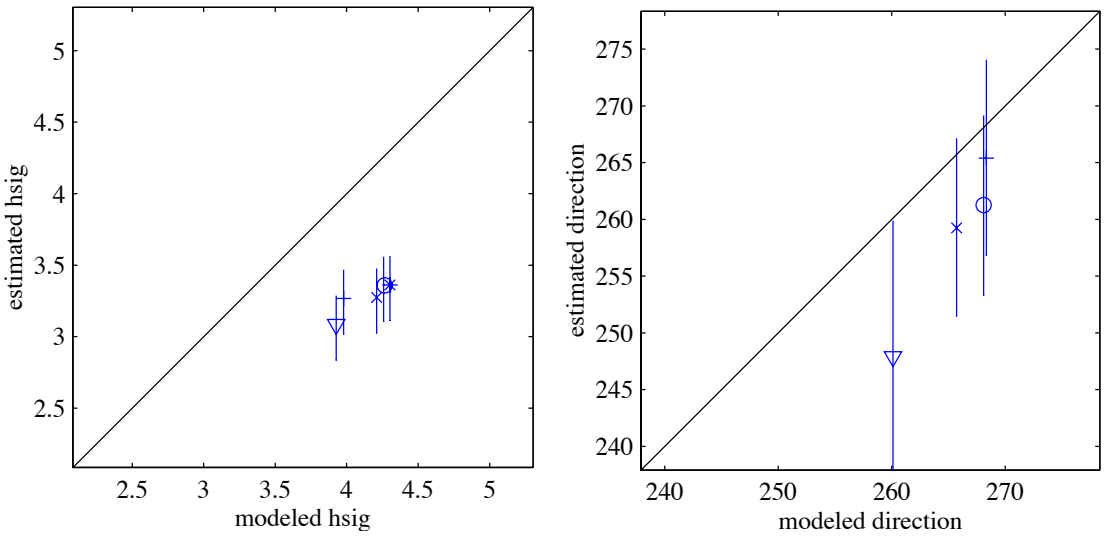

Figure 67. Model results from CR2 compared with field data.

Calibration Study

The purpose of the SWAN model calibration was to choose correct formulations for modeling wave characteristics along the southwest Washington coast. The time period for the SWAN calibration study was chosen according to several criteria. Relatively intermediate conditions in terms of significant wave height, peak period, and peak direction were used for model calibration. Conditions remained stable over the time period used for calibration so uncertainty was not introduced due to variable wind conditions or changing wave conditions. The NDBC buoy and CDIP buoy used to determine model boundary conditions were required to function throughout the calibration time period. The time period between 12/6/99 19:00 and 12/7/99 8:00 met these criteria and was used for the calibration run. Conditions during this time period are plotted in Figure 64. Significant wave height at 46005 was 4.2 m. Peak period was 12 s and average wind speed was 12.3 ms^{-1} with wind direction from 270°. Wave direction at the model boundary was collected at the Grays Harbor CDIP buoy. The measured wave direction refracted to the offshore boundary according to Snell's Law was 271°. Estimated wave heights at the tripod locations were lower than the offshore buoy due to dissipation. Wave direction at the tripods varied between 245° and 270°. Bathymetry was a nested grid of 750 m resolution and 500 m resolution. The model was initially run with the SWAN model's default formulations. Results

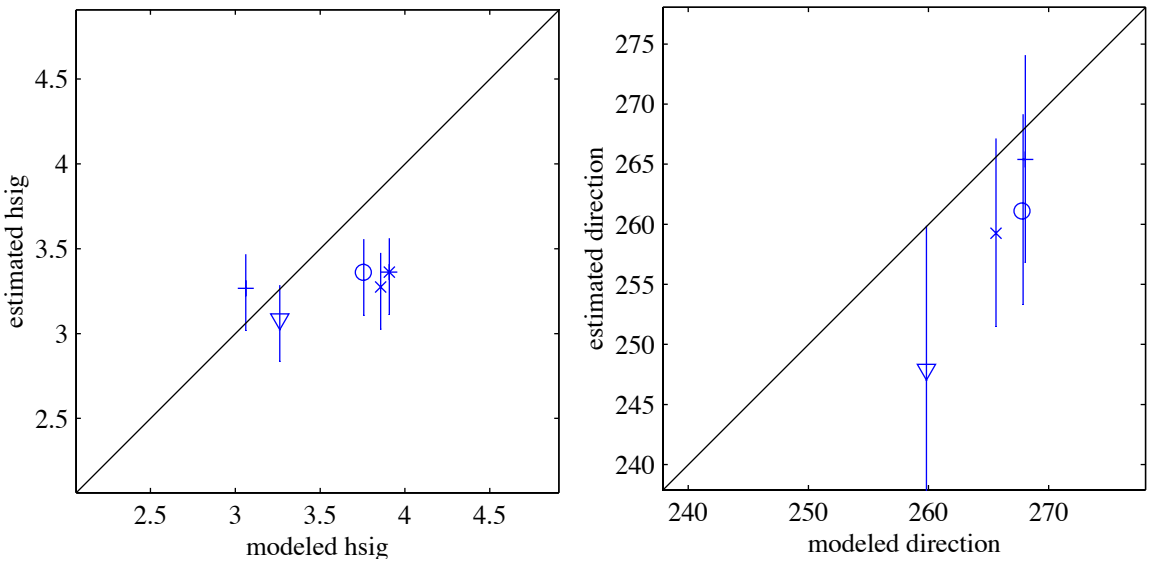

Figure 68. Model results from CR3 compared with field data.

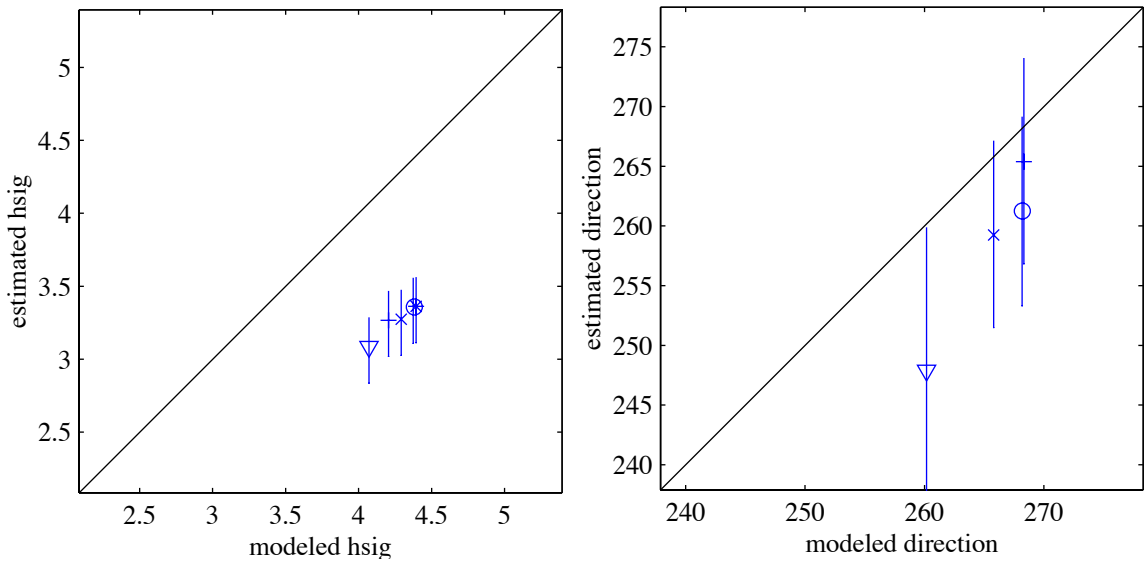

Figure 69. Model results from CR13 compared with field data.

from this initial run (CR1) at the station locations are plotted in Figure 65 along the x-axis with estimated wave height and direction plotted along the y-axis. Model results were statistically compared with estimated wave height using equations in the methods section. The statistical comparisons show a weak relationship between modeled and estimated wave height. RMS error is very high. The RMS-error normalized by mean of observed wave parameters, or SI, was an order of magnitude larger than an acceptable value. The MPI, or comparison between a perfect model run and rms error of the model run relative to the rms of observed changes, is very low.

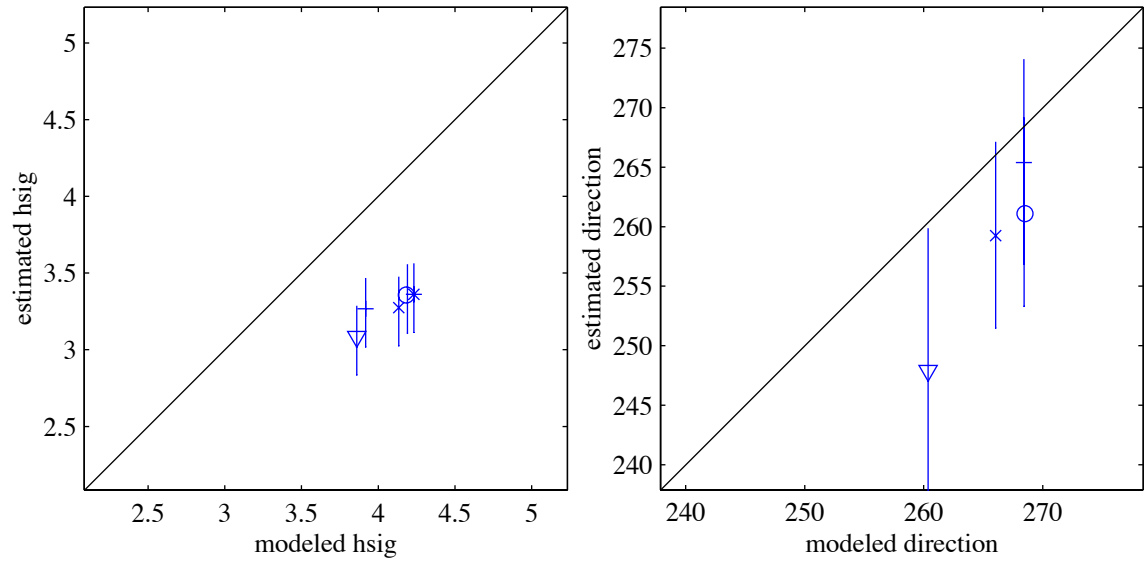

Figure 70. Model results from CR4 compared with field data.

The OPI, which expresses error in terms of model input is high. Modeled wave height from CR1 was approximately 25% greater than estimated wave height. Modeled wave direction is within 11° of estimated wave direction at all stations.

As noted in the methods, variation of two formulations with in the SWAN model, the formulation for dissipation due to bottom friction and dissipation due to whitecapping, produced greater than 3% changes in wave height. After producing an initial run based on the SWAN model's default formulations these two formulations were varied in small steps within ranges recommended in the literature. Two formulations for bottom friction were tested while the coefficient for dissipation due to whitecapping in the Komen formulation for wind input/whitecapping

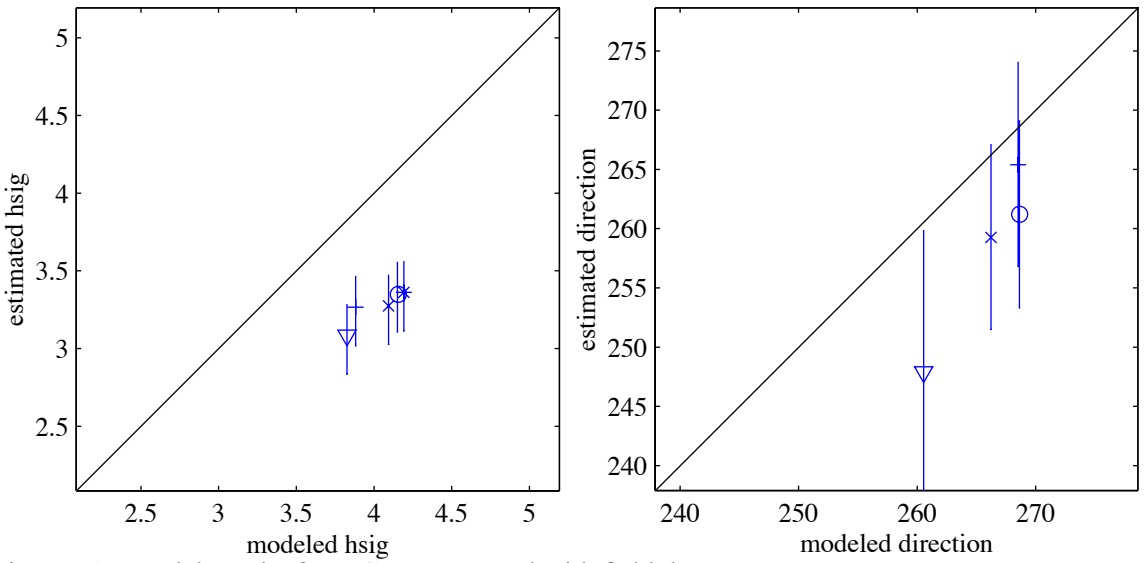

Figure 71. Model results from CR5 compared with field data.

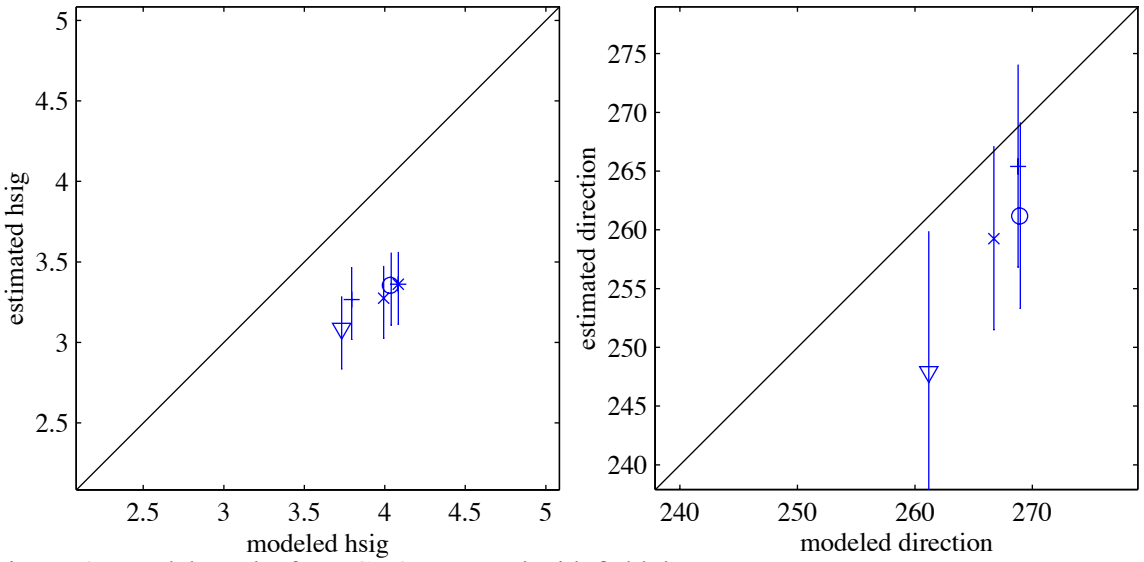

Figure72. Model results from CR6 compared with field data.

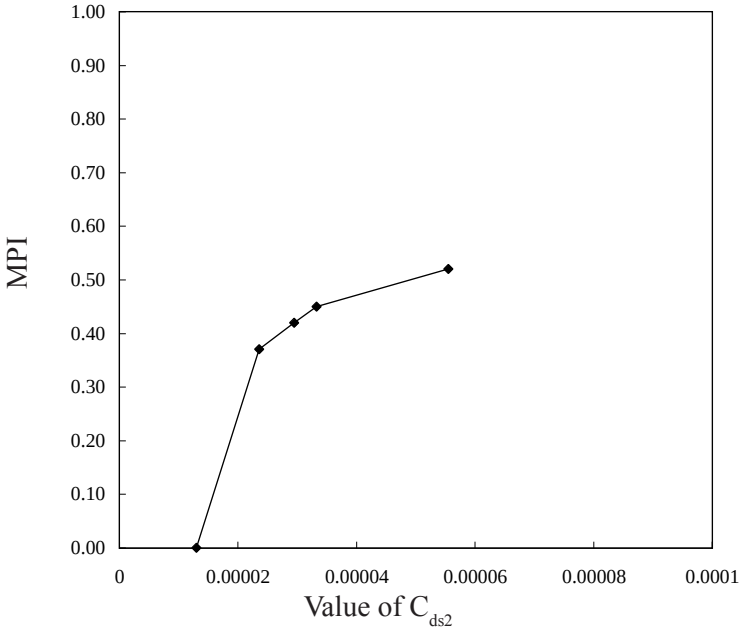

Figure 73. Plot showing MPI for CR4, CR5,CR6, and CR14 (Table 3) where each model run used a different value for C_{ds2} in the Komen formulation for whitecapping. Model performance is proportional to value of C_{ds2}. However, values of MPI show that for all values of C_{ds2}, the Komen formulation for whitecapping does not reproduce field data well.

(C_{ds2}) was held constant. Modeled wave heights improved slightly in CR2 when using the Madsen drag law formulation for bottom friction with a roughness value (K_N) of 0.05 rather than empirical JONSWAP formulation for bottom friction developed for swell waves in the North Sea (Figure 67). Weber (1991) assumes that K_N is two to four times ripple height. Therefore, ripple height in this run is equivalent to 0.025 m to 0.013 m. The goodness of fit parameter in CR2 was barely improved relative to CR1. The RMS-error slightly decreased. Similarly, SI, MPI, and OPI were slightly improved upon. Wave direction in CR2 was not significantly different from CR1.

The purpose of CR3 was to study the effect of a very large bottom roughness length on wave height and direction. In CR3, the Madsen formulation for bottom friction was used, with Kn = 0.5. The formulation for bottom friction was the Komen formulation where $C_{ds2} = 2.36 \times 10^{-5}$ and the value for wave steepness for a Pierson-Moskowitz spectrum ($\tilde{s}_{pm}$) was set to the default of 3.02×10^{-3}. Modeled wave height was decreased from the default run when a large value for bottom friction was used. At NS and SS, wave modeled wave heights were lower than wave height estimated from field data. Although the statistical comparisons between modeled and estimated wave heights are improved relative to CR1, it is misleading because K_N maybe

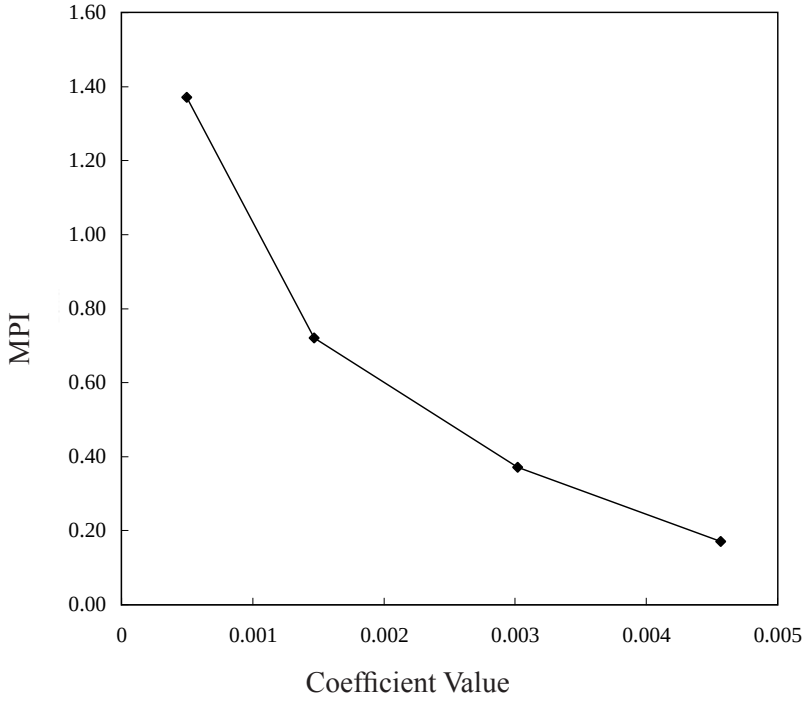

Figure 74. Plot showing MPI for CR2, CR7,CR12, and CR21 (Table 3) where each model run used a different value for $\tilde{s}_{pm}$ in the Komen formulation for whitecapping. Model performance is inversely proportional to value of $\tilde{s}_{pm}$. However, values of MPI demostrate the sensitivity of the SWAN model to the value of $\tilde{s}_{pm.}$

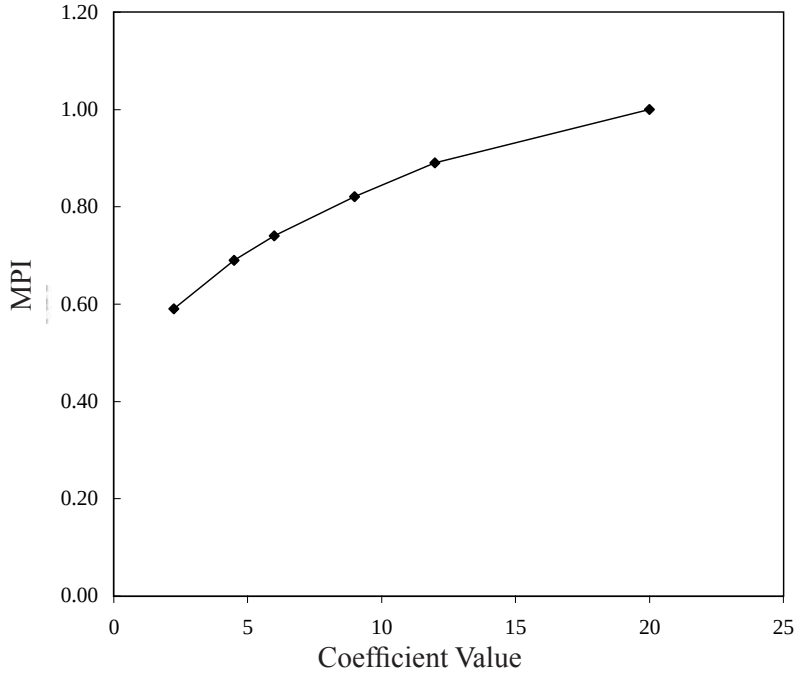

Figure 75. Plot showing MPI for CR9, CR10, CR15, CR16, CR17, and CR18 (Table 3) where each model run used a different value for C_{ds1} in the Janssen formulation for whitecapping. Model performance is proportional to value of C_{ds1}.

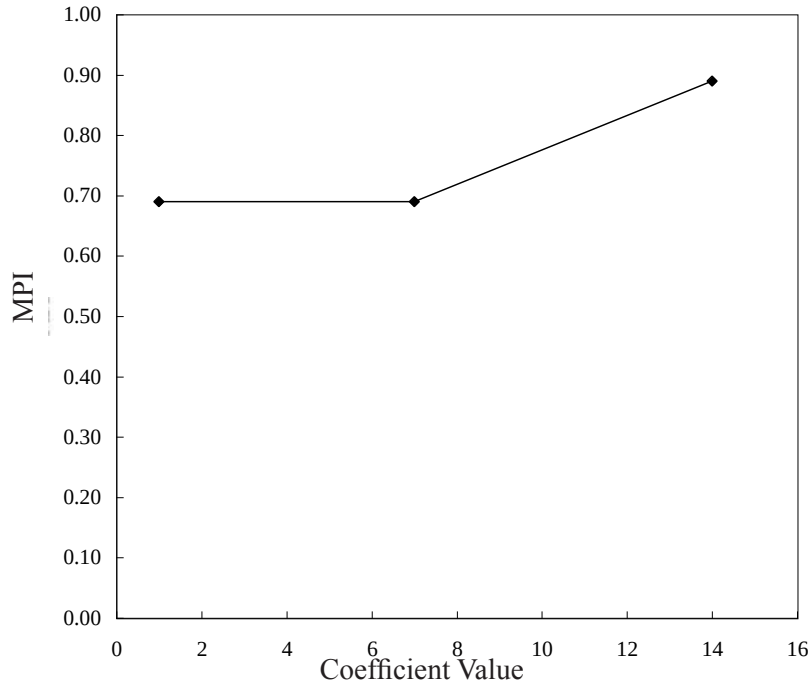

Figure 76. Plot showing MPI for CR8, CR23, and CR24 (Table 3) where each model run used a different value for directional spreading. Model performance increases with value of ms.

unrealistically large for most of the model domain. This would imply a roughness length of 0.25 m to 0.13 m which may be the case for areas of the model domain where large ripples occur, but would certainly be an overestimate for most of the model domain (Twitchell et al, 2000).

In contrast to CR3, the objective of CR13 was determining the effect of a very small bottom roughness length on model results. The Madsen bottom friction formulation with a bottom roughness value of 0.005 m. This value of Kn represents a muddy bottom. The whitecapping/wind input formulation used in this model run is the Komen formulation with default values. Modeled wave height is slightly greater than that produced by the default run. Wave height is over predicted, which may be expected because the value for bottom friction is very low. Statistical comparisons between the field data and the model results are very similar those of the default run. CR13 does not reproduce field data as well as CR2, in which a realistic value for K_N is used.

CR4 tested the effect of varying the coefficient for rate of dissipation in the Komen formulation for whitecapping (C_{ds2}). Formulation for bottom friction in CR4 was Madsen K_N = 0.05 m. C_{ds2} was set to 2.95 x 10^{-5} as suggested by Bender (1996). Statistical comparisons between modeled and estimated wave heights were slightly improved relative to CR2 where

C_{ds2} = 2.36 x 10^{-5}. CR5 and CR6 also evaluated the effect of increasing C_{ds2} according to recommendation in Bender (1996) and Komen et al (1984). In CR5 C_{ds2} was 3.3 x 10^{-5} and the Madsen bottom friction formulation was used where K_N = 0.05. Statistical comparisons were improved slightly relative to CR2. However, error in CR5 greater than in CR4. C_{ds2} in CR6 was 5.0 x 10^{-5}, a rather large value for dissipation due to whitecapping. Statistical comparisons were slightly improved relative to previous runs, however, the value of C_{ds2} is larger than recommended by the literature and the improvement in modeled wave height is not significant. Wave direction varied little in CR4, CR5, and CR6.

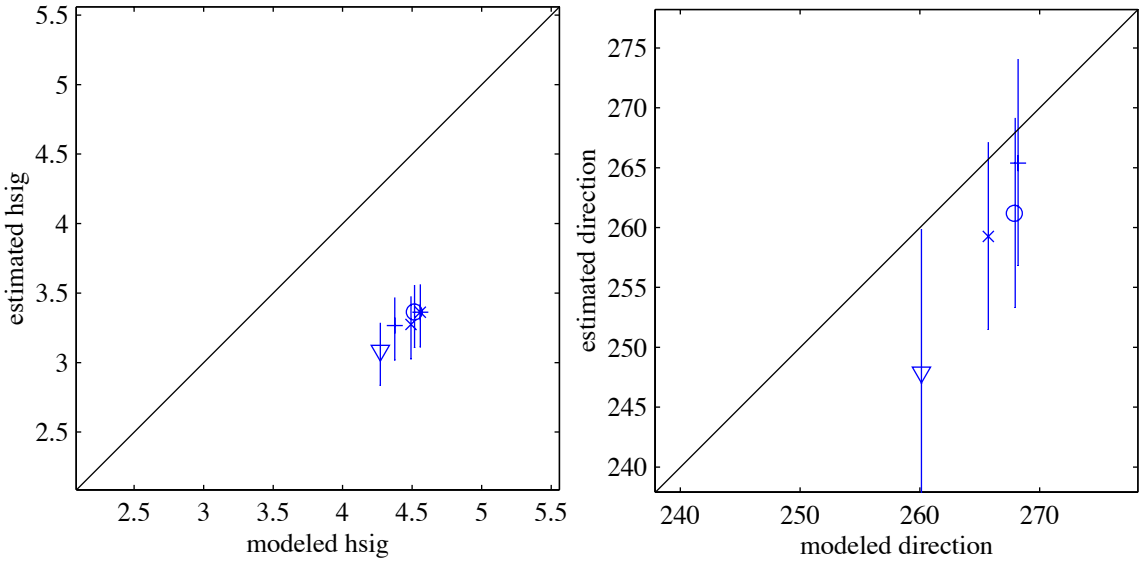

Figure 77. Model results from CR14 compared with field data.

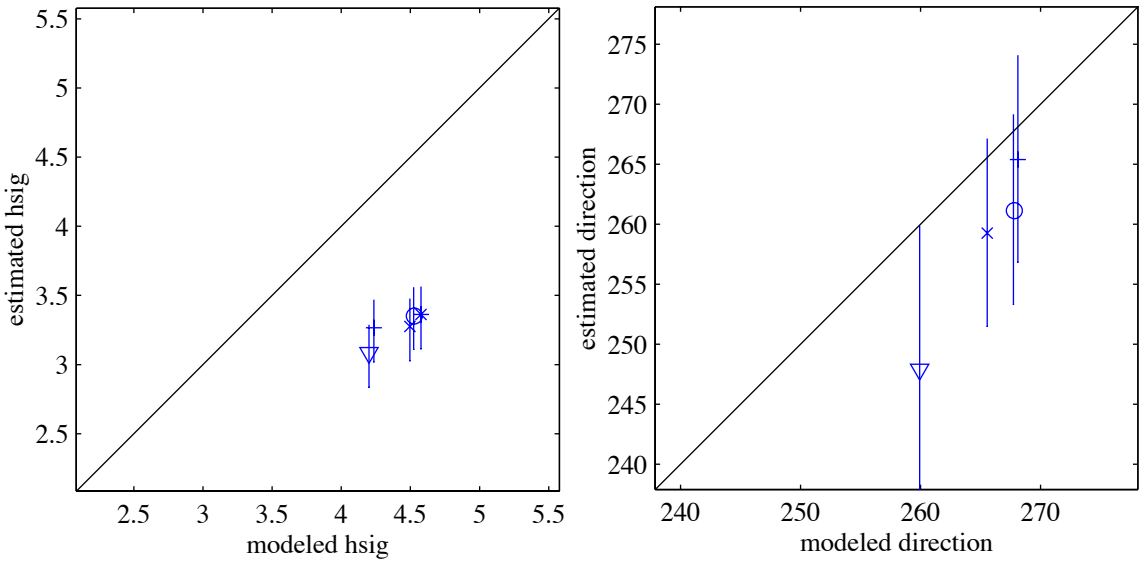

Figure 78. Model results from CR7 compared with field data.

In an effort to determine the best value for C_{ds2}, its value was set below the default value to 1.3 x 10^{-5} in CR14. Model results relative to field data were not improved by decreasing the value of C_{ds2}. CR2, CR4,CR5, and CR6 produced better results than CR14. Wave direction was unaffected by the change in the value of C_{ds2}.

Within the Komen formulation for bottom friction is the value of s_{pm}. Run CR7 tested the effect of increasing the value for wave steepness from the default value of 3.02 x 10^{-3} to 4.57 x 10^{-3} as suggested by Bender (1996). This resulted in slightly worse statistical comparisons relative CR2. Wave direction was similar to CR2.

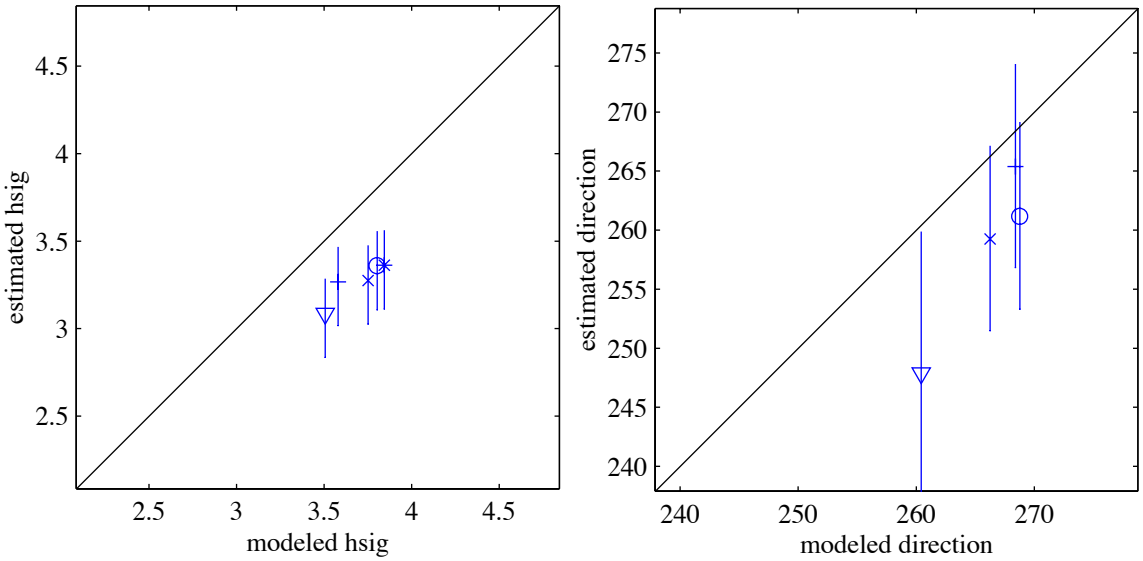

Figure 79. Model results from CR8 compared with field data.

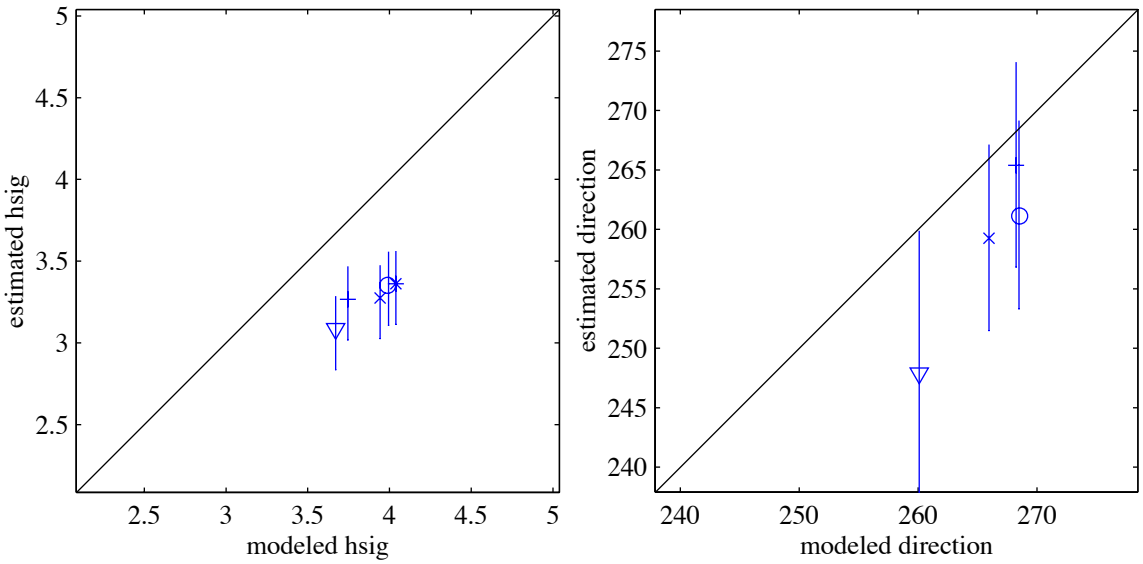

Figure 80. Model results from CR9 compared with field data.

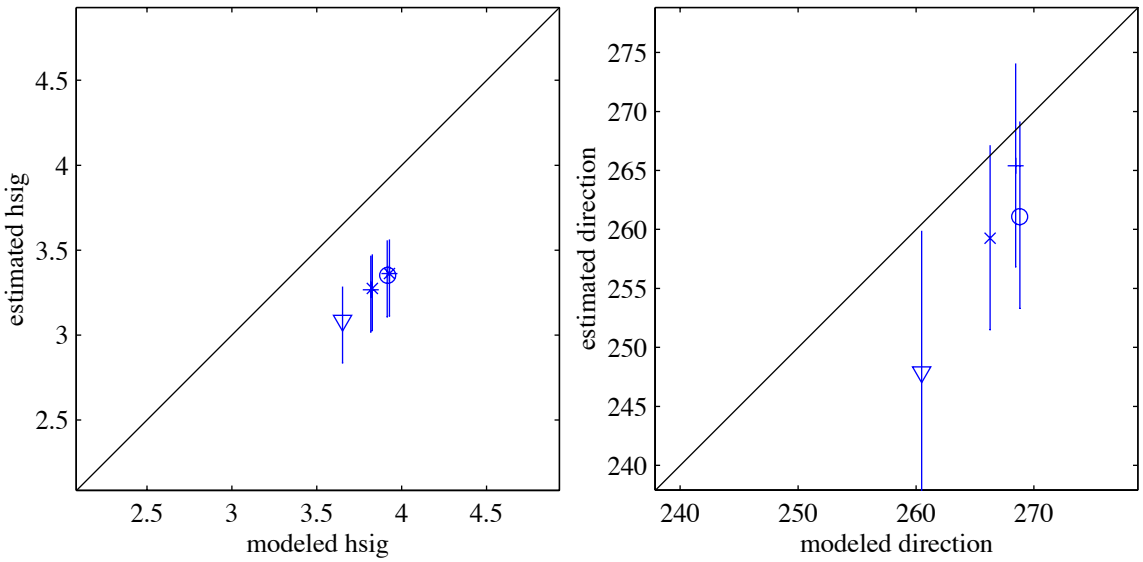

Figure 81. Model results from CR10 compared with field data.

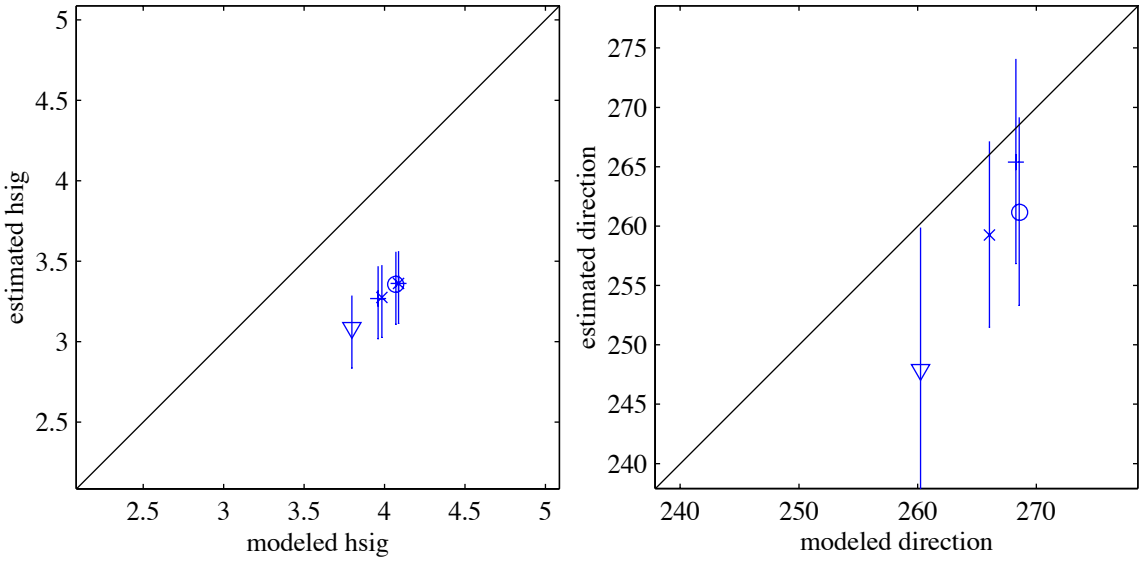

Figure 82. Model results from CR11 compared with field data.

The five calibration runs studied the effect of utilizing the Janssen formulation for dissipation due to whitecapping. In CR8, the coefficient dissipation due to whitecapping (C_{ds1}) was set to 4.5 and δ was 0.5. The Madsen bottom friction formulation with K_N = 0.05 was utilized in CR8. The use of the Janssen formulation for whitecapping improved modeled wave height significantly. All statistical comparisons of wave height were improved relative to CR2. Wave direction was similar to previous runs. The same formulation for whitecapping was used in CR9, while bottom friction was set to the JONSWAP formulation with a coefficient of 0.038 for swell

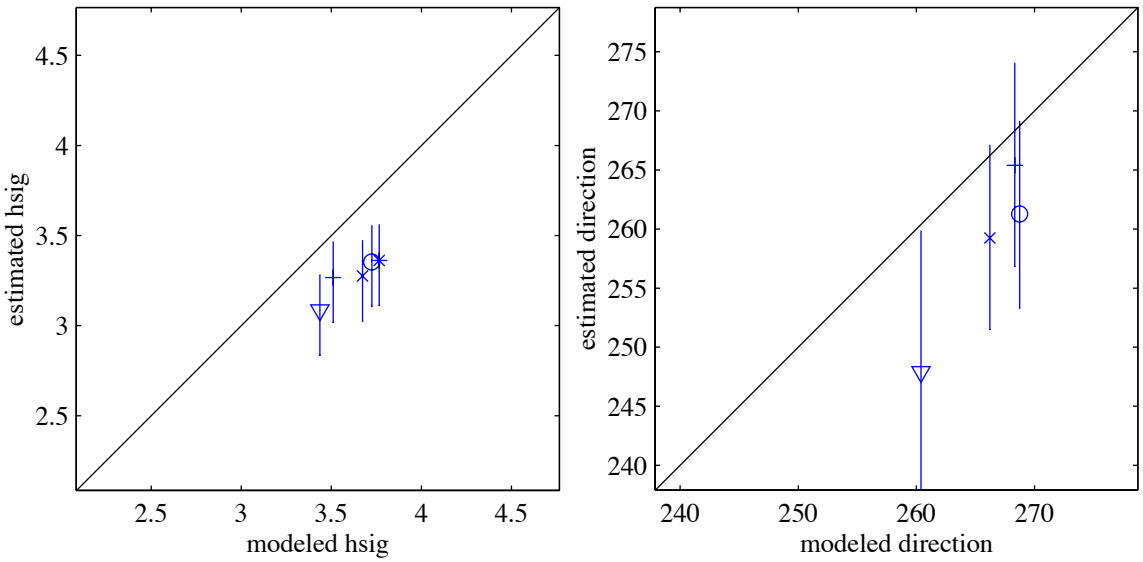

Figure 83. Model results from CR15 compared with field data.

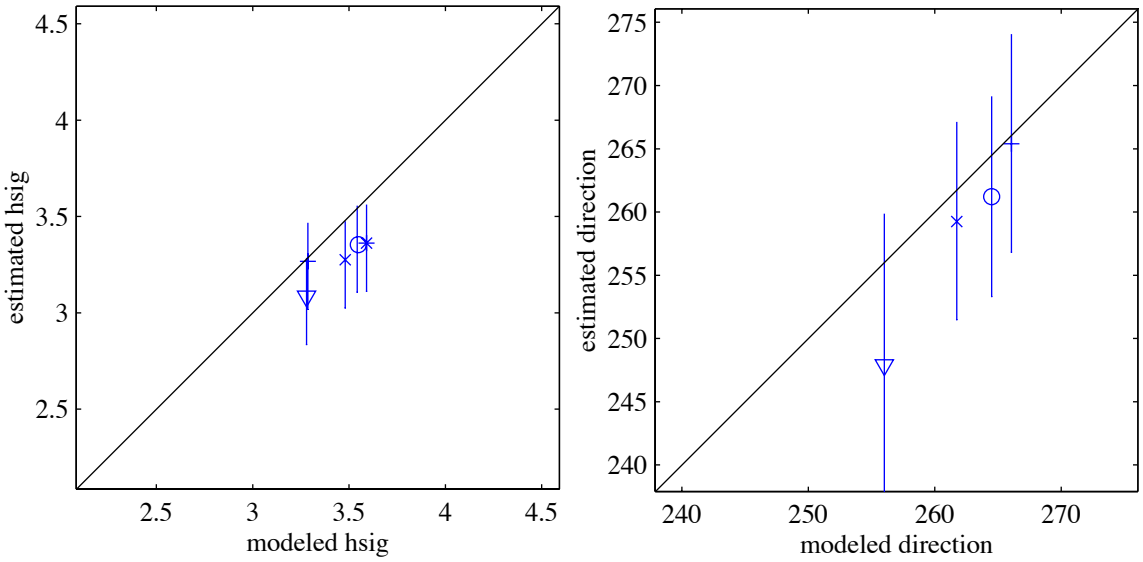

Figure 84. Model results from CR23 compared with field data.

conditions. This resulted in slightly worse statistical comparisons with estimated wave height relative to CR8, but improved statistical comparisons relative to CR1. CR10 and CR11 used a value of 2.25 for C_{ds1} and 0.5 for δ. Madsen bottom friction formulation with K_N value of 0.05m was used in CR10. Statistical comparisons were not improved relative to CR8, where C_{ds2} is 5.0×10^{-5} and $K_N = 0.05$, but was significantly better than CR2. CR11 used the JONSWAP formulation for bottom friction with swell waves. Statistical comparisons were not improved over CR8 or CR10, but significantly better CR2. CR15 tested the effect of increasing the value of C_{ds2} to 6 while using the Madsen formulation for bottom friction with a K_N value of 0.05 m.

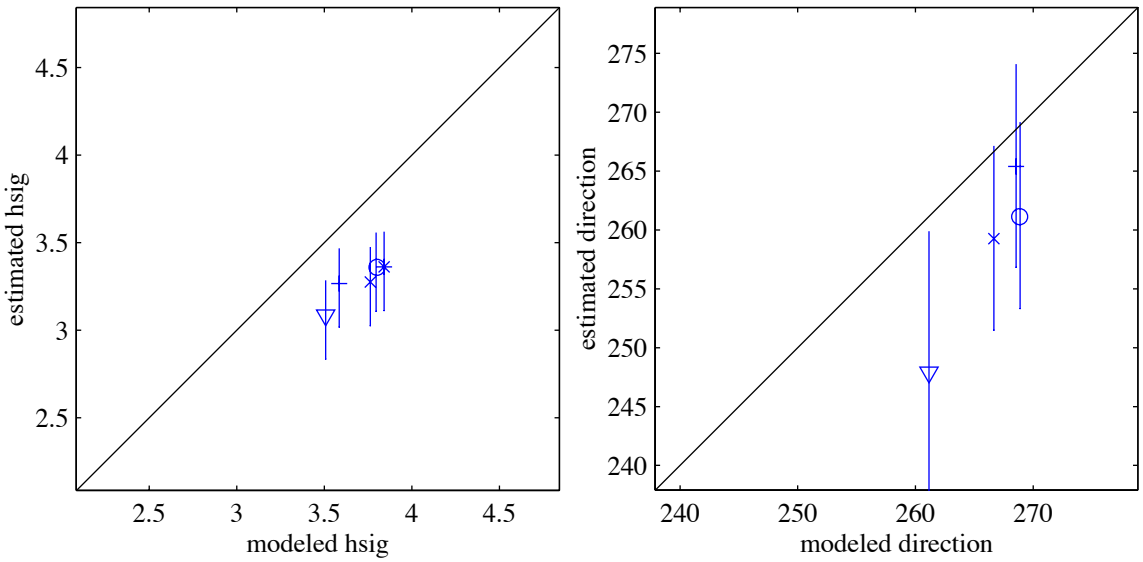

Figure 85. Model results from CR24 compared with field data.

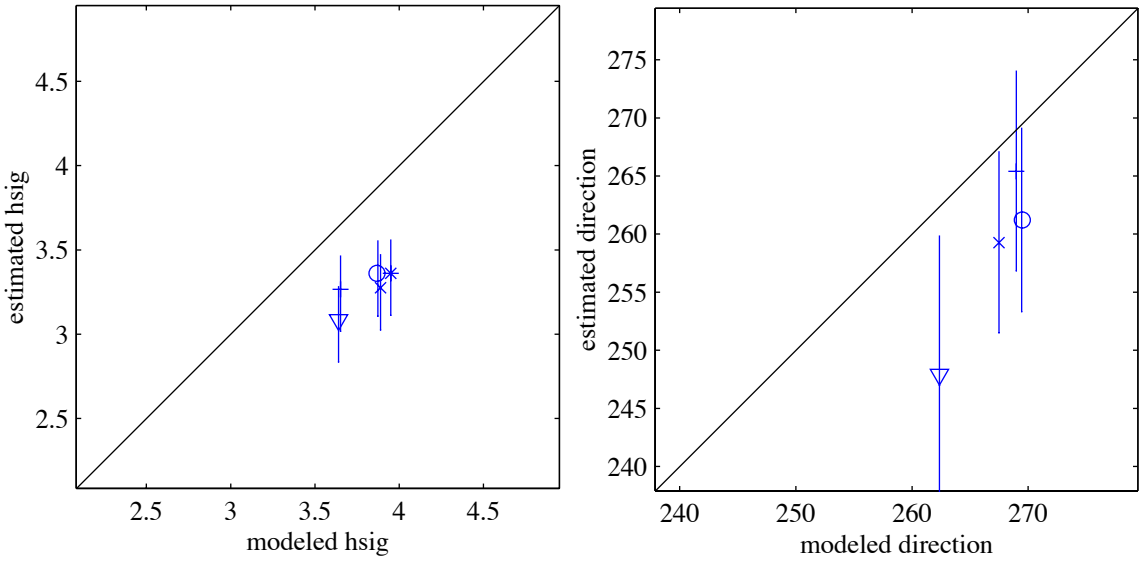

Figure 86. Model results from CR18 compared with field data.

The comparison between modeled wave height and wave height estimated from field data was improved over runs where C_{ds2} was equal to or less than the default value. Wave height was unaffected by increasing the value of C_{ds2}.

The modeler sets directional spreading in the SWAN model. The value of directional spreading in the calibration runs was constant at ms = 7. This value was calculated for the peak period using the Donnelan-Banner method. The object of CR23 and CR24 was to compare model accuracy using directional spreading values of ms = 1 and 14, respectively. ms = 1 indicates

very low direction spreading expected from a wind sea. ms values of 7 and 14 indicate greater directional spreading resulting from swell conditions. Wave heights were slightly over predicted using ms = 1 (Figure 84). Error statistics for wave height and direction indicate an excellent model run. Increasing the value of ms to 14 in CR24 increases model error for wave height and direction, relative to CR23. However model results from CR24 for significant wave height are identical to results for CR8. Modeled wave direction was slightly better predicted by CR8 than CR24.

The SWAN model may be initialized with a parameterized wave spectrum, as in all prior model runs in the calibration study or with an observed wave spectrum and a constant or variable value for directional spreading. The purpose of CR18 was to model the same frequencies used in other calibration runs with an observed wave spectrum, rather than the JONSWAP spectrum and a constant value for directional spreading. Significant wave height was over predicted in CR18 (Figure 86) and model performance decreased slightly relative to CR8, where the JONSWAP spectrum was used. Modeled wave direction was slightly better predicted in CR8 than CR18. An observed frequency spectrum and a variable value for directional spreading calculated using the Donnelan-Banner method was used in CR19. Error increased for wave height and direction in CR19 relative to CR8 and CR18 (Table 4).

Based on model results from the calibration study, formulations for the SWAN model on the southwest Washington inner continental shelf were chosen. The Janssen formulation for wind input/whitecapping was utilized. This formulation produced greater dissipation of wave energy resulting in modeled wave height nearer to estimated wave height than modeled wave height using the Komen formulation. Within the Janssen formulation, the value of C_{ds1} remained at the default value of 4.5 as it produced acceptable results. The least empirical and most dissipative formulation for bottom friction, the Madsen formulation, was adopted for the southwest Washington continental shelf. The bottom roughness value (K_N) was set to 0.05, representing a sandy, rippled bottom. Value of directional spreading was set to ms = 7, from the Donnelan-Banner method for the calibration study. This value may be altered for conditions where directional spreading is greater, but need not be adjusted for less directional spreading.

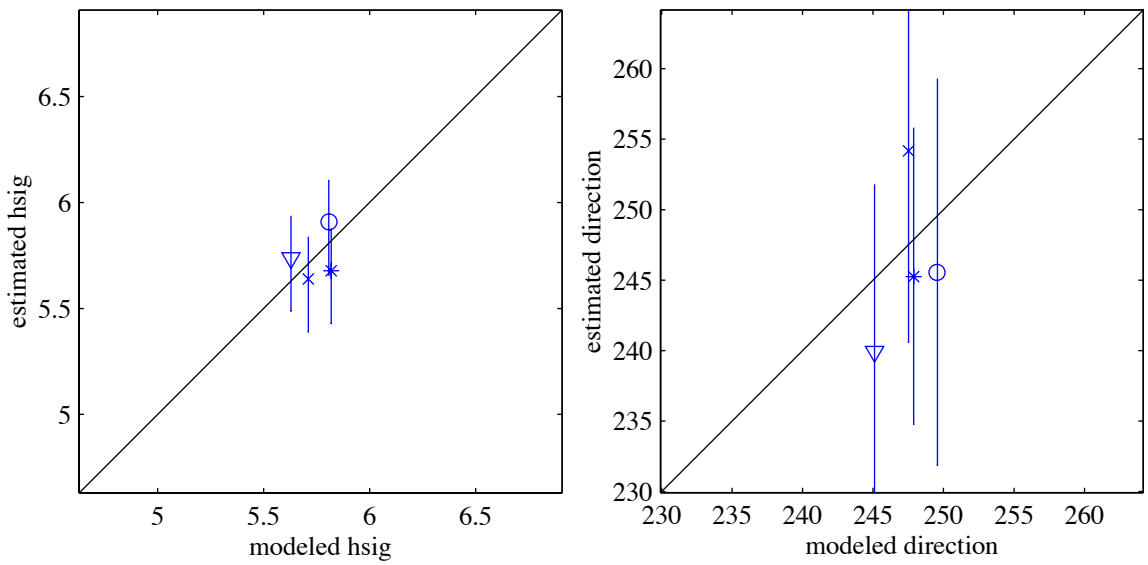

Figure 87. Plot of modeled significant wave height and direction against field data for the time period between 10/28/99 12:00 and 10/29/99 02:00.

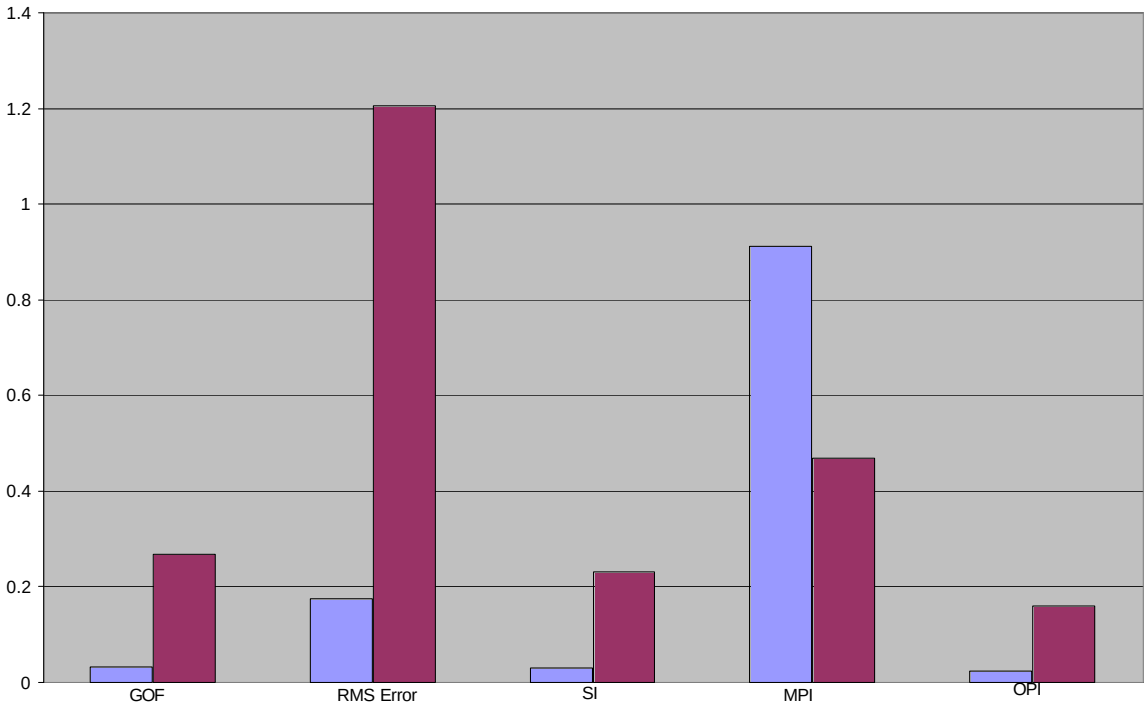

Figure 88. Reduction in model error for time period between 10/28/99 12:00 and 10/29/99 02:00 due to changes in model formulation. The x axis shows types of error measurements, the y axis represents scale of the error. The light bar represents the error for a tuned model run and the dark bar represents error for a default model run.

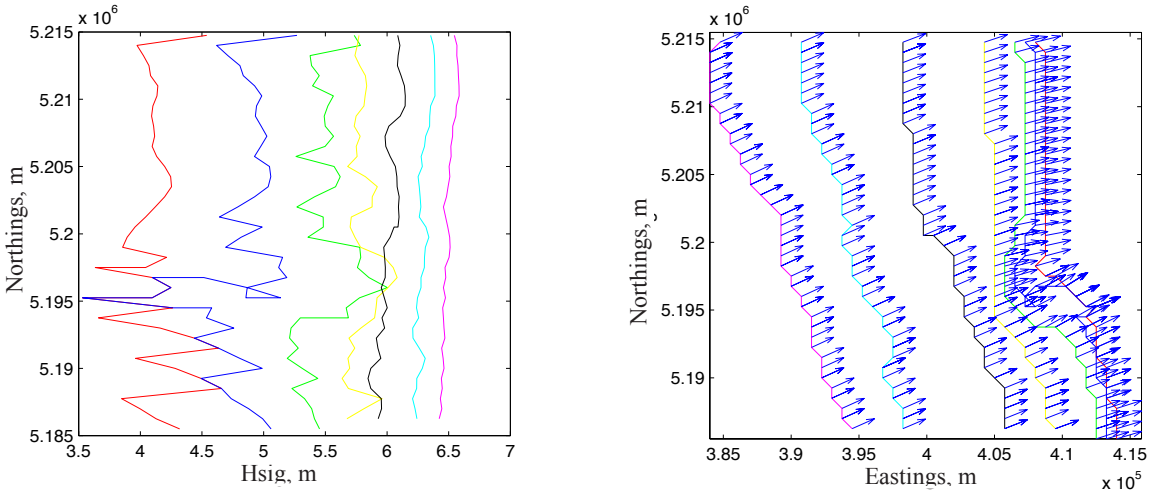

Figure 89. Plot of significant wave height and wave direction along isobaths for time period between 10/28/99 12:00 and 10/29/99 02:00. Each isobath is represented by a different color; red (10 m), blue (12 m), green (15 m), yellow (25 m), black (40 m), cyan (55 m), magenta (70 m).

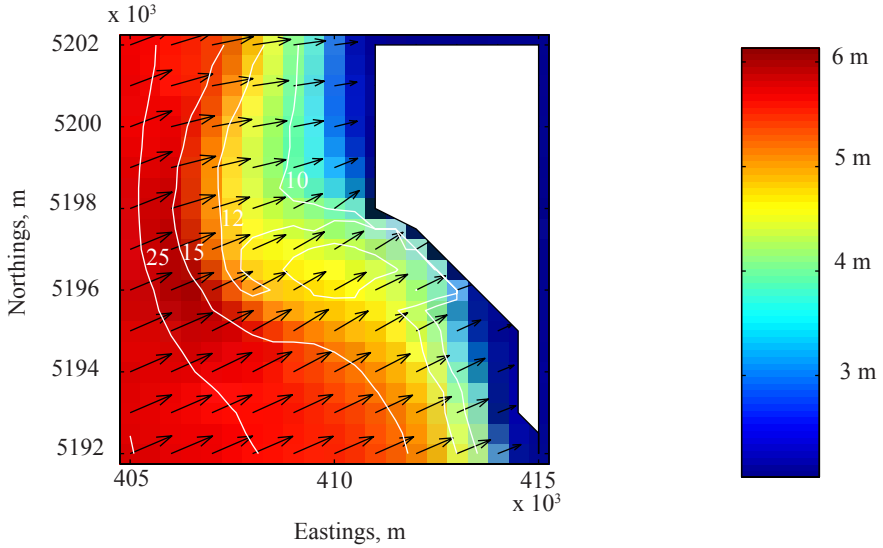

Figure 90. Vector plot of Significant wave height in color and wave direction with arrow for time period between 10/28/99 12:00 and 10/29/99 02:00.

Validation Study

The model was tuned using the results of the calibration study. Non-default values were selected for the formulation for wind input/whitecapping (Janssen formulation where $C_{ds1} = 4.5$) and the formulation for bottom friction (Madsen formulation with $K_N = 0.05$ m). Boundary conditions were given as significant wave height, wave direction, and peak period. The JONSWAP spectrum was calculated from the given boundary conditions.

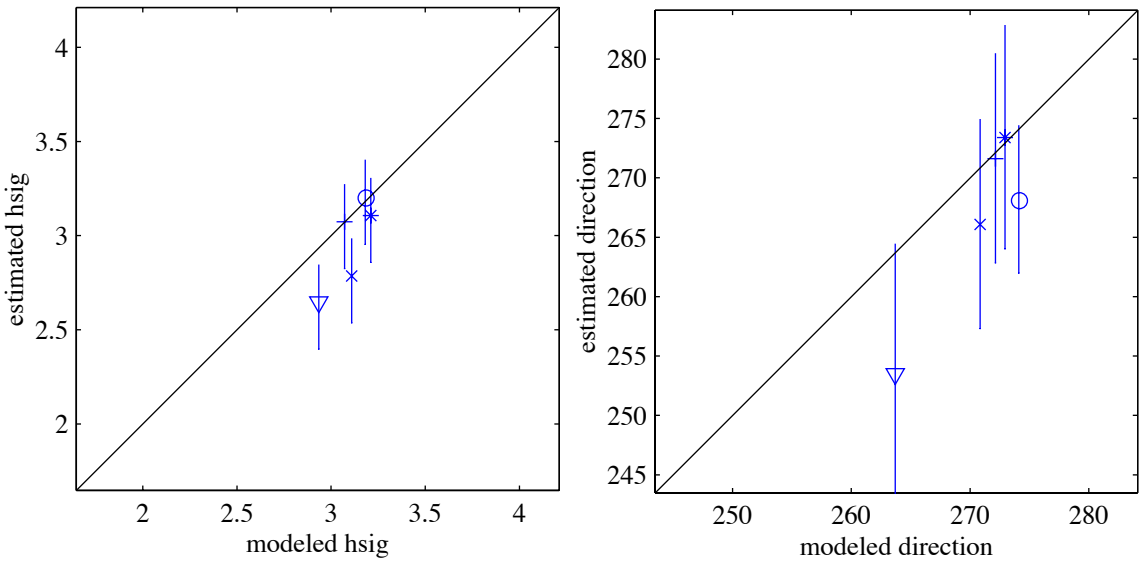

Figure 91. Plot of modeled significant wave height and direction against field data for the time period between 11/22/1999 12:00 to 11/23/1999 12:00 from a tuned model run.

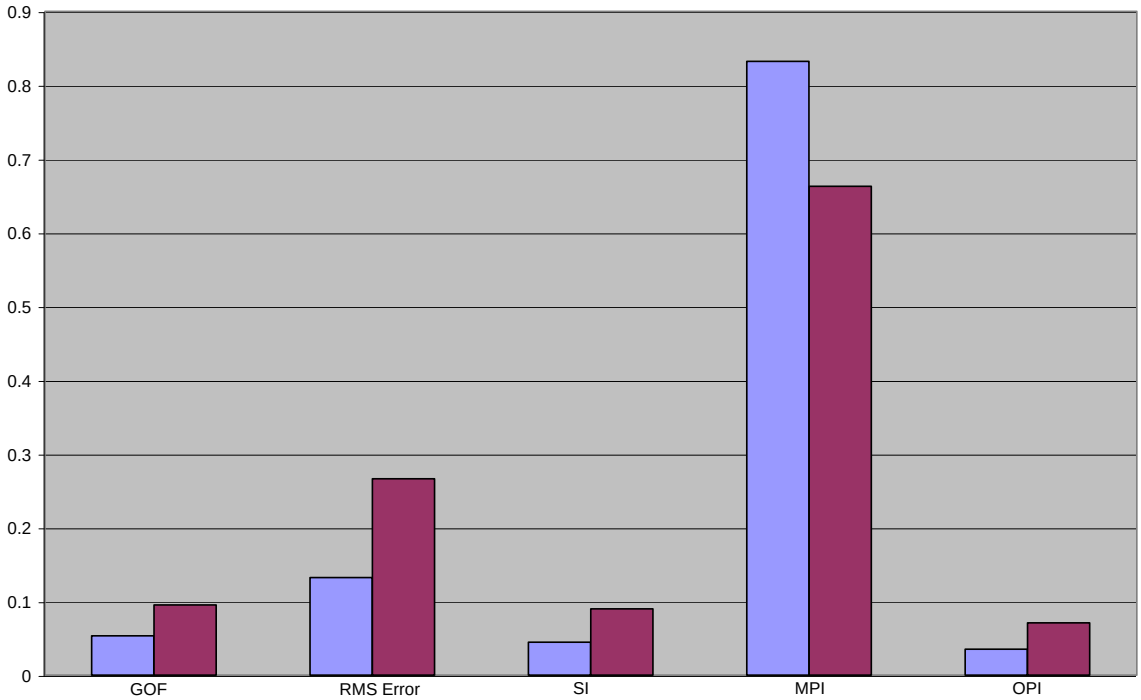

Figure 92. Reduction in model error for time period between 11/22/1999 12:00 to 11/23/1999 12:00 due to changes in model formulation.The light bar represents the error for a tuned model run and the dark bar represents error for a default model run.

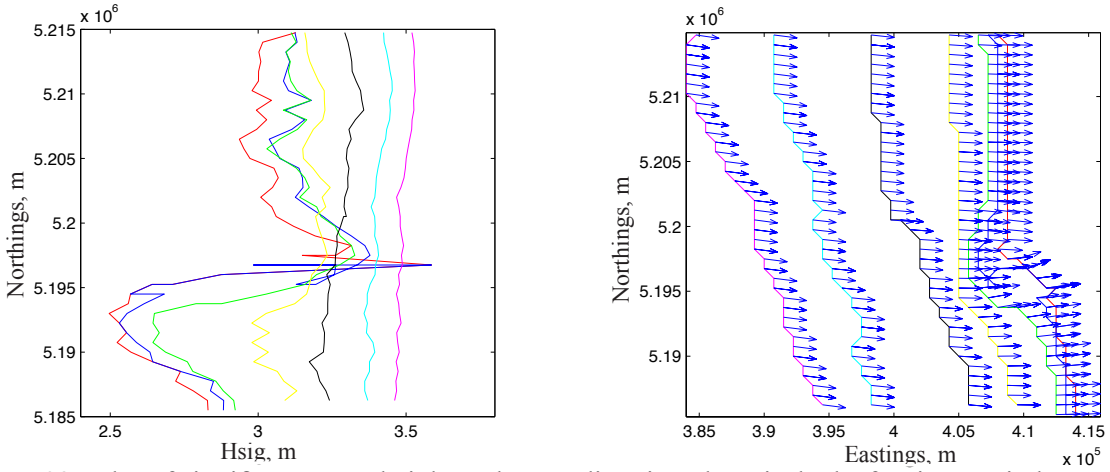

Figure 93. Plot of significant wave height and wave direction along isobaths for time period between 11/22/1999 12:00 to 11/23/1999 12:00.

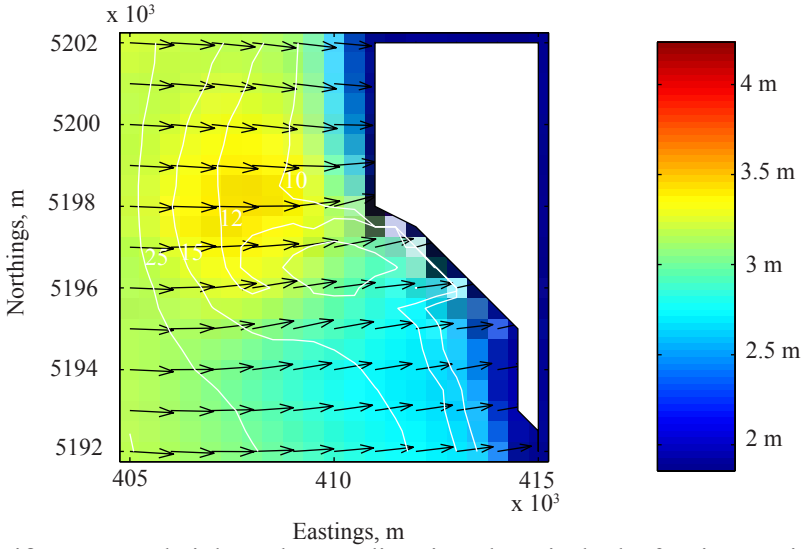

Figure 94. Plot of significant wave height and wave direction along isobaths for time period between 11/22/1999 12:00 to 11/23/1999 12:00.

Error statistics were calculated for model runs using the default settings and calculated again for tuned model runs. Comparisons were made for other time periods during the field data collection including 10/28/1999 12:00 to 10/29/1999 02:00, 11/22/1999 12:00 to 11/23/1999 12:00, and 12/2/1999 14:00 to 12/3/1999 05:00. Note that wave direction was near the wind direction with an offshore wind blowing in these cases. Offshore wave height in the October case was 7.53 m, peak period was 13.3 s, wind speed was 12.5 ms^{-1}, and offshore wave direction was 243°. RMS error in between modeled and estimated wave height was reduced from 0.17 in the default run to 0.05 in the tuned model run (Figure 88). SI was reduced to 0.009 in the tuned run from an initial value of 0.031 in the default run. MPI increased in the tuned run to 0.97 from

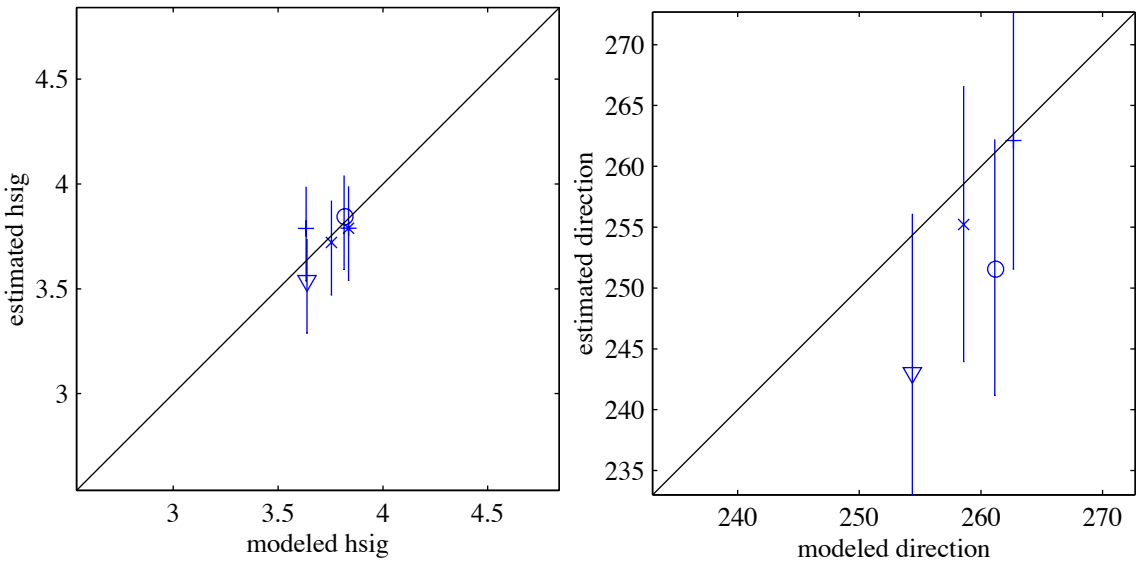

Figure 95. Plot of modeled significant wave height and direction against field data for the time period between 12/2/1999 14:00 to 12/3/1999 05:00 from a tuned model run.

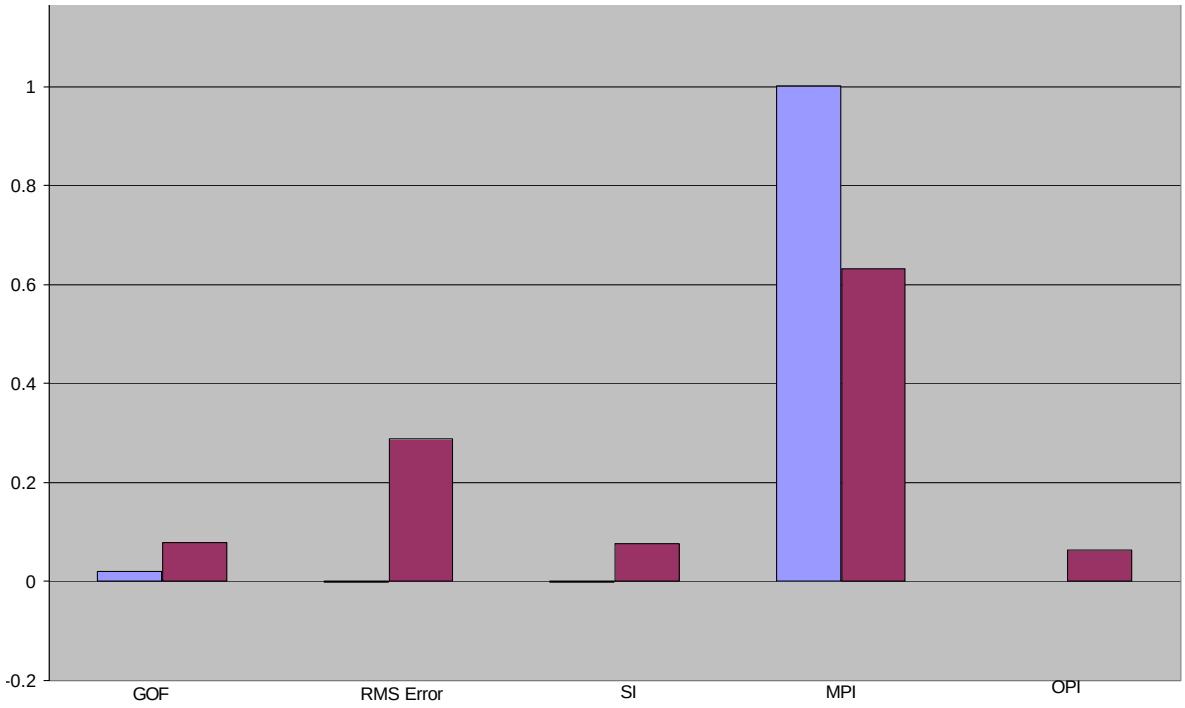

Figure 96. Reduction in model error for time period between 12/2/1999 14:00 to 12/3/1999 05:00 due to changes in model formulation.

the default value of 0.91. OPI was reduced from 0.023 in the default run to 0.007 in the tuned run. Raw comparisons between modeled and estimated wave height were very reasonable with the largest difference of 0.15 m at MD in the tuned model run.

During the November case, offshore wave height was 5.07 m, peak period was 16.67 s, wind speed was 9.6 ms^{-1}, and wind direction was 250°, and wave direction was 282°. RMS error was reduced by nearly half from 0.27 to 0.13 (Figure 92). SI was improved upon from 0.09 in the default run to 0.04 in the tuned model run. MPI was increased from 0.66 to 0.83 in the tuned model run. OPI was reduced from 0.07 to 0.03.

Offshore wave height during the December case was 4.52 ms^{-1}, peak period was 12.42 s, wind speed was 9.23 ms^{-1}, wind direction was 270°. RMS error was greatly reduced between the default (0.29) and the tuned model run (just below 0.00) (Figure 96). The default SI value was reduced from 0.08 in the default run to just below 0.00 in the tuned model run. MPI was

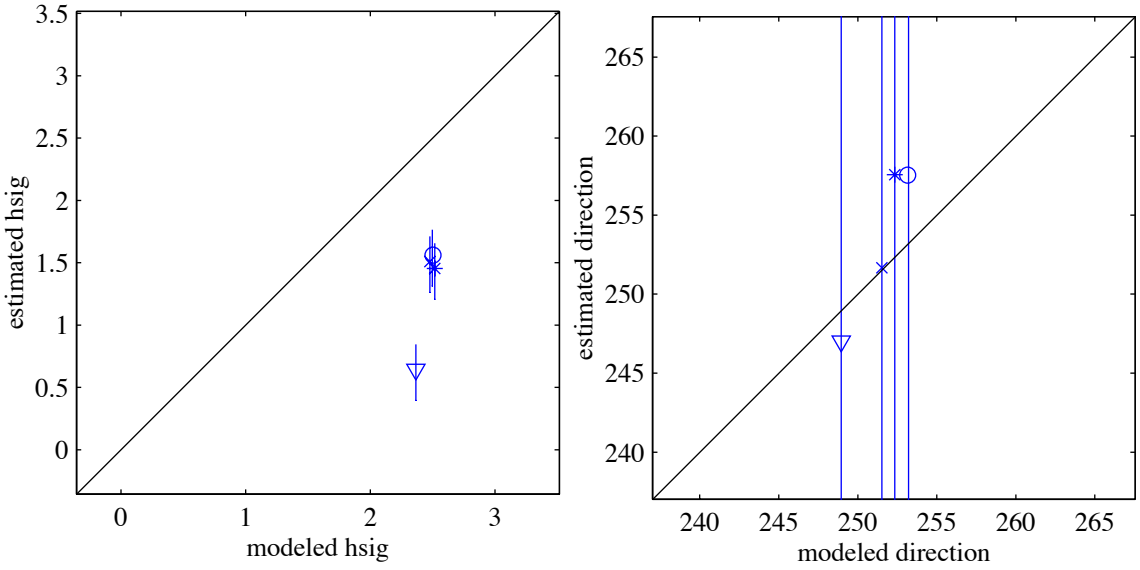

Figure 97. Plot of modeled significant wave height and direction against field data for the time period between 10/13/1999 02:00 to 10/13/1999 22:00 from a tuned model run.

increased slightly over 1.00 in the tuned run from 0.63 in the default run. OPI was reduced from 0.06 in the default run to below 0.00 in the tuned model run. The negative RMS, SI, and OPI values and the MPI value greater than one denotes that some modeled wave heights were lower than wave height estimated from field data.

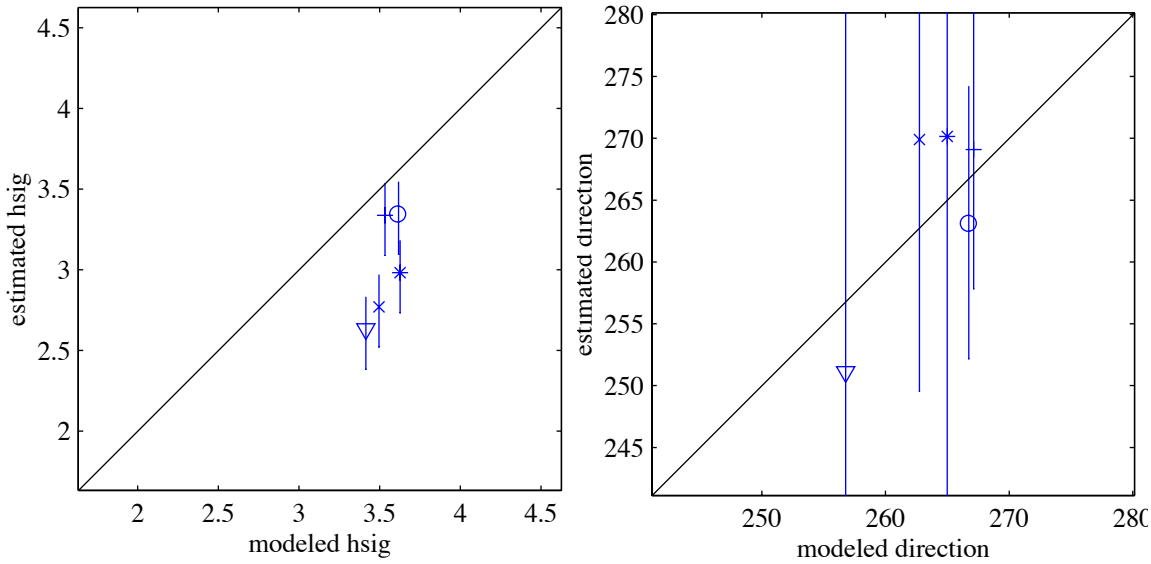

Figure 98. Plot of modeled significant wave height and direction against field data for the time period between 11/15/1999 02:00 to 11/15/1999 14:00 from a tuned model run.

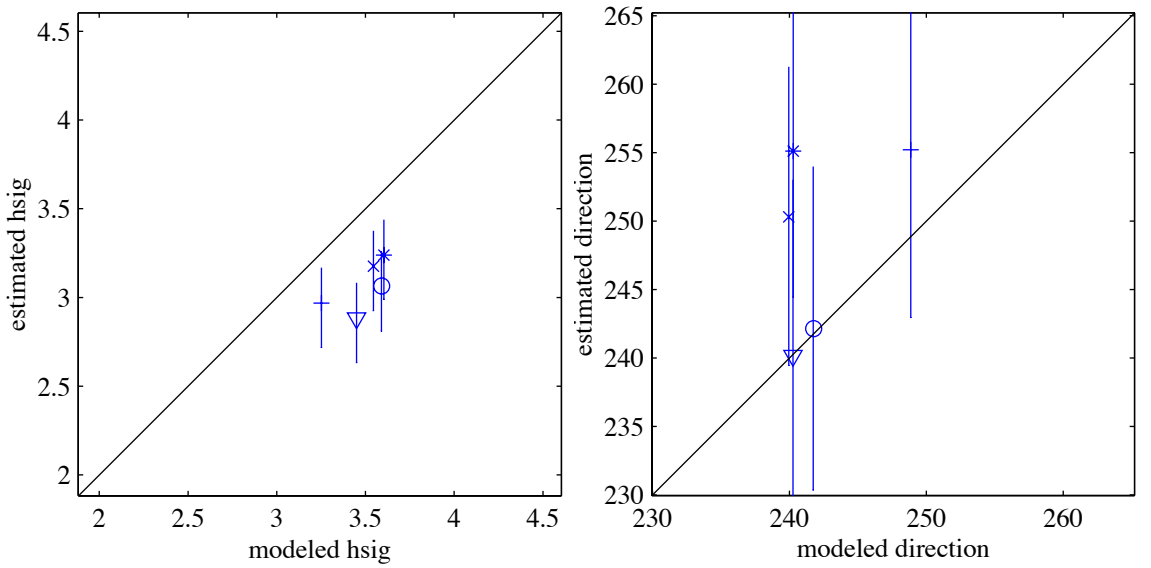

Figure 99. Plot of modeled significant wave height and direction against field data for the time period between 11/20/99 00:00 and 11/20/99 20:00 from a tuned model run.

The previous validation runs compared very well with field data. In contrast, many validation runs produced unacceptable results. This second group of validation runs is presented here. Low wave heights and a wind blowing from northwest while waves at the CDIP buoy approached from the southwest characterized the time period between 10/13/99 02:00 and 10/13/99 22:00. The model (Figure 97) overestimated field conditions. Error statistics (Table 5) show this model run has poor results. Wave direction was close to wave direction estimated from field data.

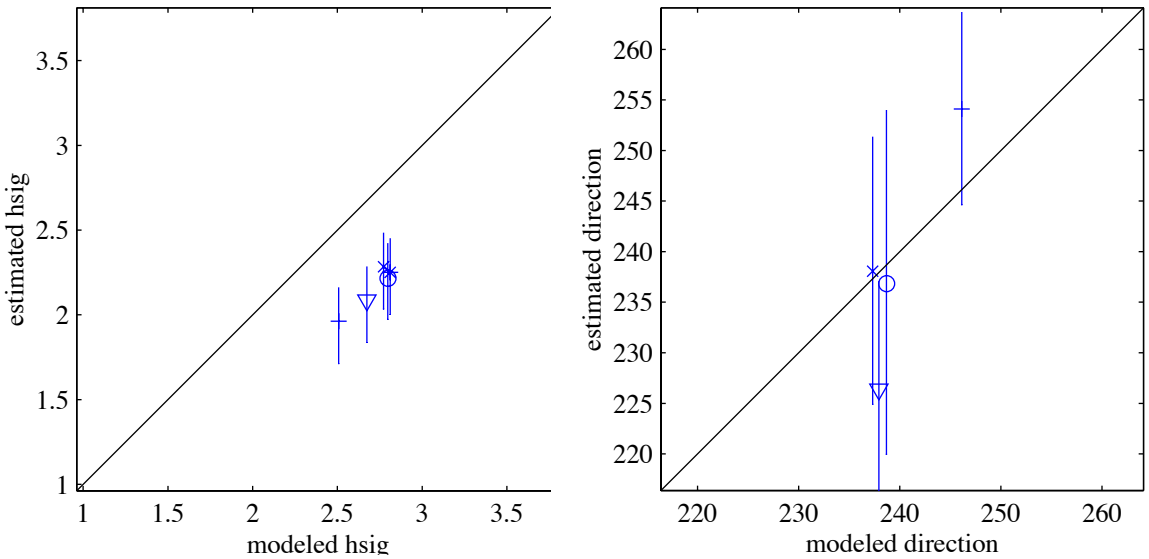

Figure 100. Plot of modeled significant wave height and direction against field data for the time period between 12/01/99 02:00 and 12/02/99 00:00 from a tuned model run.

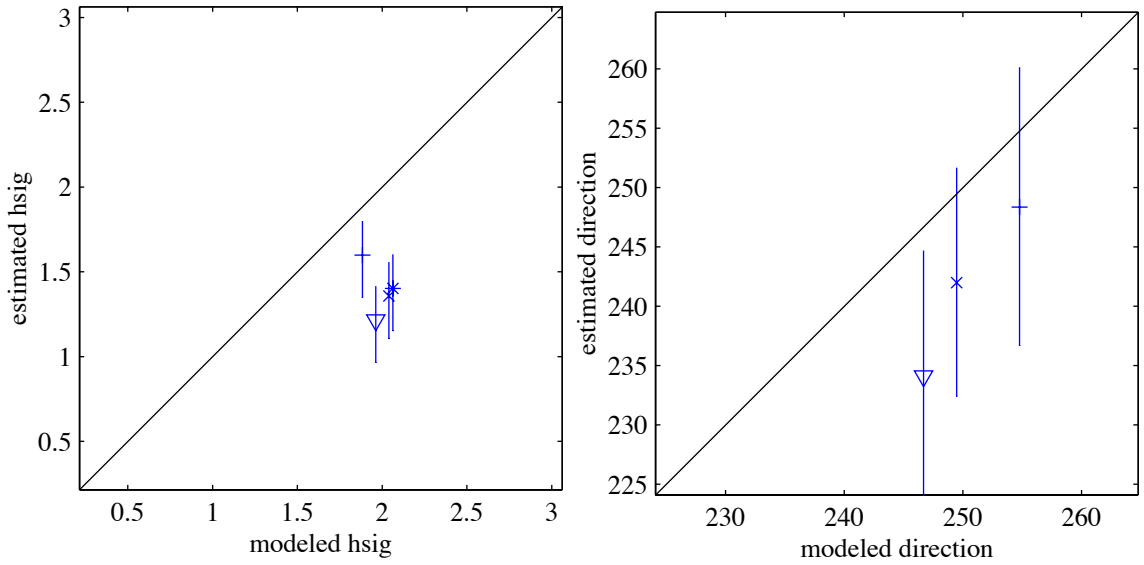

Figure 101. Plot of modeled significant wave height and direction against field data for the time period between 12/24/1999 17:00 to 12/25/1999 08:00 from a tuned model run.

Wave height for the time period between 11/15/99 02:00 and 11/15/99 14:00 was modeled moderately well (Table 5). Modeled wave heights at ND and NS compare better with field data than modeled wave heights at other locations. Modeled wave direction at all locations compares well with wave direction calculated from field data. Wave height during the time period between 11/20/99 00:00 and 11/20/99 20:00 was 4.55 m at the offshore buoy. Peak period was 11.0 s. Wave direction was from 244°, while wind direction was from 268°. Conditions during this time period are very similar to the conditions during the calibration study,

however wind is from a more southerly direction. Error statistics are also very similar to those from the CR8, tuned result of the calibration study (Table 3 and Table 5). Wave height at NS,MD, and SD are more accurately modeled in this validation run than in CR8, while ND and SS are more accurately modeled in CR8 (Figure 99). Modeled wave direction between 11/20/99 00:00 and 11/20/99 20:00 matches well with field data. Note the large error bars on directional plots. The time period between 12/01/99 02:00 and 12/02/99 00:00 was characterized by an offshore significant wave height of 3.47 m. Wind direction offshore was 226^{o} and wind speed was 10.4 ms^{-1}. Wave height offshore, calculated from the CDIP buoy, was 226^{o}. Wave height was over predicted in the model run (Figure 100), resulting in error statistics of moderate quality (Table 5). Wave height was modeled with reasonable accuracy in this model run. Low wave height and a light onshore wind characterized the time period between 12/24/99 17:00 and 12/25/99 08:00. Figure 101 shows the poor comparison between modeled and estimated significant wave height. Comparisons between modeled and estimated wave directions are reasonable.

Chapter Four

Discussion

Dynamics of the Grays Harbor ETD play an important role in the development of the coast near the entrance to Grays Harbor (Figure 2). Jetties constructed over the last century at the north and south sides of the entrance to the Grays Harbor increased the velocity of tidal flow and increased scour of the ETD and entrance channel. The ETD migrated offshore as a result of the higher current velocities and the beaches to the north and south of the inlet accreted as waves pushed sediment from the flanks of the ETD towards the shoreline (Buisjman, 2000). Prior to jetty construction the ETD and shoreline were considered stable features with no significant gradient in sediment transport (Kaminsky and Gelfenbaum, in press). Prehistorically, sediments were redistributed northward from the Columbia River, feeding the Grays Harbor ETD (Woxell, 1998). Annual average sediment supply from the Columbia River has decreased ~50-60% relative to the late 19th century (Jay and Naik, 2000). An application of the validated SWAN model is to explore whether the ETD has migrated to a stable position over the last century, or will waves be expected to enhance or destroy the feature, particularly with a reduced sediment supply from the south?

Stability of the ETD, and therefore the coastline, may be qualitatively explored through interpretation of SWAN model results. The purpose of the modeling exercise previously described is to provide calculated values of significant wave height and wave direction which may be used to determine of longshore energy flux, which is proportional to longshore sediment transport due to waves. The equation for longshore energy flux on a straight coast with plane parallel contours is given below,

$$P_\ell = \frac{\rho g}{16} H^2 C_g \sin 2\alpha \qquad 42$$

where ρ is water density, g is gravity, H is wave height, C_g is group velocity and a is the angle waves make with a bottom contour or shoreline. Magnitude of longshore energy flux

is proportional to the wave height statistic used, therefore significant wave height will produce greater longshore energy flux than H_{rms}. This equation was derived to predict longshore energy flux along a straight coast with parallel bathymetry contours and therefore is difficult to solve along a complex ETD. Although this equation will not be explicitly solved, it will be used to interpret relative magnitude and direction of longshore energy flux and asymetry in orbital velocity it would produce to infer changes that may occur to the ETD. Position of the ETD used in the modeling exercise is from 1998 bathymetry.

Prediction of Wave Characteristics

To provide accurate estimates of wave height and direction at the Grays Harbor ETD, sensitivity, calibration and validation of the SWAN model took place. Several of the model elements in the SWAN model produced little change in modeled wave height, while other model elements had a strong influence on wave height. The objective of the sensitivity study was to determine which elements of the SWAN model must be tuned to produce accurate model results and which model elements may remain untuned while determining the reason that an element must be tuned or left as a model default.

Model formulations for the nonlinear source term in the SWAN model produced little change in modeled wave height. These terms were the coefficients related to the equation for triad interactions and the method of computing quadruplet interactions. These formulations had little influence on wave height because the function of the nonlinear source terms is to redistribute energy within the spectrum rather than input or dissipate wave energy. Use of the linear growth term for waves due to wind had no significant effect of wave height in the study area. This may be expected as the linear growth term only has a significant effect on wave evolution over very short fetches (Ris, 1997). Modeled wave direction was very insensitive to changes in most formulations in the SWAN model because source terms have little influence on the computation of wave refraction in the SWAN model.

Several of the many elements in the SWAN model produce significant changes in modeled wave height. The default parameters in SWAN were set for a depth and fetch limited environment. This is very different from the southwest Washington inner continental shelf, making it important to tune influential formulations in the SWAN model for a high wave

energy environment. Model formulations used to calculate the source terms for energy input and dissipation were most influential on model results. These terms were the wind input/whitecapping and bottom friction formulation.

Two formulations for exponential growth of wave by wind are available in the SWAN model. These formulations are coupled with formulations for whitecapping. The sensitivity of modeled wave height to wind input, whitecapping was turned off, while the formulation for wind input was varied between the Komen and Janssen formulations. Although the two formulations have different formulations for wind input, there is little difference between resulting wave heights. The amount of energy input to the waves by wind may be small relative to the size of the waves modeled. Therefore, choice of wind input formulation on the southwest Washington inner continental shelf is unimportant from a scaling argument.

Variations in formulations for energy dissipation had the greatest influence on model. Whitecapping formulation is important in modeling wave height. As shown in the Figure 16, there is a significant increase in wave height when whitecapping is turned off and formulation for exponential growth remains constant but wind input remains on. The use of the whitecapping term has great influence on wave height in the study area, as whitecaps are more likely to be present on waves of longer wavelength (Komen et al., 1994) as in this study. Therefore, a whitecapping formulation should always be included in SWAN model runs.

The Komen formulation for whitecapping produced larger wave heights than the Janssen formulation when compared using the default coefficients. The two formulations have different wind input (which produce similar results) and different dissipation mechanisms, resulting in different wave heights. In the Komen formulation, changes in wave height were inversely proportional to the value of C_{ds2}, the coefficient for dissipation. Increasing the value of the coefficient for dissipation results in an increase in the value of the source term for energy dissipation (S_{ds}). This is expected with examination of Equation 11 for dissipation due to whitecapping. $\tilde{s}_{pm}$, the steepness of the Pierson-Moskowitz spectrum, produced changes in wave height when it was adjusted by a factor of two or greater. However, changes this large are not recommended in the literature. Adjusting the value of $\tilde{s}_{pm}$ produces the same effect on dissipation as varying the value of C_{ds2}, however, $\tilde{s}_{pm}$ has a physically different meaning. From the equation, increasing the value of $\tilde{s}_{pm}$ will effectively decrease the steepness of the wave. The Komen

formulation depends on wave steepness to determine whitecapping coverage, so lower wave steepness results in less dissipation due to whitecapping and higher waves as show in Figures 27 and 28. Although waves in the study area have longer periods than in previous SWAN model validation studies, wave heights are quite high in less steep waves, as a result, $\tilde{s}_{pm}$ should not be varied.

Similar to the Komen formulation, the Janssen formulation for whitecapping also includes a coefficient for dissipation. Like C_{ds2} in the Komen formulation, C_{ds1} in the Janssen formulation was inversely proportional to wave height. The default value of C_{ds1} (4.10×10^{-5}) is nearly twice the value of C_{ds2} (2.36×10^{-5}). This is one of two reasons the Janssen formulation appears to be more dissipative than the Komen formulation. The second variable in the Janssen formulation $\delta = 0.5$. This value of δ produces greater dissipation at the high frequencies in the spectrum than the Komen formulation where the value for δ is 1. Ris (1997) found varied values of δ produce little change in wave height. This is true for that case where wave heights and wind speeds were very high. In this sensitivity study it was found that δ is sensitive for variation, particularly at low wave heights and wind speed. This is the result of energy at high frequencies being relatively more important when there is less energy near the peak frequency. Therefore, the second component to lower wave heights modeled with the Janssen formulation may be greater dissipation at high frequencies.

Bottom friction is the second mechanism for dissipation of wave energy in the SWAN model. Three formulations for bottom friction in the SWAN model use slightly different mechanisms to calculate dissipation. However, two of the formulations produce very similar results. The JONSWAP formulation for bottom friction was determined empirically for swell waves in the North Sea and assumes a constant bottom velocity. Although this approximation gives good results, it is certainly not valid. In contrast, the Collins formulation depends on a simplified form of the quadratic drag law using wave induced bottom velocity, where dissipation is determined from bottom velocity and a drag coefficient determined experimentally in the Gulf of Mexico. The Madsen formulation for bottom friction is more dissipative than the other two formulations for bottom friction in the SWAN model (Figure 29). A different modification of the quadratic drag law is used in this formulation where the friction factor depends on a value for bottom roughness and local bottom velocity. The Madsen formulation produced the best results

for the southwest Washington continental shelf and appears to be most adaptable to different environment by using a local bottom velocity and a variable value for bottom friction.

Frequency and directional resolution are two elements in the SWAN model that affect model computational time. It was important to understand the sensitivity of these two parameters in order to achieve model results that compared well with data, while being able to compute model results in a relatively short period of time. Frequency resolution had an insignificant effect on wave direction. Cavaleri and Bertotti (1994) suggest modeling 20-25 frequencies produced sufficiently accurate model results. 15 or more frequencies must be modeled in SWAN to produce accurate wave height results. Modeling a larger number of frequencies will produce nearly the same results and increase computational time. Hence, 15 frequencies were calculated for model runs in the calibration study. Differences in wave height caused by modeling fewer than 15 frequencies were the result of the inability of the model to reproduce an accurate spectrum with too few frequencies. The range of frequencies modeled was not explicitly tested in the sensitivity study, however it was important to model the range of frequencies that are will induce realistic sediment transport. Therefore a range of frequencies between 0.05 and 0.25 were modeled.

Unlike frequency resolution, directional resolution had a significant effect on wave direction. Binned wave direction in the SWAN model is calculated for the median value in the bin. A directional resolution of 30^{o} or greater produced significant differences in wave direction, while directional resolution of fewer than 30^{o} did not result in a significant difference in wave direction. However, model runs took longer to compute. Differences in wave direction with varying directional resolution are due to differences in the calculation of wave refraction at different resolutions. Wave height was proportional to bin size. Wave height calculated with a directional resolution of 20^{o} or greater was significantly different than wave height calculated with a directional resolution of 15^{o} or less. As in the calculation of wave direction, wave refraction calculated with different resolutions has an effect on wave height. Model runs in the calibration study were completed with a directional resolution of 15^{o}.

The sensitivity study showed that variation in wind speed results in variation in modeled wave height. Also, a following wind produces larger wave heights than a crossing wind.
The sensitivity of modeled wave height to wind input illustrates the importance of valid wind information for input into the model. Measured wind information is not available over the entire

model domain in this experiment. Modeled wind information may be available for the model domain, but output from wind models are often at too large a resolution for the smaller scale SWAN model. Wind information was available at the offshore model boundary for this study. It should be noted that wind input may vary greatly from that at the offshore boundary and therefore, inaccurate wind input may have introduced error into model results.

Time periods chosen for modeling were based on the criteria of stable conditions while waves traveled from 46005 to the Grays Harbor study area. Wave group travel time between 46005 and the study area were calculated using linear wave theory. It was difficult to isolate time periods to model as wave conditions and wind conditions are rarely stable over several hours. Many of the time periods used in the modeling effort contain slight changes in wave height or wind direction at the offshore boundary. During one burst of the 10/13/99 time, wave period jumped at MD and SS while wave period at all other mooring locations remained constant. This type of deviation from a stable condition generates some uncertainty in comparisons made between modeled and estimated wave statistics. These uncertainties were accounted for in error bars on wave statistics calculated for the modeled time periods.

Model calibration described in the Results section measured the accuracy of model results relative to wave conditions estimated from field data. Error statistics from model results obtained in the calibration run determined which formulations for whitecapping and bottom friction dissipation produce wave heights and directions that best agree with estimated wave heights and directions.

Two formulations for bottom friction are available in the SWAN model. Comparing error statistics for CR1 and CR2 (Table 4), it is evident that model runs using either formulation produces similar results in wave height and direction with CR2 being slightly, but not significantly better. It is then a subjective choice whether the modeler chooses to use the empirical JONSWAP formulation for bottom friction or Madsen's drag law formulation (Luo and Monbaliu, 1994). The Madsen formulation was chosen for this study as it took into account variations in bottom orbital velocity. The bottom friction factor may be adjusted in the Madsen formulation according to roughness length. Another option in the Madsen formulation is to include a spatially varying value for bottom friction. A variable value of bottom friction would allow greater realism in the formulation of bottom friction, particularly in the study area, where bottom type varies greatly

(Figure 3 and Figure 4). The greatest difficulty with the Madsen formulation is the lack of well-defined parameters for determining bottom friction in the field. This is in contrast to the SWAN calibration study by Ris (1997) where the JONSWAP bottom friction with $C_j = 0.067$ was chosen because it produced a better results in lacustrine and estuarine environments, where the frequency spectrum is dominated by wind generated waves.

Within the Madsen formulation for bottom friction, the modeler sets the roughness length (K_N). Without considering physical characteristics of the environment, an unrealistically high K_N value might be chosen, as in CR3, because it produces better overall results. However, a K_N value of 0.5 as in CR3 implies ripple heights of 0.125 m to 0.25 m, covering the entire continental shelf. While a small portion of the inner continental shelf may have a K_N value of 0.5, this is certainly an overestimate in locations covered by fine sand and mud. In CR3 at NS and SS, where bottom friction can be expected to be greater than at the deeper tripods, wave heights were under predicted when $K_N = 0.5$ m. Even though this under prediction is not of great magnitude, it implies that the value of K_N is too great. $K_N = 0.05$ m will be used in the calibrated model because it is a conservative estimate of bottom roughness length and well accepted in the literature (Luo and Monbaliu, 1994).

The second formulation within the SWAN model that produced significant change in wave height was the formulation for wind input and dissipation due to whitecapping. Wind input and dissipation may be modeled according to two schemes, the Komen formulation and the Janssen formulation. The Komen formulation for wind input and whitecapping dissipation was utilized in CR1-CR7 and is the default formulation in the SWAN model. Running the model with this formulation tended to over predict wave height (Figures 66 - 74). Within this formulation for wind input/whitecapping, the modeler may vary the coefficient for dissipation (C_{ds2}). Variation of the C_{ds2} using values recommended in the literature (between 2.36×10^{-5} and 3.33×10^{-5}) over predicted wave heights, which is reflected in low values for MPI (Figure 73). Larger values of C_{ds2} produced results more like field data, however using a large value for C_{ds2} may not be physically accurate.

The second coefficient within the Komen formulation for wind input/whitecapping that may be altered is the value of wave steepness for the Pierson-Moskowitz spectrum ($\tilde{s}_{pm}$), increasing the value of $\tilde{s}_{pm}$ as suggested by Bender (1996) decreased the value of MPI (Figure 74).

Decreasing γ_{pm} well below the accepted value increases dissipation and improves MPI, but may not be physically accurate. Therefore, γ_{pm} should remain at the default value.

The other formulation for wind input and dissipation due to whitecapping is the Janssen formulation. This formulation was used in CR8-CR11. It produced significantly better results in wave height than the default Komen formulation. This result contrasts with the results of the SWAN calibration study by Ris (1997) for shallow barrier inlets. In that study, a wind sea, rather than swell dominated. The Janssen formulation tended to over predict wave heights over short distances and low energy and under predict wave heights over long distances in that study. The Janssen formulation applies a different method for determining whitecapping dissipation than the Komen formulation. In the Komen formulation, from Hasselman (1974), whitecaps are small compared with the length and period of a wave with the whitecap. Because this relationship is weak in the mean, it is quasi-linear. Therefore, the dissipation source function is linear in spectral density and the frequency. It has been shown that this may not be the most physically accurate formulation (Komen et al., 1994). The Janssen formulation assumes there may not be a linear relationship between waves and whitecaps at high frequencies and dissipation may depend on wavenumber. This formulation is often used with trepidation in the SWAN model because it depends on the high frequency tail of the spectrum, which is parameterized in the SWAN model and may produce incorrect results. In this calibration study, the Janssen formulation appeared to produce better results than the Komen formulation. The Janssen formulation was used in the tuned model run. The SWAN model produced the least error when the coefficient for determining dissipation due to whitecapping (C_{ds1}) within the Janssen formulation was set at a value of 1.09×10^{-4} (Figure 75). This value is nearly four times larger than the default value which was determined with extensive tuning to produce results that agree well withwave growth and dissipation data (Komen et al., 1994). The default value of C_{ds1} reproduced field data moderately well (MPI = 0.68). Komen et al. (1994) suggest that C_{ds1} should be retuned for different conditions. Therefore, it may be appropriate to vary C_{ds1} for the swell dominated environment of the Washington inner continental shelf, however, based on the literature, varying the value by an order of magnitude or more may not be appropriate. The default value of C_{ds1} was used in the validation study.

The second coefficient within the Janssen formulation for whitecapping, δ, allows the user to alter the influence of wavenumber on whitecapping. The default value of δ was also determined by tuning (Komen et al., 1994). Although this coefficient may be tuned, it was left at the default of 0.5 as the value produced good results and is accepted in the literature.

Directional characteristics of the wave field in the SWAN model are estimated using a value for directional spreading. A value of ms = 7, determined at the peak period using the Donnelan-Banner method was used in the calibration runs. The purpose of CR23 (ms = 1) and CR24 (ms = 14) was to determine whether this was the best estimate of directional spreading (Figure 76). CR23 produced the best model results, however this value of directional spreading is extremely high and is unrealistic for swell conditions. Increasing the value of ms to 14 (decreasing spreading) did not affect modeled wave height, but did slightly decrease accuracy of modeled wave direction. Therefore, a value of 7, as determined by the Donnelan-Banner method produces the most reasonable model results.

The SWAN model may be initialized with a parameterized spectrum or an observed wave spectrum with constant or variable directional spreading. Comparison of CR18 (Figure 86 and Table 5) and CR8 (Figure 79 and Table 5) indicate that model results from an observed spectrum produce less accurate wave heights at the tripods than the parameterized spectrum. Examples of the average observed and the parameterized JONSWAP wave spectra used in this comparison are shown in Figures 102 and 103. Although both spectra contain the same amount of total energy, the JONSWAP spectra has more energy at lower frequencies. In contrast the observed spectra contains more energy higher frequencies. Greater dissipation due to bottom friction would be expected at lower frequencies. The greater dissipation in CR8, where the JONSWAP spectra was used, relative to CR18, where the observed spectrum is used, is due to the greater amount of energy at lower frequencies and therefore greater dissipation due to bottom friction. This greater dissipation is an artifact of the modeling technique and an observed spectrum should be used. In contrast to these results from the calibration study, observed spectra used in the sensitivity study appeared to be similar in shape to the JONSWAP spectra, having more energy at low frequencies relative to the energy at high frequencies. These results were nearly identical to those obtained using the parameterized JONSWAP spectrum. In this study, it was important to consider shape

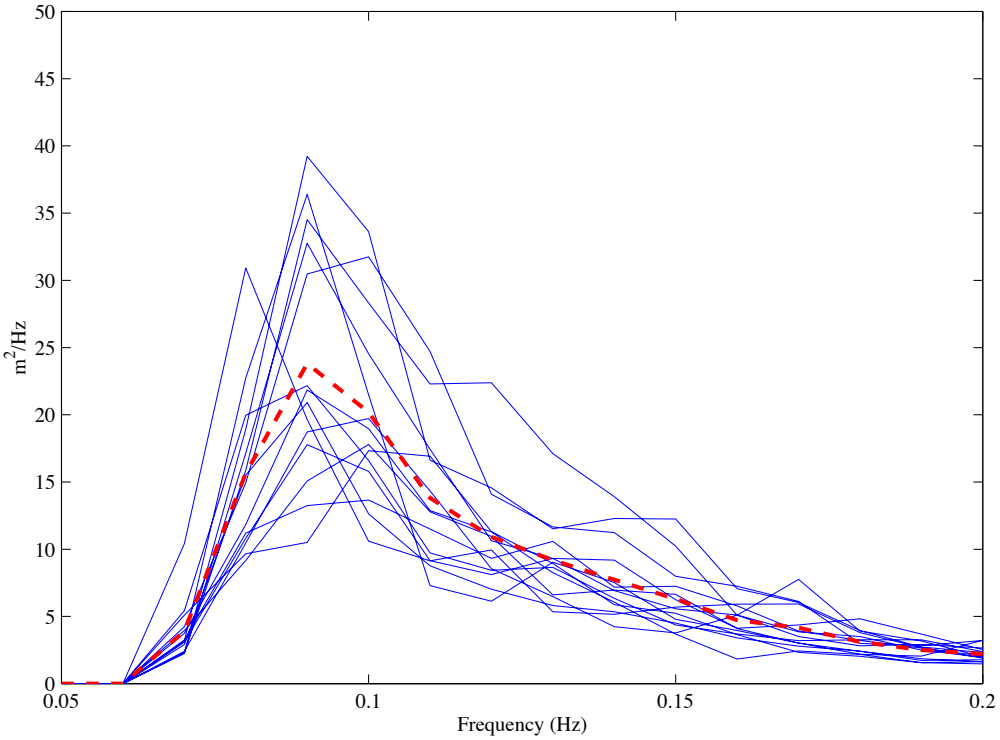

Figure 102. Dashed line is average observed spectra over time period modeled in the calibration runs.

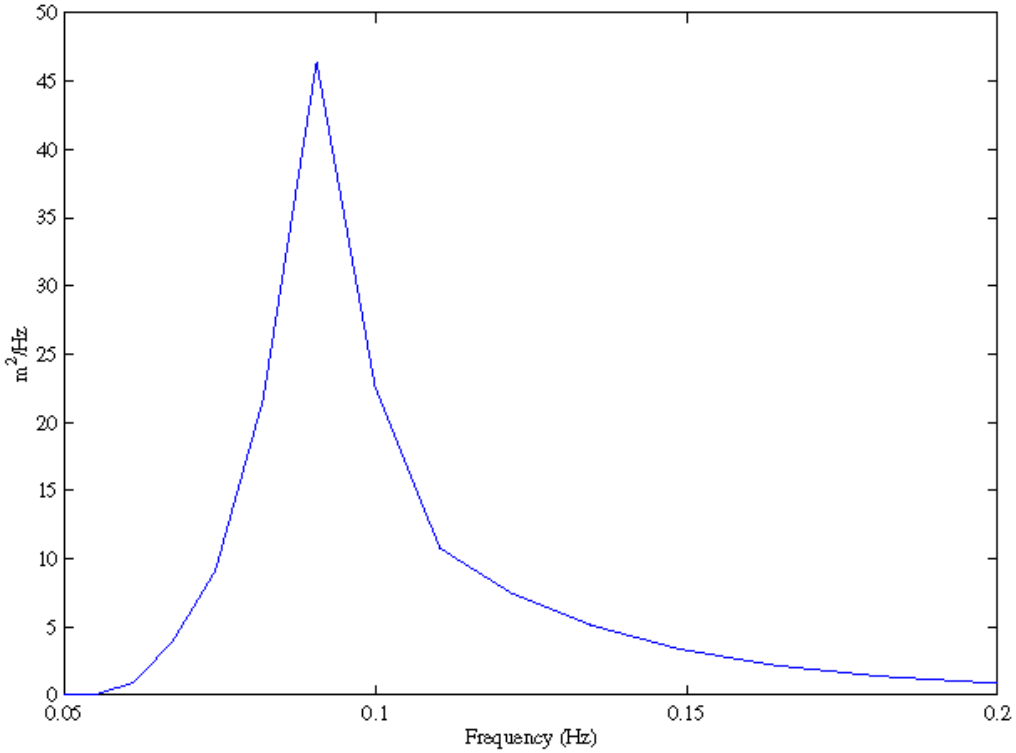

Figure 103. JONSWAP spectra over time period modeled in the calibration runs.

of the observed spectrum when choosing whether to use an observed or parameterized spectrum at the model boundary.

In many cases, model results improved for the tuned model runs relative to the default model run. Modeled wave height at each tripod was compared with wave estimated from the field data. Both modeled wave statistics compare well with wave statistics from the field data. Figures 87 - 90 show model validation results during the largest wave event of the field experiment. Error statistics from the model default run show very poor agreement with field data, while error statistics from the tuned model run show excellent agreement with field data. Figure 87 shows the agreement between modeled and estimated wave height and direction. In this case it appears energy input by wind and dissipation due to whitecapping and bottom friction are well balanced.

Figures 91-94 show a time period with medium wave heights. The default model run produced fairly accurate results, which were improved upon by the tuned model run. The source terms for wave energy input and dissipation are well balanced as modeled wave heights fall close to the values for wave heights estimated from field data. Modeled wave direction appears to be slightly more northerly than in wave direction estimated from field data.

Medium wave conditions dominated for validation runs shown in Figures 90 and 91. Comparison between modeled and estimated wave heights is very good, showing that formulations for energy input and dissipation are well tuned. As in other validation cases, wave direction is biased towards a higher value. Wave statistics show an improvement between the default and tuned model run, showing that indeed, the tuning increased accuracy of the SWAN model on the southwest Washington continental shelf.

Wave height was over and under estimated by the SWAN model for validation runs. However, the error bars on the estimated wave height overlap the 45^{o} line, showing a good relationship. The overestimates in wave height may be due to a conservative estimate of bottom friction in the model. Bottom friction was set with a roughness length of 0.05 m which is representative of small sand ripples. Although this is a conservative estimate, it is not entirely accurate. Twichell et al (2000) show the continental shelf in the model domain includes silty-sand near the shelf edge, sand, coarse sand near the beach, gravel, rock outcrops, megaripples, and sand dollars, which all have vastly different values for bottom roughness (Figure 2).

Wave direction was biased towards waves from the north by several degrees in the SWAN model. Refraction in the SWAN model is calculated according to Snell's Law. It is known that change in wave direction is greater with smaller resolution when calculating refraction with Snell's Law. Therefore, better agreement with field data may occur with smaller grid size. Another aspect of the mismatch between estimated and modeled wave direction are the large directional resolution errors resulting from calculation of direction using pressure and horizontal velocities. Hence, a close match between modeled and estimated direction may be difficult.

The cases discussed above were times when the model could be properly initialized. Many time periods during the deployment when both buoys were working were not usable as boundary conditions because wind direction was not from offshore. Figures 56 and 97, Figures 58 and 98, Figures 59 and 99, Figures 61 and 100, and Figures 64 and 101 are examples of this situation. Wind was 42^{o} northwest of wave direction in the 10/13/99 case. Wind was light and from onshore, while wave direction at the CDIP buoy refracted offshore was 249^{o} in the 12/24/99 to 12/25/99 case. Similarly on 11/15/99, wave direction at the CDIP buoy was 275^{o} while wind direction was from 151^{o}. Because wave direction was measured at the Grays Harbor CDIP buoy and refracted to the offshore boundary using Snell's Law, this method was only accurate when peak direction at the offshore NDBC buoy was equal to that at the CDIP buoy. In this case wind was blowing offshore, this was not the case. At this time, the wind input at the CDIP buoy is minimal, resulting in a short fetch. At the same time the wind has blown over a large fetch to the NDBC buoy the peak wave direction has been influenced by the offshore blowing wind. This is reflected in an offshore wave direction, where wave energy is moving out of the model domain. However, this direction is not the result calculated using Snell's Law from the CDIP buoy. This idea is supported by reverse shoaling wave height from the CDIP buoy to 46005 using linear wave theory. In the 10/13/99 case, wave height at the CDIP buoy was 1.74 m. Wave height calculated with reverse shoaling from the CDIP buoy to 46005 was 1.60 m, while measured wave at 46005 was 2.73 m. In the 12/24/99 to 12/25/99 case, wave height at the CDIP buoy was 1.42 m. Wave height at 46005 was calculated as 1.30 m using reverse shoaling and measured at 2.32 m. The discrepancy between reverse shoaled wave height and measured wave height is due to energy input from wind moving in the offshore direction. Upon inspection of the spectra, the large amount of energy at high frequencies due to wind input is evident. In both cases where

wind was blowing offshore, wave heights at the northern tripods were modeled with acceptable accuracy, while wave height at the southern tripods was not well modeled. This effect is the combination of too much energy at the model boundary and the convergence and divergence of that energy around the ETD due to refraction.

As a result of inaccurate boundary conditions, much of data collected during the experiment is unusable due to lack of offshore wave direction information. This situation often occurs when wave heights are low, reducing the number of low wave height cases available to be modeled. The experiment would have been improved if wave directional measurements were available at the offshore buoy. Output from the WAM oceanic wave model has been shown to be very inaccurate in this area when compared with field data, so it was not used for model boundary conditions (Allen and Komar, 2000).

Another example of model inaccuracy due to boundary conditions occurred between 12/01/99 00:00 and 12/02/99 02:00. Wave height at 46005 was 3.47 m. Wind direction was 226^{o} and wave direction offshore, calculated from the CDIP buoy was 226^{o}. Modeled significant wave height was overpredicted by 0.48 to 0.58 m during this period. Wave height offshore, calculated by reverse shoaling from the CDIP buoy is 2.32 m. Therefore, it appears that wave height at 46005 is not representative of wave height reaching the moorings at Grays Harbor. According to the calculation of offshore wave direction, wave energy at Grays Harbor is approaching from a more southwesterly direction than the location of 46005, so offshore energy at 46005 may not be the origin of the wave energy measured at Grays Harbor. Because wave direction and wind direction coincide, it is not likely that wave energy in the wind frequencies is propagating offshore as in the cases described above. Once again, lack of information about boundary conditions results in model error.

Conditions during the time period modeled between 11/20/99 00:00 and 11/20/99 20:00 were very similar to those modeled in the calibration study, although, wave direction was more northerly in the calibration study. The difference in wave direction influences wave heights in the field as well as those modeled. A larger amount of directional spreading may be expected when waves and wind are from different directions. Therefore, reducing the value of ms to 4 increased directional spreading. Modeled wave height was improved in 11/20/99 by adjusting directional spreading as described in calibration runs.

Influence of Waves on the Stability of the Ebb Tidal Delta

Sediment transport and the balance of sediment transport on an ETD are largely the result of three mechanisms. Tidal currents are obviously important. Tide dominated ebb tidal deltas are characterized by a well developed tidal channel and may extend several kilometers offshore (Boothroyd, 1978). Shoaling waves will tend to transport sediment in the onshore direction. Wave dominated ebb tidal deltas terminate nearer to the shoreline than tide dominated ebb tidal deltas (Boothroyd, 1978). Longshore current skews the orientation of the ebb tidal in the direction of the current (Boothroyd, 1978). Morphology of an ebb tidal delta results from the relative magnitude of each of these mechanisms as well as sediment size.

Along-isobath energy flux is a measure of wave orbital motions skewed from the cross-shore direction. Wave orbital motions are responsible for moving sediment, therefore, the magnitude and direction of along isobath energy flux is used as a proxy for magnitude and direction of longshore sediment movement. The results from calibration and validation of the SWAN model may be interpreted to explore stability of the ETD at Grays Harbor. Lower energy waves from the west and high energy storm events from the southwest were measured during the fall deployment. Two time periods from the validation study are chosen as representative of the low and high-energy events. During the high-energy event on 10/28/99, waves of 7.53 m approached from 243^{o}. Figure 104 shows the along-isobath energy flux, from interpretation of modeled significant wave height and direction patterns shown in Figures 89 and 90. Arrows to the north and south of the delta are of equal magnitude because wave heights and directions are very similar on stretches of coast trending north and south with relatively parallel contours. Along-isobath energy flux decreases on the southern side of the ETD as the orientation of the contours rotates abruptly to northwest and southeast trending, which are more perpendicular to waves approaching from the southwest. Deposition of sediment may occur where the gradients in along-isobath energy flux decreases. Along-isobath energy flux increases on the northern side of the ETD where in angle between waves and bathymetery contours increases at the same location that wave height increases. Erosion may occur at the increasing gradient in along-isobath energy flux on south side of the ETD. Erosion may contribute to the steep bathymetry gradient on the northern edge of the ebb tidal channel (Figure 10). Deposition would occur north of the ETD

where along-isobath energy flux decreases. The decreasing gradient in along-isobath energy flux on the nothern side of the ETD corresponds to the rapidly accreting section of the coastline in Figure 2. During high energy events from the southwest, along-isobath energy flux is directed northward. This is reflected in the elongation of the ETD in the towards the north. The northward direction of sediment transport at depths up to 24 m or more during high energy winter storms is confirmed with measurements of suspended sediment and currents by Sherwood et al. (2000) made during this time period at the tripod locations.

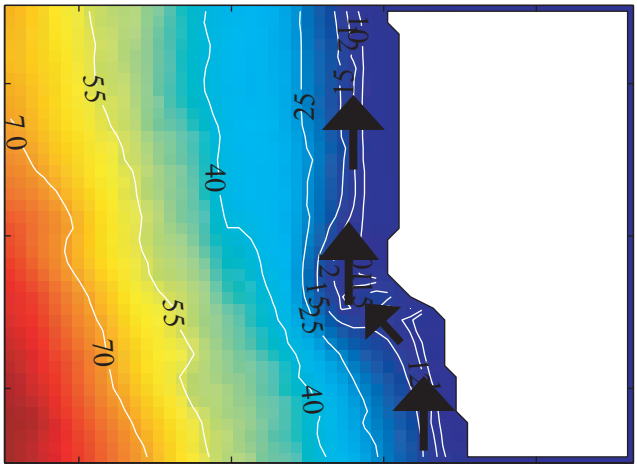

Figure 104. Patterns in along-isobath energy flux for winter storm conditions. Arrow direction and magnitude was determined using Equation 42 to interpret spatial variation of wave height and direction along isobaths.

The second general set of conditions observed during the field deployment is low wave energy events with wave direction from west or north of west. These conditions are exemplified during the time period between 11/22/99 12:00 and 11/23/99 12:00. Significant wave height offshore was 3.76 m and offshore waves were from 279°. Interpretation of Figures 93 and 94 using Equation 42 resulted in Figure (105). Along-isobath energy flux is interpreted to be small and directed southerly north and south of the ETD as waves would be approaching nearly perpendicular to the contours. Magnitude of along-isobath energy flux increases on the northern flank of the ETD as wave height increases, direction is southerly. Along-isobath energy flux reverses direction to the south of the delta due to wave refraction. Erosion would be expected at the location of divergence in along-isobath energy flux. Although southerly transport during long periods low energy conditions is expected balance northerly along-isobath energy flux, it appears that northerly along-isobath energy flux dominates morphology of the ETD. Sherwood et

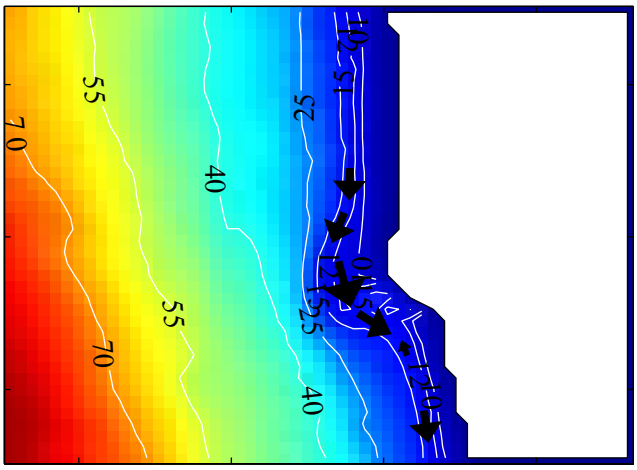

Figure 105. Patterns in along-isobath energy flux for low energy conditions. Arrow direction and magnitude was determined using Equation 42 to interpret spatial variation of wave height and direction along isobaths.

al. (2000) agree that transport direction may vary, but conclude that northerly transport dominates over the time scale of a year.

The interpretation of gradients in along-isobath energy flux implies changes that have occurred prior to the 1998 position of the delta will continue to occur as long as wave climate continues to follow the pattern of high energy events from the south west and low energy events from a more westerly direction. Decreasing sediment supply from the Columbia River combined with net northerly along-isobath energy flux will exacerbate the patterns of erosion. Therefore the ETD has not reached a stable position and reorientation of the ETD to the north will only occur more rapidly as sediment supply from the south diminishes.

Chapter Five

Conclusions

The SWAN model was developed for use in all gravity wave environments, however published model calibration are for wind dominated wave conditions in lacustrine or estuarine environments. Therefore, it was necessary to recalibrate the model for the high energy, swell dominated study area. This wave modeling study of the southwest Washington continental shelf was undertaken to provide accurate information about wave climate for interpretation of along-isobath energy flux or use in a sediment transport model. The study area has experienced a large amount of accretion and erosion associated with damming of the Columbia River and emplacement of jetties at Grays Harbor. An application of the model results examined the contribution of along-isobath energy flux due to waves to the stability of Grays Harbor ETD.

Sensitivity of the SWAN model was determined by varying model elements to determine which elements were important for accurate model calibration. Field data were collected for comparison with model results in the calibration and validation study. Formulations within the SWAN model were retuned for conditions on the southwest Washington shelf. Finally, the tuned model was applied to stable time periods during the field experiment. The model was then analyzed to determine reasons for model error.

The sensitivity study showed only formulations for energy dissipation due to whitecapping and bottom friction were important to modeling wave height. The SWAN model was very insensitive to changes in wave direction. The calibration study determined the most accurate formulation for wind input/whitecapping in the SWAN model on the southwest Washington coast is the Janssen formulation. This formulation was choosen because dissipation is greater than in the Komen formulation used in other enviroments. The Madsen formulation for

bottom friction produced the most accurate model results because it utilizes a variable value for bottom velocity, unlike the JONSWAP formulation, and the bottom friction coefficient depends on a local value for bottom roughess, unlike the Collins formulation. Error statistics in the validation model runs always improve relative to the default model runs. Error statistics in the tuned model run are reasonable when compared with error statistics in the tuned model of Ris (1997).

Spatial patterns in significant wave height and wave direction for two validated model runs representing low and high energy events were interpreted using Equation 42 to determine direction and relative magnitude of along-isobath energy flux. High energy events are characterized by northerly longshore energy flux with gradients resulting in deposition north and south of the ETD and erosion near the center of the ETD. This interpretation corresponds well with historical changes in bathymetric data as well as calculated sediment flux from measured velocites and sediment concentrations. Low energy conditions are characterized by gradients in longshore flux resulting in deposition and erosion at the same locations as during high energy events, however transport direction is in different directions and of lower magnitude than high energy events. The ETD at Grays Harbor is not located in a stable postion and will continue to reorient itself as a result of wave driven along-isobath energy flux and diminishing sediment supply from the south.

References

Allen, P., and P. Komar, Spatial and temporal variations in the wave climate of the North Pacific, Report to the Oregon Department of Land Conservation and Development, 46 pp., 2000.

Battjes, J., and P. Janssen, Energy loss and set-up due to breaking of random waves, in Coastal Engineering 1978, Proceedings of the 16th International Conference, ASCE, Hamburg, Germany, 59-587, 1978.

Bender, L., Modification of physics and numerics in a third-generation ocean wave model, Journal of Atmospheric and Oceanic Technology, 13, 726-750, 1996.

Boothroyd, J., Mesotidal inlets and estuaries, Coastal Sedimentary Environments, edited by R. Davis, 287-360, Springer-Verlag, New York, 1978.

Bouws, E. and G. Komen, On the balance between growth and dissipation in an extreme depth-limited wind-sea in the souther North Sea, Journal of Physical Oceanography, 13, 1653-1658, 1983.

Buijsman, M., The relation between jetty construction/rehabilitation and shoreline change at the entrance to Grays Harbor, Southwest Washington coastal erosion workshop report 2000, edited by G. Gelfenbaum and G. Kaminsky, 115-122, U.S. Geological Survey Open File Report, in press.

Collins, J., Predictions of shallow water spectra, Journal of Geophysical Research, 77, 2,693-2,707 pp., 1972.

Cavaleri, L. and L. Bertotti, Sensitivity of wave model results to directional resolution, Il Nuovo Cimento, 17 C, 635-644, 1994.

Cross, V., D. Twichell, K. Parolski, S. Harrison, Archieve of boomer seismic-reflection data collected aboard RV CORLISS cruise CRLS97007 off northern Oregon and southern Washington inner continental shelf, U.S Geological Survey Open File Report 98-351, 2 CD-ROM, 1998.

Ewans, K., Observations of directional spectrum of fetch-limited waves, Journal of Physical Oceanography, 28, 495-512, 1998.

Gelfenbaum, G. and G. Kaminsky (Eds), Southwest Washington coastal erosion workshop report 1999, U.S. Geological Survey Open File Report 00-439, 187, 2000.

Gelfenbaum, G. and G. Kaminsky, Motivation, goals, and status of the southwest Washington Coastal Erosion Study, Southwest Washington coastal erosion workshop report 2000, U.S. Geological Survey Open File Report, in press.

Gibbs, A., M. Buijsman, C. Sherwood, Gridded bathymetry data Washington-Oregon coast: 1926-1998, U.S. Geological Survey Open File report 00-448, 36 pp., 2000.

Guza, R., and E. Thornton, Local and shoaled comparisons of sea surface elevations, pressures, and velocities, Journal of Geophysical Research, 83(C3), 1,524-1,530 pp., 1980.

Hasselman, K., On the nonlinear ernergy transfer in a gravity-wave spectrum, part 1: general theory, Journal of Fluid Mechanics, 12, 481-500, 1963.

Hasselman, K., On the spectral dissipation of ocean waves due to whitecapping, Boundary-Layer Meteorology, 6, 107-127 pp., 1974.

Hasselman, S., K. Hasselman, J. Allender, T. Barnett, Computations and parameterizations of the nonlinear energy transfer in a gravity-wave spectrum. Part II: Parameterizations of the non-linear energy transfer for application in wave models, Journal of Physical Oceanography, 15, 1378-1391, 1985.

Herb, A., Holocene stratigraphy and sediment volumes for the Columbia River littoral cell, Pacific Northwest, USA, M.S. Thesis, Portland State University, 168 pp., 2000.

Janssen, P., Wave-induced stress and the drad of air flow over sea waves, Journal of Physical Oceanography, 19, 745-754, 1989.

Janssen, P., Quasi-linear theory of wind-wave generation applied to wave forecasting, Journal of Physical Oceanography, 21, 1,631-1, 642 pp., 1991.

Jay, D., and P. Naik, Separating human and climate impacts on Columbia River hydrology and sediment transport, Southwest Washington coastal erosion workshop report 2000, edited by G. Gelfenbaum and G. Kaminsky, 23-24, U.S. Geological Survey Open File Report, in press.

Jonsson, I., Wave boundary layers and friction factors, 127-148, in Coastal Engineering 1966, Proceedings of the 10th International Conference, 1966.

Kaminsky, G., M. Buijsman, P. Ruggiero, G. Gelfenbaum, An integrated contemporary sediment budget for the Columbia River Littoral Cell, Southwest Washington coastal erosion workshop report 2000, edited by G. Gelfenbaum and G. Kaminsky, 141-148, U.S. Geological Survey Open File Report, in press.

Komen, G., S. Hasselmann, K. Hasselmann, On the existence of a fully developed wind-sea spectrum, Journal of Physical Oceanography, 14, 1271-1285, 1984.

Komen, G., L. Cavaleri, M. Donelan, K. Hasselmann, S. Hasselmann, P. Janssen (Eds), Dynamics and Modelling of Ocean Waves , 532 pp., Cambridge University Press, New York, 1994.

Li, C., and M. Mao, Spectral modelling of typhoon-generated waves in shallow water, Journal of Hydraulic Research, 30, 611-622, 1992.

Luo, W., and J. Monbaliu, Effects of the bottom friction formulation on the energy balance for gravity waves in shallow water, Journal of Geophysical Research, 99(C9), 18501-18511, 1994.

Madsen, O., Y. Poon, H. Graber, Spectral wave attenuation by bottom friction: experiments, in Coastal Engineering 1988, Proceedings of the 21st International Conference, 492-504, 1988.

Madsen, O., and M. Rosengaus, Spectral wave attenuation by bottom friction: theory, in Coastal Engineering 1988, Proceedings of the 21st International Conference, 849-857, 1988.

Ris, R., 1997. Spectral modeling of wind waves in coastal areas, Report no 97-4, Communications on Hydraulic and Geoltechnical Engineering, Department of Civil Engineering, Delft University of Technology, 160 pp., 1997.

Snyder, R., F. Dobson, J. Elliott, and R. Long, Array mearuements of atmospheric pressure fluctuations above surface gravity waves, Journal of Fluid Mechanics, 102 1-59 pp., 1981.

Thornton, E., T. Dalrymple, T. Drake, E. Gallagher, B. Guza, A. Hay, R. Holman, J. Kaihatu, T. Lippman, T. Ozkan-Haller, Nearshore processes research: Report based on the nearshore research workshop, St. Petersburg, FL, pp. 3, 2000.

Thornton, E., and R. Guza, Energy saturation and phase speeds measured on a natural beach, Journal of Geophysical Research, 87(C12), 9,499-9,508 pp., 1982.

Tillotson, K., and P. Komar, The wave climate of the Pacific Northwest (Oregon and Washington) a comparison of data sources, Journal of Coastal Research, 13(2), pp. 440-452, 1997.

Tolman, H., A third-generation model for wind waves on slowly varying unsteady, and inhomogeneous depths and current, Journal of Physical Oceanography, 21, 782-797 pp., 1991.

Twitchell, D., V. Cross, and K. Parolski, Sidescan-sonar imagery, surface sediment samples, and surficial geologic interpretation of the southwestern Washington inner continental shelf based on data collected during Corliss cruises 97007 and 98014, U.S. Geological Survey Open File Report 00-167, 26 pp, 2000.

Twitchell, D., V. Cross, and K. Parolski, Evolution of the southwest Washington inner shelf since the last lowstand of sealevel, In Southwest Washington Coastal Erosion Workshop Report 1998, edited by G. Gelfenbaum and G. Kaminsky, pp. 24-28, U.S Geological Survey Open File Report 99-524, 1999.

Weber, N., Bottom friction for wind seas and swell in extreme depth-limited situations, Journal of Physical Oceanography, 21, 148–172, 1991.

Woxell, L., Prehistoric beach accretion rates and long-term response to sediment depletion in the Columbia River littoral system, USA, M.S. Thesis, Portland State University, 137 pp., 1998.

Venkatarathnam, K. and D. McManus, Origin and distribution of sands and gravels on the northern continental shelf off Washington, Journal of Sedimentary Petrology, 43, 799-811, 1973.

Young, I., and R. Gorman, Measurements of the evolution of ocean wave spectra due to bottom friction, Journal of Geophysical Research, 100(C6) 10,987-11,004 pp., 1995.

Young, I., and G. Van Vledder, A review of the central role of nonlinear interactions in wind-wave evolution, Philosophical Transactions The Royal Society, 342, 505-524, 1993.

Zambresky, L., A verification of the global WAM model December 1987-November 1988, Technical report 63, European Center for Medium-Range Weather Forecasts, Reading, England, 86 pp., 1989.